FINAL REPORT

FUEL GRADE ETHANOL RECOVERY BY SOLVENT EXTRACTION

By

D. W. Tedder
Project Director

Under

Contract No. E-19-669
Georgia Tech Research Institute
Solar Energy Research Institute
Golden, Colorado

August 1984

GEORGIA INSTITUTE OF TECHNOLOGY
A UNIT OF THE UNIVERSITY SYSTEM OF GEORGIA
CHEMICAL PROCESS DESIGN INSTITUTE
SCHOOL OF CHEMICAL ENGINEERING
ATLANTA, GEORGIA 30332-0100

Contract No. E-19-669
Georgia Tech Research Institute
Solar Energy Research Institute
Contract No. XX-2-02180-1

FUEL GRADE ETHANOL RECOVERY BY SOLVENT EXTRACTION: FINAL REPORT

D. W. Tedder
Project Director

August 1984

Georgia Tech
Chemical Process Design Institute
School of Chemical Engineering
Altanta, GA   30332-0100   U.S.A.

Table of Contents

LIST OF TABLES

LIST OF FIGURES

CHAPTER 1

EXECUTIVE SUMMARY
(D. W. Tedder)

The comparative costs of solvent extraction and distillation for ethanol recovery from a continuous fermentor are discussed. The reference cases are based upon feedstock received from an orange concentrate plant processing 100,000 boxes/day of Valencia oranges for 180 day/year. The estimated ethanol production rate is 864,000 200 proof gal/year recovered from the fermentation of citrus molasses. The net sugar costs are 4.5¢/lb.

The estimated net production costs are 92-101¢/gal for the solvent extraction and distillation processes respectively. Solvent extraction increases the estimated cash flow about 12%, but also requires about 12% more in capital investment ($1.65 vs. $1.46 million in 1983). The solvent extraction case saves approximately $100,000 annually in actual utility costs.

As a first approximation, both cases exhibit about the same percentage return on investment (% ROI). Three year ACRS depreciation and straight line capital recovery have been assumed. Both investments are assumed to qualify for a 20% tax credit in the first year and 10% in the second. With these and other assumptions, the base case ROI is about 9% in the 1st year of investment and 21% in the 4th year.

Net profits can be increased by adjustments in the assumed plant operating period, the plant size, and the estimated ethanol f.o.b. selling price. Operating the ethanol plant 300 days/year yields about a 67% increase in the % ROIs (15% in the 1st year, 35% in the 4th year). On the other hand, a 400,000 box/day plant should earn 15% ROI in the 1st year operating 180 days/year or about 25% ROI in the 1st year operating 300 days/year. An 800,000 box/day plant operating 300 days/year should earn 35% ROI in the first year with an ethanol selling price of $1.70/200 proof-gal. f.o.b.

During the period in which the Solar Energy Research Institute has supported this work, considerable progress has been made toward the identification of ways in which liquid/liquid extraction may be used to reduce ethanol production costs. Tests during the past year have included the measurement of solvent toxicity on Saccharomyces cerevisiae and several attractive solvent systems have been identified. These solvent mixtures exhibit low toxicities, but adequate solvent capacity and selectivity to extract an 80-85% product from an 8-10% beer in the presence of inextractable dissolved solids such as dextrose. In addition, considerable progress has been made in measuring

the vapor/liquid equilibria which are relevant for solvent regeneration and in defining conditions under which the ethanol product may be removed without the use of refrigerant during product condensation.

A two-cycle concept using liquid/liquid extraction has been largely demonstrated on a pilot-scale basis although questions remain as to the long-term effects of solvent cross contamination. It has been demonstrated, however, that fuel-grade ethanol can be produced in a suitable drying cycle from a 50% ethanol/water mixture. Conditions are even more favorable for the drying cycle when the feed is 80-85% ethanol as discussed below.

The toxicity tests which have been completed thus far suggest that the solvent mixtures under active consideration exhibit negligible effects on ethanol production rates by Saccharomyces cerevisiae. However, it has not been proven at this point that the solvents do not affect the long term viability of this microorganism. Toxicity tests by others (see Chapter 3) yielded similar results.

Chapter 2
Economic Considerations
(D. W. Tedder)

2.1 Introduction

Fuel-grade ethanol is a potentially attractive transportation fuel whose use could decrease crude oil imports if it is derived from biomass or agricultural wastes rather than petrochemicals. Although there is considerable interest in Gasahol (1), there is also some controversy about whether or not it represents an energy resource (2) when it is recovered from dilute fermentation liquors. Beer stills and azeotropic distillation systems (3-5) are capable of producing a 99+% product from an 8 wt% beer with an energy expenditure of about 24,000 BTU/gal (See Fig. 2.1). Alternatively, a beer still/extractive distillation combination (6) may be capable of producing the same product at an energy expenditure of about 14,000 BTU/gal. On the other hand, the current solvent extraction concepts offer the possibility of producing a 96 wt%, fuel-grade product (2% solvent and 2% water) with an energy expenditure of about 10,000 BTU/gal. An improved solvent extraction/extractive distillation combination, however, may be capable of recovering a 99+% product with an energy expenditure of about 9,000 BTU/gal.

The current research effort focuses on the application of solvent extraction recovery with other unit operations such as continuous fermentation and extractive distillation to achieve further reductions in energy and ethanol production costs. Although the current flow sheets are attractive, it appears that further improvements are now possible. For example, some benefits may exist through partial water recycle to reduce sugar concentration requirements. For another example, a single solvent processing system may be achievable through solvent extraction followed by extractive distillation. If feasible, such a concept will further reduce the estimated capital requirements and avoid the contamination problems which often results from the use of multiple solvents in a processing scheme.

Currently, steam costs are in the range of $8 - $10 per 10^6 BTUs. This cost amounts to an energy charge of about 22¢/gal to produce 99+% ethanol from an 8% beer using an optimized beer still/azeotropic distillation system. One goal of this program, therefore, has been to demonstrate that solvent extraction can be coupled with continuous or batch fermentation and extractive distillation to reduce the energy expenditure to about 8¢/gal.
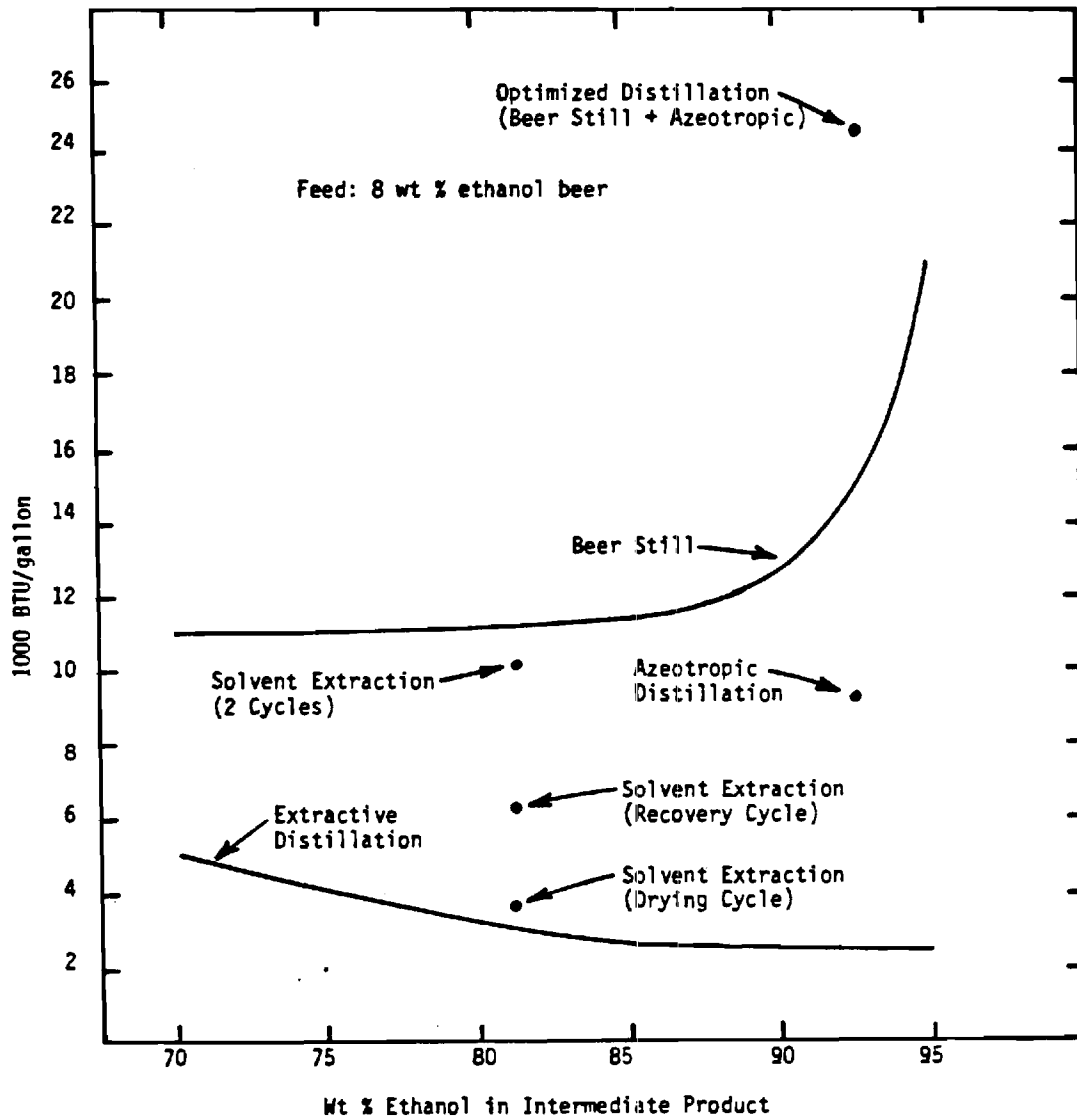
Fig. 2.1 Estimated energy requirements for ethanol recovery by liquid/ liquid extraction, extractive distillation, azeotropic distillation, and a beer still from an 8 wt % beer feed.

Liquid/liquid extraction is particularly attractive for use with large scale fermentation systems because of the ease with which it can be scaled up and its tolerance for feed stream impurities, such as unc.ssolved solids. In addition, it offers the possibility of reduced energy requirements for ethanol production through the exploitation of physical properties other than the relative volatilities of ethanol and water alone to facilitate ethanol dehydration and recovery.

2.2 Economic Analysis and Design Summary

The current reference flowsheet is based on ethanol production from citrus molasses. An orange concentrate plant, operating continuously for 180 days annually, produces 84.5 tons of 72 Brix molasses (10, 11) recovered from 100,000 boxes of Valencia oranges. The ethanol plant requires (11, 12) 3.85 gal of 72 Brix molasses to produce one gallon of 200 proof ethanol. The ethanol plant produces, therefore, 4800 gal/day as 200 proof product or about 864,000 gallons annually.

Citrus molasses is a by-product which currently sells for $70-90/dry ton (12) as an ingredient in cattle feed. Approximately 50% of the molasses solids are fermentable. A key assumption is that the unfermentable solids, together with excess biomass, may be returned to the orange concentrate plant for the same price as the feedstock (i.e. $90/dry ton). Discussions with industry representatives suggest that this assumption is reasonable as long as the processed solids are still valuable as a cattle feed.

Experimentally, it has been found that the diluent, ISOPAR-M, and the modifier, tri-n-butyl phosphate (TBP), have little effect on the fermentation rates associated with Saccharomyces cerevisiae. Other investigators have obtained similar results for TBP (7-9) for several types of microorganisms.

It has also been learned that inextractable dissolved solids improve ethanol recovery by solvent extraction. The dissolved solids (dextrose, thus far) appear to enhance the ethanol distribution coefficient (a salting effect) and to decrease water extraction (presumably by decreasing the water activity). Consequently, solvents which are equilibrated with ethanol/water/dextrose solutions yield both higher ethanol distribution coefficients and selectivities than when the same solvents are equilibrated with ethanol/water solutions under comparable conditions. Experimentally, the following correlations have been identified for ethanol and water extraction into the solvent 20 vol% TBP in ISOPAR-M at room temperature:

$$\ln D_e = -1.61 - 1.779\ X_e + 1.321\ X_D \qquad (2.1)$$

$$\ln D_w = -5.63 + 2.91\ X_e + 1.27\ X_D \qquad (2.2)$$

where:

X_e = weight fraction ethanol in equilibrated aqueous

phase $0 < X_e < 0.2$

X_D = weight fraction dextrose in the equilibrated aqueous phase $0 < X_D < 0.4$

As can be seen from eqn. 2.2, the dextrose also increases the water distribution coefficient (since the term 1.27 X_D is positive). However, the amount of water extracted is decreased since:

$$Y_W = D_W X_W \simeq D_W (1 - X_e - X_D) \tag{2.3}$$

where:

Y_W = weight fraction ethanol in the solvent phase.

The effect of temperature is also important for this system. However, temperature elevation is not required in order to achieve an economical operation. Consequently, the extraction column in this design study is assumed to operate at the same temperature as the fermentor (27°C). On the other hand, the effective operation of the drying cycle requires higher temperatures ($\sim 85^{\circ}$C) and, therefore, the drying cycle is opeated at this state using the solvent, ISOPAR-M.

Figure 2.2 summarizes the flowsheet utilizing the two cycle concept for producing fuel-grade ethanol from an 8% beer. The product in this case is 98 wt% ethanol on a solvent-free basis and it contains about 2% solvent (primarily ISOPAR-M). Vapor-liquid equilibrium data suggest that solvent carry over can be held to this level using a reflux ratio of 0.20. Table 2.1 summarizes the major stream material balances for this system. The estimated purchases costs for major equipment items are summarized in Table 2.2 for the fermentation and plant storage systems, and in Tables 2.3 and 2.4 for the recovery and drying cycles in Fig. 2.2. Tables 2.5 and 2.6 summarize estimated purchase equipment costs for distillation equipment to perform about the same separation (i.e. 99+% ethanol from an 8% beer).

The estimated energy use rates for these two processing concepts are summarized in Table 2.7. As can be seen, optimized distillation for the case is expected to require about 24,000 BTU/gal whereas the solvent extraction system is expected to require about 10,000 BTU/gal exlcuding pumps and drivers. At an energy value of $8/10^6 BTU, this savings is equivalent to 13¢/gal of absolute ethanol.

From Table 2.8, it appears that the solvent extraction process requires about 12% more in capital investment compared to conventional distillation. In addition, both processes have other manufacturing costs which should be considered when gross profits are computed. These cost elements, together with the estimated annual sales, are

Fig. 2.2 Conceptual flowsheet for ethanol recovery by liquid/liquid extraction using the two cycle concept.

Table 2.1 Material balances for ethanol recovery by solvent extraction using the two cycle concept.

STREAM NUMBER	1	2	3	4	5	6	7	8	9	10	11	12	13
STREAM LABEL	FEED 37 BRIX	FERM ØG	FERM AIR	FERM YEAST	BEER	1A EXT	1A ORG	1A RAFF	HOT 1A EXT	1B EXT	FEED STM	1A REBOIL STM	1B CW
T (°F)					95	95	95	95	300	300	401	401	85
P (PSIA)					15	15	15	15	15	2	250	250	15
Cp (BTU/lb °F)									0.5	0.5			
FLOWRATES (1000 lb/hr)													
TOTAL	14.26				13.00	110.12	108.74	12.03	110.12	110.12			
SUGARS	2.40				0.07			0.07					
TOTAL DISS. SOLIDS	5.10				2.77			2.77					
WATER	9.16				9.16	0.25	---	9.06	0.25	0.25			
ETHANOL		0.005			1.04	1.15	0.02	0.01	1.15	1.15			
BIOMASS					0.19			0.19					
SOLVENT						108.72	108.72	---	108.72	108.72			
CARBON DIOXIDE		0.94											
AIR		0.30	0.30										

Table 2.1 (Cont)

	14	15	16	17	18	19	20	21	22	23	24	25	26
	2A LIQUID FEED	1B ØRG	WARM ØRG	1A CW	SOLVENT MAKE UP	DAY PRODUCT	2A EXT	HOT 2A EXT	2B CW	2B STM	2B ØRG	WARM 2B ØRG	2B RAFF
T (°F)	95	310	105		95	95	185	225				185	95
P (PSIA)	2	15	15		15	15		2					
Cp (BTU/lb °F)	0.92	0.5	0.5								•		0.97
FLOWRATES (1000 lb/hr)													
TOTAL	1.54					0.02	1.08	41.28	41.28				
SUGARS													
TOTAL DISS. SOLIDS													
WATER	0.25						0.02	0.02	0.02			----	----	0.23
ETHANOL	1.15						1.04	1.20	1.26			0.21	0.21	0.10
SOLVENT	0.02	108.70	108.70		0.02	0.02	40.02	40.02			40.00	40.00	----
TOTAL FLOW (GPD)						4796							

Table 2.3   Estimated Purchased Equipment Costs to Produce 81% Ethanol by Solvent Extraction (Mid-1983) from an 8% Beer

Item	$1,000[a]
Extraction Column (5.4' ∅ x 55', cs)	46
Intervals	3
Heat Exchangers	
H1, 11,300 ft^2, cs	75
H2, 190 ft^2, cs	5.3
H3, 100 ft^2, cs	4.7
H4, 700 ft^2, cs	10.2
Stripper Column (4' ∅ x 20', cs)	13
Intervals	1
Pumps and Drivers	6
TOTAL	164.2

[a] M&S index = 773.2

Table 2.4   Estimated Purchased Equipment Costs to Produce 98% Ethanol from 81% Feed by Solvent Extraction

Item	$1000[a]
Extraction Column (2.3' ∅ x 40', cs)	14
Intervals	3
Heat Exchangers	
H5 (10 ft^2, cs)	4.0
H6 (1600 ft^2, cs)	16.4
H7 (470 ft^2, cs)	9.5
H8 (770 ft^2, cs)	10.2
H9 (410 ft^2, cs)	7.8
Stripper Column (1.5' ∅ x 20', cs)	5
Intervals	1
Pumps and Drivers	4
TOTAL	74.9

[a] M&S index = 773.2

Table 2.5   Estimated Purchased Equipment Costs to Produce 92.5% Weight Percent Ethanol by Distillation from an 8 Weight Percent Beer

Item	$1000[a]
Distillation Column (6' ∅ x 90', cs)	78
Sieve Trap (50 trays, cs)	15
Condenser (1400 ft^2, cs)	14.6
Reboiler (200 ft^2, cs)	5.4
Feed Preheat (500 ft^2, cs)	8.1
Reflux Tank	6.0
Pumps and Drivers	5.0
TOTAL	132.1

[a] M&S index = 773.2

Table 2.6   Estimated Purchased Equipment Costs to Produce 99+% Ethanol from 81% Feed Using Azeotropic Distillation

Item	$1000[a]
Azeotropic Distillation Column (1.8' ∅ x 39', cs)	11
Intervals	
Stripper Column (0.8' ∅ x 25', cs)	3
Intervals	
Heat Exchangers	
Azeotropic Condenser (262 ft^2, cs)	6.6
Azeotropic Reboiler (90 ft^2, cs)	4.4
Stripper Condenser (32 ft^2, cs)	4.2
Stripper Reboiler (26 ft^2, cs)	4.1
Pumps and Drivers	4
Decanter	5
Reflux Tanks	4
TOTAL	46.3

[a] M&S index = 773.2

Table 2.7   Energy Use for Ethanol Recovery by Solvent
             Extraction and Distillation

| | BTU/gal 200 proof Ethanol | |
	Distillation	Solvent Extraction
Media Sterilization	2,500	2,500
Beer Still	15,000	
Azeotropic Column	7,447	
Stripper Column	1,983	
Recovery Cycle		6,280
Drying Cycle		3,870
Pumps and Drivers	600	647
TOTALS	27,530	13,297

Table 2.8   Estimated Installed Costs for Solvent Extraction
             Distillation and Fermentation Systems

| Item | $1000[a] | |
	Solvent Extraction	Distillation
Distillation		
Ethanol Concentrator		132
Azeotropic Purification		46
Solvent Extraction		
Recovery Cycle	164	
Drying Cycle	75	
Fermenter System	256	256
Plant Storage	54	54
Purchased Equipment Costs (PEC)	549	488
Installed Costs (3 x PEC)	1,647	1,464

[a] M&S index = 773.2

summarized in Table 2.9. It is assumed at this point that the ethanol plant is cosited with an existing orange concentrate plant. Utilities are estimated, therefore, using internal pricing.

Slightly different sales prices have been assumed for each ethanol product because slight differences exist in product quality. The ethanol product from solvent extraction contains slightly more water (1-2%) than the ethanol distillate. On the other hand, the solvent extraction product also contains about 1-2% ISOPAR-M which increases the ethanol value as a fuel.

The two products are assumed, therefore, to have slightly different values. Specifically, the cost of the ISOPAR-M is recovered in the solvent extraction product. Actually, the solvent extraction produces a slightly increased amount of product which has a lower value ($1.69/gal) versus the distilled ehtanol product ($1.73/gal). The extraction produces, therefore, about 900,000 gals of product annually whereas the distillation process produces about 864,000 gal/year.

Examination of the gross profits calculations in Table 2.9 suggests that the solvent extraction process will reduce the annual utility costs by about $100,000. On the other hand, the 12% increase in capital outlay increases the fixed costs of solvent extraction. The estimated gross profits are, nevertheless, 15% higher for the solvent extraction process.

As the cost of steam increases, this cost difference will also increase. For example, steam costs of $12/10^6 BTU leads to a utility charge difference of about $122,000 or a 30% difference in annual gross profits.

Current assumptions for a beer still producing a 95% product are equivalent to utility charges of about 17¢/gal. Small producers today are paying 18-20¢/gal to produce this same product. Hence the current assumptions ($8/10^6 BTU) remain on the low side of current utility costs.

Table 2.10 compares these two processes with respect to net production costs. As can be seen, the solvent extraction process is expected to reduce steam costs about 1.1¢/gal and yield a net savings of about 9¢/gal of 200 proof ethanol.

Table 2.9　　　Estimated Annual Gross Profits for 98-99% Ethanol Production from Citrus Molasses Using Either Distillation or Solvent Extraction

Item	Process Cost ($1000/year)	
	Solvent Extraction	Distillation
Annual Costs (C)		
Molasses ($90/dry ton)	991	991
Solvent (17,000 gal)	34	
Pentane		4
Cooling Water (15¢/1000 gal)	7	13
Steam (250 psia, $8/$10^6$ BTU)	87	182
Electricity ($50/$10^6$ w-hr)	10	3
Labor	100	100
Nutrients and Yeast	10	10
Fixed Charges (10% of Investment)	165	146
TOTALS	1,404	1,449
Annual Sales (S)		
Dry Ethanol (864,000 gal)	1,525	1,495
By-product Solids ($90/dry ton)	575	575
	2,100	2,070
Gross Profits (GP = S-C)	696	621

Table　2.10　　　Net Production Costs for Fuel Grade Ethanol Recovered from Citrus Molasses Excluding Capital Recovery

Item	¢/gal 200 proof ethanol	
	Solvent Extraction	Distillation
Molasses	48.1	48.1
Solvents	0.5	0.5
Nutrients and Yeast	1.1	1.1
Cooling Water	0.8	1.5
Steam	10.1	21.1
Electricity	1.1	0.3
Labor	11.6	11.6
Fixed Charges	19.1	16.9
	92.4	101.1

Table 2.11   Net Profit Calculations for Ethanol Production Using Solvent Extraction and Distillation

(3 year capital recovery)

Item	$1000/year	
	Solvent Extraction	Distillation
FIRST YEAR		
Gross Profits (S-C)	696	621
Net Taxable Income (GP-0.25 I)	284	255
Taxes (0.5 NTI)	142	127
Total Credits (0.2 I)	329	293
Excess Credits	187	166
Cash Flow (GP-0)	696	621
Net Profit (CF-I/3)	147	133
(NP/I) x 100	8.9%	9.1%
SECOND YEAR		
Gross Profits (S-C)	696	621
Net Taxable Income (GP-0.38 I)	70	65
Taxes (0.5 NTI)	35	33
Total Credits	165	146
Excess Credits (0.1 I)	130	113
Cash Flow (GP-0)	696	621
Net Profit (CF-I/3)	147	133
(NP/I) x 100	8.9%	9.1%
AFTER THIRD YEAR		
Gross Profits (= NTI)	696	621
Taxes (0.5 NTI)	348	311
Cash Flow (= NP)	348	311
(NP/I) x 100	21.1%	21.2%
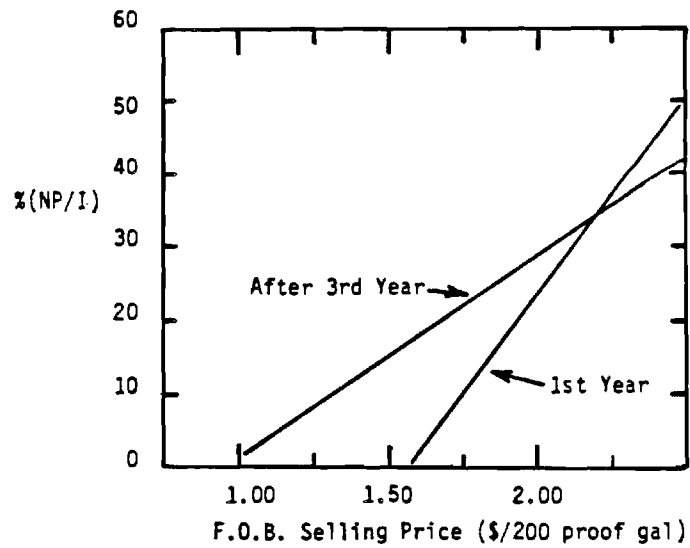
Fig. 2.3 Effect of ethanol product selling price on the estimated return on investment.
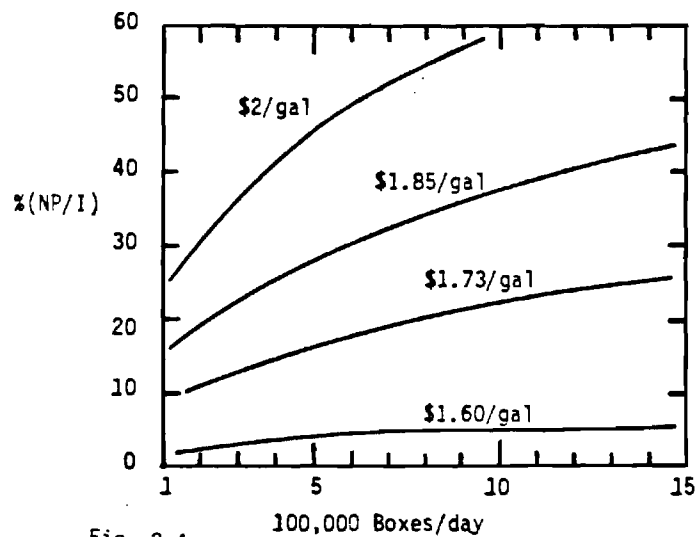
Fig. 2.4 Effect of the plant size and ethanol selling price on the estimated first year return on investment.

Table 2.11 compares the two processes in terms of net profits and return on investment. In this case, a three year payback period was assumed. Also, no differential in tax credits was assumed between the two processed although the solvent extraction process should qualify for an additional energy conservation credit which has not been considered. Despite the slightly higher capital investment requirements which are associated with solvent extraction, it appears to yield greater net profits than the distillation system. On the other hand, the return on investment is slightly lower for the solvent extraction system. Initially, both systems should earn at least 9% on the investment. After capital recovery, the estimated return on investment is about 20%.

A key assumption is the value of by-products. Since only half of the soilds in citrus molasses are fermentable, the residuals represent a significant cost factor. If it is not possible to incorporate the unfermentable residuals into cattle feed, then both processes become uneconomical. In this case, the residuals become a waste material which requires disposal at an additional cost. However, with the current assumptions, sugar is purchased at a net cost of about 4.5¢/lb. Without by-product credits, the sugar price would essentially double.

Net profits for the base cases are about 9% in the first year. This conclusion is affected by the ethanol selling price and the plant size. These factors can be considered, however, through the use of Figs 2.3 - 2.5 which approximate these effects. Also, the time value of money between the 1st and 4th years have been ignored in these figures.

In Fig 2.3, the % ROI in the 1st and 4th years after the investment is estimated as a function of the ethanol product selling price before shipment to the user. (The adjustment for transportation costs may be on the order of 5-10¢/gal). With the current assumptions, the net profits approach zero at about $1.57/gal f.o.b. On the other hand, an ethanol selling price of $2.00/gal yields about 24% in the first year. An expected value is $1.70-1.80/gal which yields an estimated 7-12% ROI in the first year and 20-23% ROI after capital recovery.

The expected %ROI is also affected by the plant size as shown in Figs 2.4 and 2.5 for the 1st and 4th years respectively for different ethanol f.o.b. selling prices. The expected 1st year % ROI for a 400,000 box/day (180 day/year) plant is 15-25%. An 800,000 box/day plant is expected to earn 21-35% ROI in the 1st year and 50-60% in the 4th year based upon these approximate calculations in which the 0.6 tenths power rule was applied to the total installed cost for solvent extraction at 100,000 boxes/day.

The reference plant is also assumed to operate for 180 day/year. A more typical work period for chemical plants is 300 day/year. If the plant is constructed for a 100,000 box/day concentrate plant which provides feed 180 days/year, but other feed materials can be supplied at the same net sugar cost for an additional 120 day/year, then the 1st and 4th year ROIs are about 15-35% respectively. Hence, the annual operating period assumptions reduce the % ROI about 67%.

2.3 Conclusions

In summary, the proposed solvent extraction system appears attractive compared to conventional distillation. It is expected to reduce production costs at least 8¢/gal and to increase both gross and net profits. Although the current concept requires slightly more capital investment than conventional distillation, it is expected that an extractive distillation/solvent extraction combination process will require less capital outlay and yield further reductions in actual energy requirements.
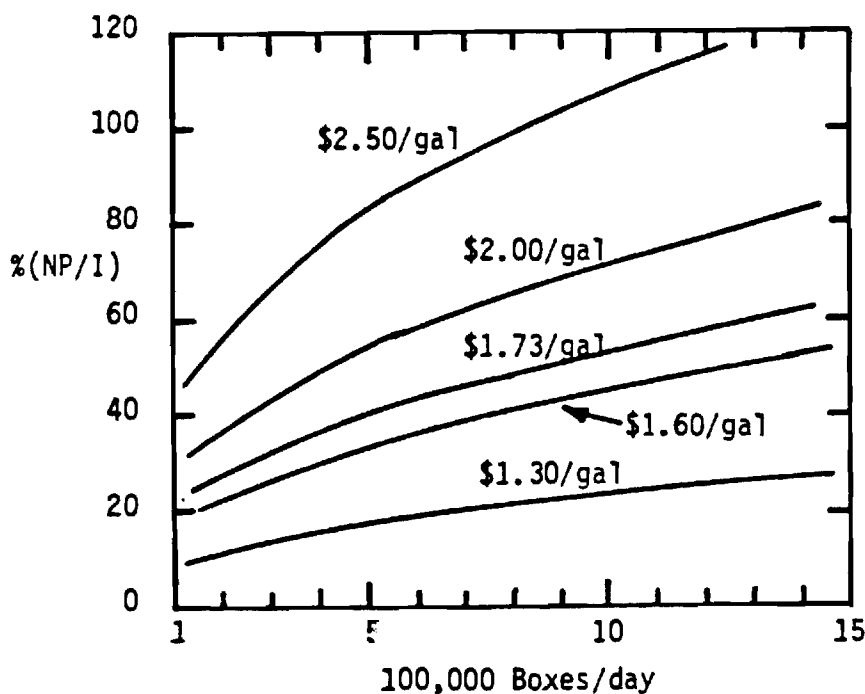
Fig. 2.5 Effect of the plant size and ethanol selling price on the estimated return on investment after the third year.

2.4 References

1. Larry Marion, "In the Spotlight: Ethanol", Chem. Eng., (Feb. 26, 1979), p. 78.

2. E. V. Anderson, "Gasohol: Energy Mountain or Molehill?" C & E News, (July 31, 1978).

3. M. L. David, et al., Gasohol Economic Feasibility Study, Development Planning and Research Associates, Manhattan, Kansas (July 1978).

4. G. R. Cysewaski and C. R. Wilke, "Process Design and Economic Studies of Alternative Fermentation Methods for the Production of Ethanol", Biotech and Bioeng., Vol. XX, (1978) 1421-1444.

5. C. Black, "Distillation Modeling of Ethanol Recovery and Dehydration Processes for Ethanol and Gasohol", CEP (September 1980), p. 78.

6. M. R. Basila, Improtec, Inc., Tyler, Texas, personal communication to D. W. Tedder (July 1983).

7. M. J. Playne and B. R. Smith, "Toxicity of Organic Extraction Reagents to Anaerobic Bacteria", Biotech and Bioeng. Vol XXV (1983) 1251-1265.

8. A. E. Torma and I. J. Itzkovitch, Appl. Environ. Microbiol. 32 (1976) 102.

9. G. Dave, H. Blanck and K. Gustafsson, J. Chem. Technol. Biotechnol. 29 (1979) 249.

10. J. W. Kesterson and R. J. Braddock, By-Products and Speciality Products of Florida Citrus, Agricultural Experiment Station, Lake Alfred, Florida, Bulletin 784 (technical) (December 1976).

11. R. Hendrickson and J. W. Kesterson, Citrus Molasses, Agricultural Experiment Station, Lake Alfred, Florida, Bulletin 677 (technical) (April 1971).

12. J. W. Kesterson and R. J. Braddock, "The Potential Production of Gasohol from Citrus", Annual Citrus Processors' Meeting, Lake Alfred, Florida (October 11, 1979).

CHAPTER 3

SOLVENTS EFFECTS ON ETHANOL PRODUCTION BY

SACCHAROMYCES CEREVISIAE

(A. S. Myerson And P. J. Ferster)

The production of ethanol from sugar by fermentation employing Saccharomyces cerevisiae has been employed for thousands of years in the production of beer and wine. In recent years, attention has been focused on the production of ethanol as a fuel replacement for oil. This attention has led to a new interest in the fermentation process along with novel separation techniques to be used in conjunction with fermentation to separate the ethanol from the fermentation broth. In this study, solvent extraction is being coupled with fermentation. In order to employ solvent extraction as a separation process, the solvent must not be toxic to the microorganisms. In this chapter, therefore, a brief literature survey on previous studies of the effects of solvents on yeast is presented. This is followed by a description of experimental procedures employed in this work and the experimental results.

3.1 Background

The growth and production of ethanol by fermentation of sugar employing Saccharomyces cerevisiae suffers from a major drawback. The product, ethanol, inhibits the fermentation process. This inhibition is noncompetitive, meaning that ethanol affects the rates of fermentation and all growth, but not its affinity for glucose. In a conventional batch or continuous system, an ethanol concentration of 10-12 wt% is normally considered the maximum value because of these inhibiting effects. Other investigators (1-7) have shown that cell growth is inhibited at very low ethanol concentrations, but that the inhibition of further ethanol production is not suppressed until the ethanol concentration in solution reaches 10-12 wt% at which point the viability of the yeast cells rapidly declines. The production of ethanol can also be affected by employing sugar concentrations above 22 wt% which also results in a loss of viability of the yeast cells.

A number of processes have been suggested to continuously remove ethanol from the fermentor thus relieving the problem of ethanol inhibition. Cysewski and Wilke (8) employed a vacuum fermentation technique with cell recycle for continuous ethanol production. Cell recycle was employed to achieve high cell densities and rapid ethanol production rates. Employing a 10% glucose feed, they obtained a cell density of 50 g dry wt/liter and an ethanol

productivity of 29.0 g/liter-hr. The vaccuum fermentor eliminated ethanol inhibition by boiling away ethanol from the fermentation broth when it was formed. This permitted a rapid and complete fermentation of concentrated sugar solutions.

Another approach to the problem of ethanol inhibition is the use of solvent extraction for the removal of ethanol from the fermentation broth. This technique requires, however, that the solvent not be toxic to the yeast cells. For example, the effects of the solvents isopropanol, propanol and butanol on the growth and fementation of S. cerevisiae was examined by Leao and Varuden (9). Their results showed that the solvents did not have an effect on the Michaelis constant, k_m, but they did reduce the maximum specific growth rate, μ_m. Butanol was found to be the most inhibitory followed by propanol and isopropanol.

Ribaud (10) examined the toxicity of a variety of solvents on the batch growth of yeast on sugar. Ribaud reported that hexanol, 1-heptanol, 1-pentanol, octanol, 3-heptanol, 2,4-dimethyl-3-pentanol, 5-methyl-1-hexanol, and 2-octanol all severely inhibited both growth and ethanol production. Dibutyl phtalate and P-1200 did not seriously affect growth and ethanol productivity.

3.2 Materials and Methods

The yeast employed in this work was Saccharomyces cerevisiae which was obtained in a pure, dry form from the Chemical Foods Corporation. The media employed in all studies is listed in Table 3.1. The toxicity studies were carried out in 250 ml shake flasks which were agitated in an American optical incubator shaker. The flasks and media were autoclaved at $121^{\circ}C$ for 15 minutes prior to innoculation. The bath was kept at a temperature of $30^{\circ}C$ with a shake speed of 200 rpm. A yeast concentration of 10 g/liter was initially employed in all experiments and a sugar concentration of 10 wt%. The solvents of interest were added so as to form a saturated solution at the conditions of the experiment. Ethanol concentrations were measured daily using gas chromatography.

A limited number of continuous studies were conducted in a 1.2 ℓ New Brunswick Continuous Fermentor equipped with pH control. A schematic on the fermentor appears as Fig. 3.1.

Table 3.1   Medium Composition for Toxicity Tests

Substance	Concentration (g/l)
KH_2PO_4	5.0
$(NH_4)_2SO_4$	1.5
EDTA (3 Na^+)	0.125
$MgSO_4 \cdot 7\ H_2O$	0.2
$Zn\ SO_4 \cdot 7\ H_2O$	0.008
$FeSO_4 \cdot 7\ H_2O$	0.02
$MnSO_4 \cdot 7\ H_2O$	0.02
$CaCl_2$	0.02
Sucrose	Variable
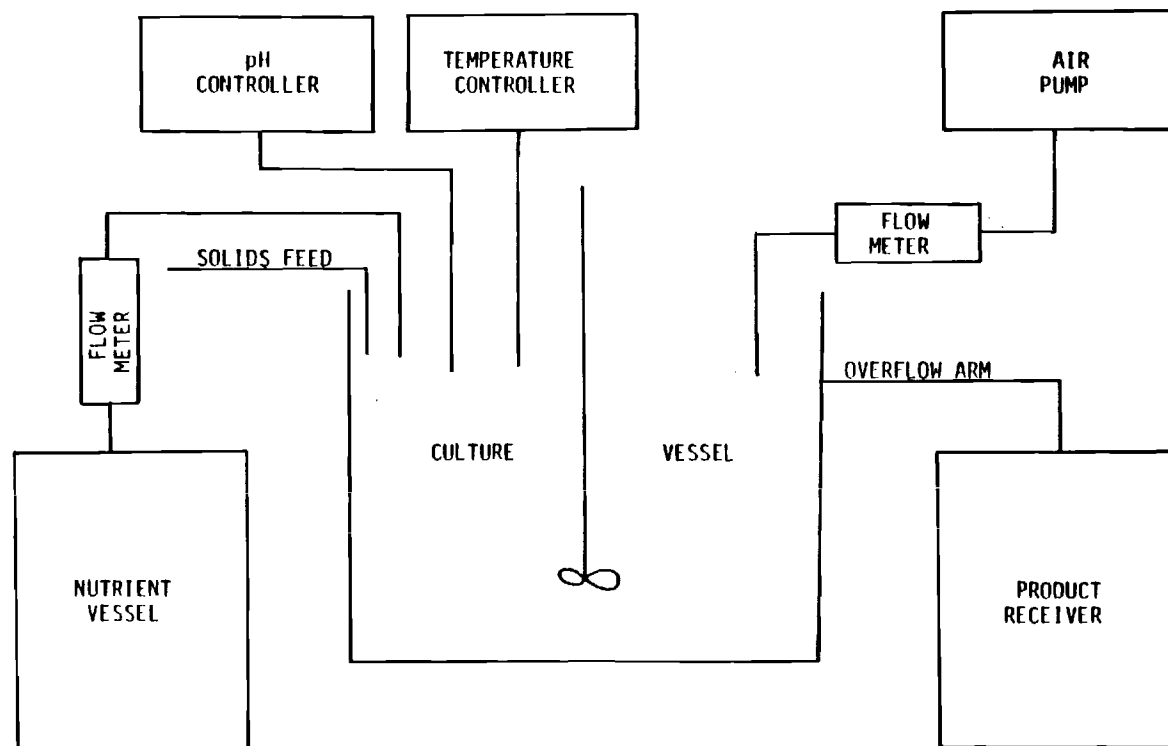
Figure 3.1   Schematic Diagram of Bioflow Fermenter

3.3 Results

Previous work resulted in the solvents tri-n-butyl phosphate (TBP), ISOPAR-M, NORPAR 12, methyl and 2-ethyl hexanol being chosen for study. Results of the batch studies are presented in Table 3.2 and show that a number of solvents and solvent concentration have no measurable effect on the ethanol production when compared to a control grown at the same conditions.

Continuous fermentation studies were conducted by first achieving a steady state ethanol concentration without the presence of solvent and examining the effect (if any) on the steady state by adding solvent to the feed. Results employing ISOPAR-M as the solvent confirmed the batch data with no effect on the steady state ethanol concentration noted. Previous workers (11-13) have also reported that ISOPAR-M and TBP were non-toxic to several other microorganisms.

Table 3.2   Batch Toxicity Test Results

Solvent	Result
30% Tridecyl in Norpar 12	No effect on ethanol concentration
30% Tridecyl in Isopar M	No effect on ethanol concentration
Methyl Ester[a]	No effect on ethanol concentration
100% tri-n-butyl phosphate	No effect on ethanol concentration
2-Ethyl Hexanol	Completely inhibited all growth and ethanol production

[a] A Procter and Gamble product, CE-1295, a high purity C_{12} cut methyl ester.

3.4 References

1. F. F. Hartline, Science, 206, 41 (1979).

2. I. Holzberg, R. K. Finn, and K. H. Steinkraus, Biotechnol. bioeng., 9, 413 (1967).

3. M. Nagatani, M. Shoda, and S. Aiba, J. Ferment. Technol., 46, 241 (1968).

4. C. D. Bazua and C. R. Wilke, Biotechnol. Bioeng. Symp., 7, 105 (1977).

5. T. K. Ghose and D. Tyagi, Biotechnol. Bioeng., 22, 1387 (1979).

6. T. W. Nagodawithana and K. H. Steinkraus, J. App. Environ. Microbiol., 31, 158 (1976).

7. M. Novak, P. Streihaiana, M. Moreno, and G. Goma, Biotechnol. Bioeng., 23, 201 (1981).

8. G. R. Cysewski and C. R. Wilke, Biotechnol Bioeng. 19, 1125, (1977).

9. C. Leao and N. Varuden, Biotech and Bioeng., 2W, 260, 1982.

10. J. Ribaud, Feasibility Study on the Use of Extractive Fermentation to Enhance Ethanol Production in the Yeast Fermentation, Department of Chemical and Biochemical Engineering, University of Pennsylvania (1980).

11. M. J. Payne and B. R. Smith, Biotech and Bioeng, 25, 1251 (1983).

12. A. E. Torma and I. J. Itzkovitch, Appl. Environ. Microbiol., 32, 102 (1976).

13. G. Dave, H. Blanck and K. Gustafsson, J. Chem. Tech. Biotech., 29, 249 (1979).

CHAPTER 4

Continuous Fermentation and Product Recovery
by Liquid/Liquid Extraction

(A. J. Eckles, P. J. Ferster, W. Y. Tawfik,
D.W. Tedder and A. S. Myerson)

4.1 Summary

This research focuses on the use of solvent extraction, coupled with continuous fermentation, to produce and recover ethanol more efficiently. These initial results suggest that a low-toxicity solvent, such as a blend of tri-n-butyl phosphate and ISOPAR-M, can be used to maintain reduced ethanol concentrations in the fermenter (8-9 wt %) and to produce an ethanol product in excess of 50 wt %. The continuous removal of the toxic end products from the fermentor results in higher productivity. Solvent extraction also facilitates ethanol recovery with less energy input than conventional distillation.

4.2 Introduction

Conventional ethanol fermentation is limited by the inhibitory effect of the ethanol end-product. This inhibition may be alleviated, however, by the continuous removal of the ethanol product from the fermentor. Vacuum fermentation (1, 2), in which an ethanol product is continuously evaporated from the fermentor, offers one approach. However, it does require the use of a large compressor. Adsorption (3), using activated carbon, is another possibility. On the other hand, fermentates containing sugars and other dissolved solids often appear to reduce ethanol loading on the adsorbent, and there are further complications due to the inherent difficulties associated with subsequent ethanol recovery from solid adsorbents.

Solvent extraction avoids many of these difficulties. For example, it is tolerant of both dissolved and undissolved solids and, in fact, inextractable dissolved solids may often enhance performance. It is also a widely used unit operation, commercially available, and relatively easy to scale up. On the other hand, many solvents are toxic both to microorganisms and mammals. Also, the solvent must be relatively inexpensive and it should have a low aqueous solubility.

Equilibrium studies (4-10), measuring the ability of various immiscible systems to extract ethanol from water, have led to several general conclusions. First, it is apparent that those solvent systems which exhibit higher

ethanol distribution coefficients also exhibit lower selectivities over water. Secondly, the extract will likely have a relatively low ethanol loading (typically, 1 - 3 wt %).

The first obsevation suggests that a solvent blend may be more useful for this application than a pure substance since a blend may be tailored to give a more appropriate compromise between selectivity and solvent capacity. The second observation suggests that the solvent should have a low volatility compared to ethanol. The alternative is a solvent system, such as supercritical carbon dioxide, where the solvent (typically 98 wt % of the extract) must be evaporated in order to recover the ethanol product.

A third observation is that the ethanol distribution coefficients arerelatively low (typically 0.1 to 0.8) compared to most solvent extraction processes. Hence the recovery process must utilize a more efficient configuration, such as a countercurrent flow system with multiple stages. Recovery using cocurrent extraction is possible (11), but it is less attractive.

4.3   Materials And Methods

4.3.1   Microorganisms and Culture Media

The yeast used in all work was <u>Saccharomyces cerevisiae</u> which was obtained in a pure, dry form from the Universal Foods Corporation. The regular medium for ethanol production included variable dextrose or sucrose concentrations, KH_2PO_4, 5 g/l; $(NH_4)_2SO_4$, 1.5 g/l; 125 mg/l of EDTA (3 Na^+), 200 mg/l of $MgSO_4 \cdot 7H_2O$, 8 mg/l of $ZnSO_4 \cdot 7H_2O$, , 20 mg/l of $FeSO_4 \cdot 7H_2O$, 20 mg/l of $MnSO_4 \cdot 7H_2O$ and 20 mg/l of $CaCl_2$.

4.3.2.   Extraction Solvents and Equipment

The solvents used were tri-n-butyl phosphate (technical grade from Fisher) and ISOPAR-M (as received from Exxon Refining). Tri-n-butyl phosphate (TBP) has a boiling point of $289^{\circ}C$ and a specific gravity of 0.97 at $25^{\circ}C$. The diluent, ISOPAR-M, is a heavy, isoparaffinic, narrow refinery cut with a boiling point range of 207 to $254^{\circ}C$ and a specific gravity of 0.78 at $25^{\circ}C$.

Ethanol extraction was carried out in a Karr reciprocating plate column with 92 stainless steel plates (about 80% void space). The column had a nominal diameter of 1 inch and an overall height of 152 inches. Positive displacement lab pumps from Fluid Metering, Inc. were used to circulate the phases.

Solvent regeneration was carried out in a custom fabricated pyrex column (a flash apparatus) with a diameter of 2 inches and an overall height of about 3 feet. This apparatus was equipped with a glass wool demister pad and condenser assembly at the top. During the extractive fermentation tests, the fermentors consisted of several 20 ℓ polyethylene carboys. Before use, this pilot equipment was decontaminated using a dilute metabisulfite wash. The basic configuration is shown in Fig. 4.1.

4.3.3 Analytical Procedures

Concentration measurements were carried out using a gas chromatograph, HP 5710A, with a Porapak Q, 80/100 mesh, 4 ft x 0.125 inch column. A Hewlett Packard 3390A peak integrator was connected to the thermal conductivity detector which was operated at $250^{\circ}C$. Helium was used as the carrier gas. The column was maintained at $150^{\circ}C$. Propanol spiking and calibration curves were used to convert the ethanol and water area percentages into weight percentages.

Dissolved solids in some cases were determined by difference. During extractive fermentation, the dissolved solids were approximated using density measurements.

4.4 Results And Discussion

4.4.1. Liquid/Liquid Equilibria

Ethanol and water equilibrium concentrations were measured for the solvent as a function of the aqueous ethanol and dextrose concentrations, the temperature, and the volume fraction of TBP initially in the organic diluent. The equilibrated phases were analyzed using a GC and led to the following empirical correlations which are valid in the operating conditions of interest:

$$\ln D_e = 1.6 + 58.5 \ X_e^2 - 19.3 \ X_e + 0.985 \ X_D$$
$$+ 3.78 \ V_{TBP} - 1007.5/T \tag{4.1}$$

$$\ln D_w = -5.31 - 6.96 \ X_e^2 + 5.36 \ X_e + 1.18 \ X_D$$
$$+ 4.95 \ V_{TBP} - 4.65.1/T \tag{4.2}$$
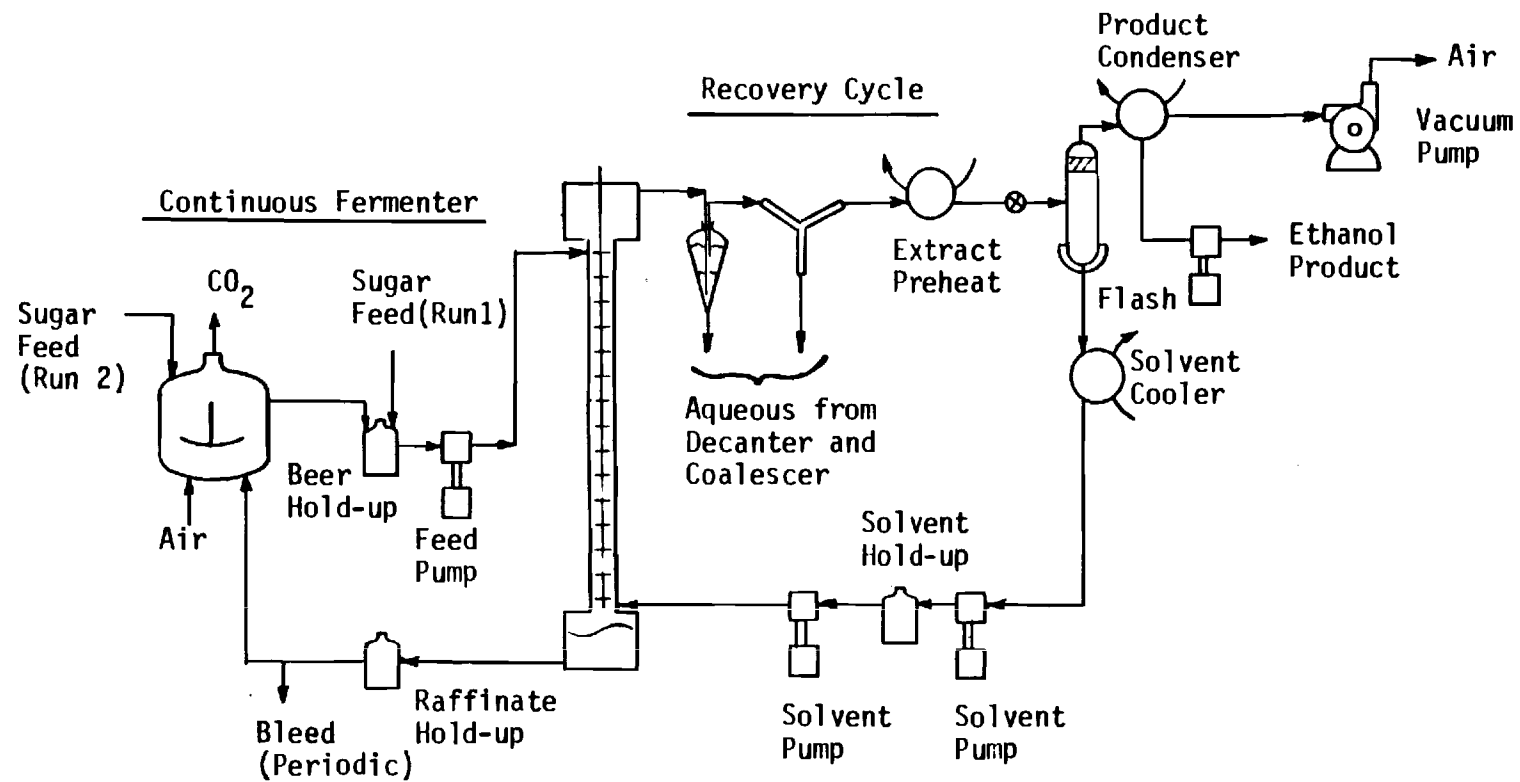
Fig. 4.1 Experimental apparatus for testing extractive fermentation. Fermenter was 20 1 capacity. Extraction column was a standard 1" diameter Karr reciprocating plate column for pilot testing.

where

D_e = ethanol distribution coefficient (weight fraction ratio)

D_w = water distribution coefficient (weight fraction ratio)

X_e = weight fraction ethanol in the equilibrated raffinate

X_D = weight fraction dextrose in the equilibrated raffinate

V_{TBP} = volume fraction of TBP used to make up the blended solvent

T = temperature, ^{O}K.

The range of applicability for these equations is limited to:

$$X_e < 0.33$$

$$X_D < 0.60$$

$$301 < T < 342\ ^{O}K.$$

These correlations for ethanol and water extraction are based upon 27 equilibrations in which the independent variables were adjusted over the ranges indicated.

4.4.2 Extractive Fermentation

The process configuration which was tested is summarized in Fig. 4.1. Glucose media and air (intermittently) were pumped into the stirred tank fermenter. Fermentate, typically 8 to 10 wt % ethanol, was removed from the fermentor by overflow, passed through a hold-up flask, and pumped into the top of the Karr reciprocating column. Solvent was pumped into the bottom of the Karr column which was operated in an organic continuous mode with the liquid/liquid interface near the bottom of the column.

Extract was taken from the top of the Karr column, passed through a decanter and coalescer, and sent to the solvent stripper. The stripper was operated at reduced pressure and slightly elevated temperatures. The ethanol

product was condensed from the stripper vapor while the regenerated solvent was recycled to the extraction column.

Because the inextractable solids (i.e. the dextrose media) increase the ethanol distribution coefficient (see Eqn. 4.1) and reduce the water activity, several runs were completed with the sucrose feed being added to the fermentate prior to extraction. The extraction raffinate, containing the inextractable media, was then recycled to the fermenter to avoid excessive sugar losses.

Results from one such run are summarized in Fig. 4.2. In this case, the sugar feed was mixed with the fermentate just prior to extraction. The inextractable solids were in excess of 10 wt %, but the ethanol feed concentration was about 5 wt %. Also, both the fermenter and Karr column were operated at ambient conditions, about 23°C.

This approach has several disadvantages. The lower ethanol concentrations and temperatures lead to extraction from a relatively viscous aqueous phase and yields reduced solvent loadings (typically < 1 wt %). Also, the height of a transfer unit increases significantly.

Nonetheless, Fig. 4.2 indicates that the extract composition, on a solvent free basis, would yield a 50 to 60 wt % product. The actual product compositions which were achieved in this case were 30 to 60   wt %, on a solvent free basis, and consistently wetter than the extract.

Extraction of the undiluted fermentate, and warming the Karr column operation through solvent preheat to around 50°C, significantly improved the process operation. In this case, the sugar feed was added directly to the fermenter as needed. The undiluted beer was pumped directly into the extraction column. The raffinate was accumulated and recycled after cooling back to the fermenter.

Figure 4.3 summarizes the results of one run using this approach. In this case, the initial ethanol concentration into the Karr column was about 10 wt %. The apparent extract composition ranged from 93 to 97 wt % while the recovered product was about 70-75 wt % ethanol on a solvent free basis.

Both Figs. 4.2 and 4.3 indicate that the recovered product will be wetter than indicated by extract analysis. This trend may be exaggerated somewhat by system air leakage in the stripper since it was operated at reduced pressures and the Atlanta air is relatively humid. However, it is also likely that water strips preferentially over ethanol from the solvent.
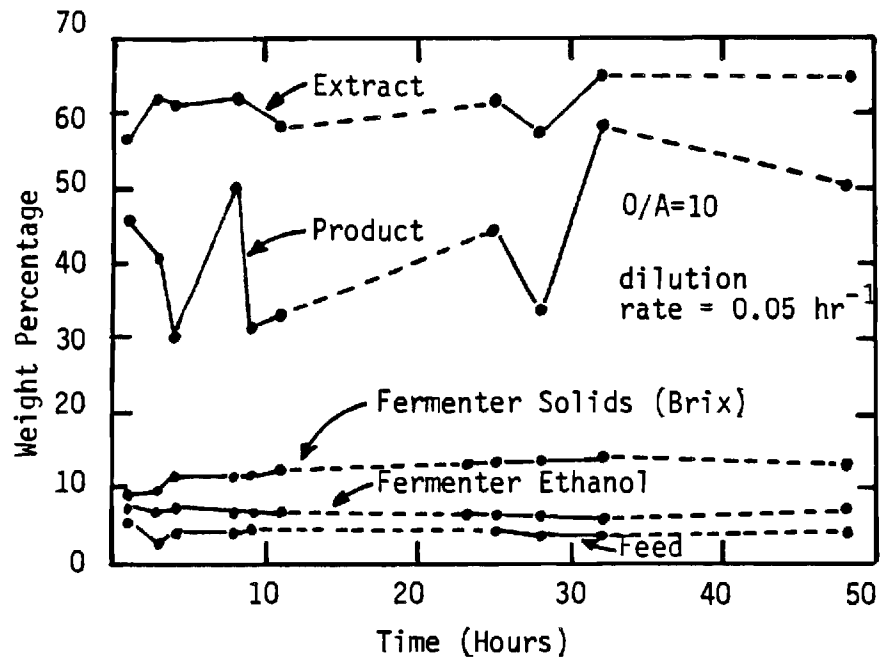
Fig. 4.2 Process conditions during first pilot run testing extractive fermentation. Sugar feed was added to beer prior to extraction. The extraction column operated at 23°C.
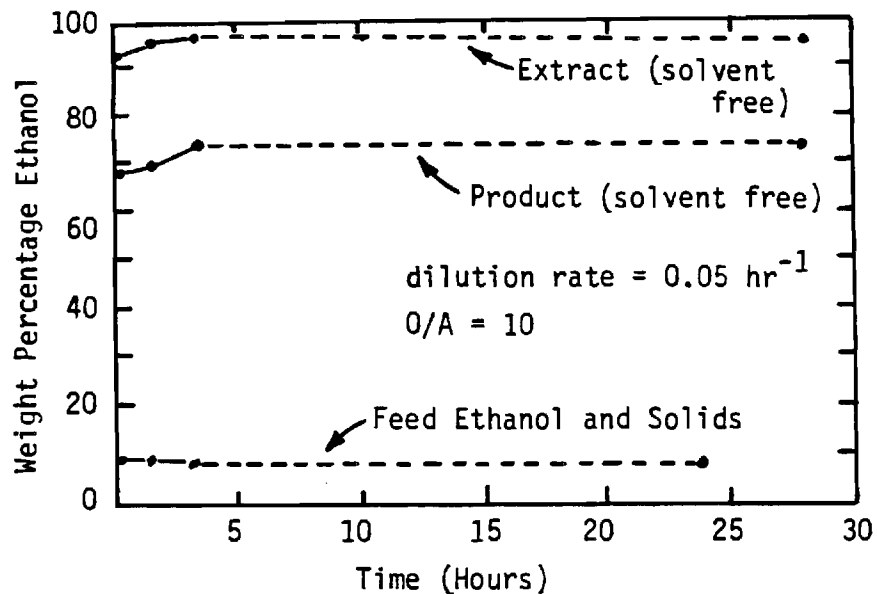
Fig. 4.3 Process conditions during the second pilot run testing extractive fermentation. The beer was added directly to the extraction column without clarification. The extraction column operated at 50°C.
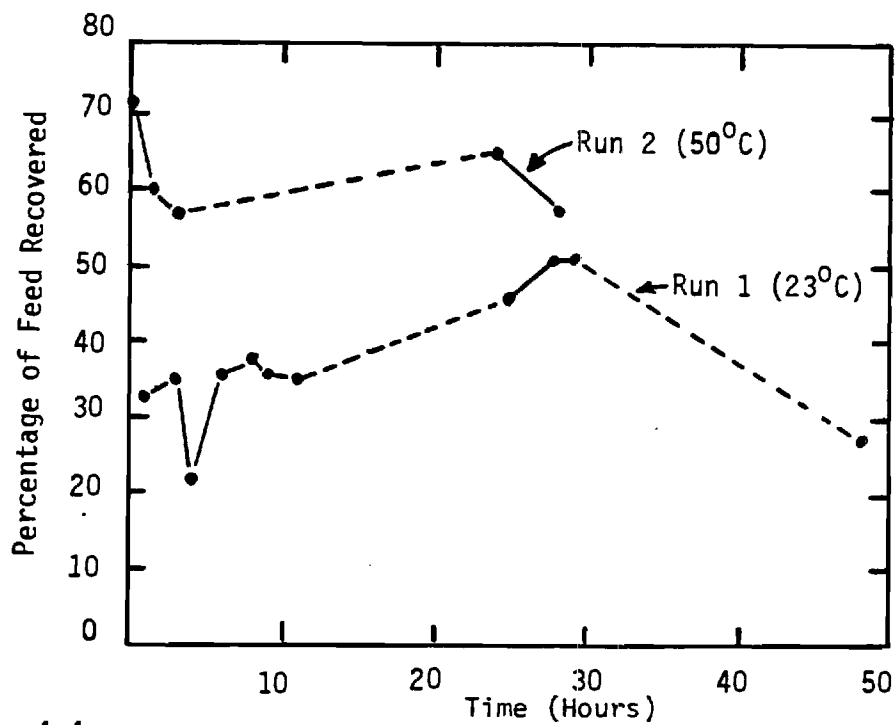
Fig. 4.4 Ethanol recoveries from two pilot runs testing extractive fermentation. Warm extraction column operation gave higher ethanol recoveries.

Consequently, it may be possible to couple liquid/liquid extraction with extractive distillation to obtain fuel-grade ethanol using a single solvent blend. In this case, the extract would be partially regenerated in a first extractive column in which fully regenerated solvent is added as a second feed above the extract. Distillate from this first stripper would be recycled to the extraction column. The bottom effluent from the first regeneration column would then be sent to a second regeneration column which would be operated at more severe conditions.

The ethanol recoveries which were achieved from runs 1 and 2 (Figs. 4.2 and 4.3) are summarized in Fig. 4.4. As can be seen, the second run at 50°C in the Karr column gave higher recoveries for the same organic to aqueous flow ratios as the first run. Although these recoveries are adequate for a raffinate recycle system as described here, a once through process would require a taller extraction column or higher organic-to-aqueous flow ratios. Typically, for example, in run 2 an 8-10 wt % feed is being extracted to about 3-4 wt % ethanol in the raffinate.

Additional process problems which have been identified include extract foaming during regeneration, low transfer unit heights during extraction and copper corrosion. In fact, the copper tubing led to a blue aqueous phase appearing in the coalescer. This phase was later determined to contain copper, sulfur, and phosphorous. The source is probably the copper tubing (which has been replaced with stainless steel) and either metabisulfite, the fermentation media salts, or TBP degradation products. At this time, it is not known whether or not TBP degradation is a significant problem, but it is a possible source of phosphorous.

From the standpoint of ethanol recovery, it apparently is not necessary to clarify the fermentate and remove the biomass. Small amounts of interfacial crud from the biomass were observed in the Karr column bottom interface, but it does not appear to be a serious problem.

With respect to the fermentor, biomass recycle has some disadvantages. However, it seems likely that microorganisms can be adapted or chosen judiciously (e.g. thermophiles) to facilitate ethanol recoveries at higher temperatures.

4.5 Conclusions

The concept of solvent blending (15) to achieve higher ethanol recoveries and quality by solvent extraction appears feasible. Although many questions remain, these initial results suggest that this approach is valid.

4.6 References

1. A. Ramalingham and R. K. Finn, Biotechnol Bioeng 19 (1977) 583.

2. G. R. Cysewski and C. R. Wilke, Biotechnol Bioeng 19 (1977) 1125.

3. H. Y. Wang, F. M. Robinson and S. S. Lee, Biotech Bioeng Sym 11 (1981) 555.

4. D. W. Tedder, Fuel Grade Ethanol Recovery by Solvent Extraction: Technical Progress Report for Period September 15, 1981 Through September 15, 1982, School of Chemical Engineering, Georgia Institute of Technology, Atlanta, GA (September 1982).

5. W. Y. Tawfik, Efficiency of Ethanol Extraction from Aqueous Mixtures, M. S. Thesis, School of Chemical Engineering, Georgia Institute of Technology, Atlanta, GA (1982).

6. K. B. Garg, Design of Liquid-Liquid Extractants for the Recovery of Fuel-Grade Ethanol, M. S. Thesis, School of Chemical Engineering, Georgia Institute of Technology, Atlanta, GA (1982).

7. J. Ribaud, Feasibility Study on the Use of Extractive Fermentation to Enhance Ethanol Production in the Yeast Fermentation, Department of Chemical and Biochemical Engineering, University of Pennsylvania (1980).

8. F. S. S. Leu, Distribution of Ethanol Between Binary Organic Solvents and Water, M. S. Thesis, Texas Tech University (1982).

9. C. J. King, "Separation Processes Based Upon Reversible Chemical Complexation," Symposium on Separation Technology, Taipei (1983) 127.

10. C. L. Munson and C. J. King, "Factors Influencing Solvent Selection for Extraction of Ethanol from Aqueous Solution," proceedings of the International Solvent Extraction Conference, Denver, CO (August 26 - September 2 1983) 509.

11. M. Minter and G. Goma, "Production of Ethanol by Coupling Fermentation and Solvent Extraction," Biotech Letters 3 (8) (1981) 405.

12. M. J. PLayne and B. R. Smith, Biotech and Bioeng 25 (1983) 1251.

13. A. E. Torma and I. J. Itzkovitch, <u>Appl. Environ.</u>
    <u>Microbiol.</u> <u>32</u> (1976) 102.

14. G. Dave, H. Blanck and K. Gustafsson, <u>J. Chem. Tech.</u>
    <u>Biotech.</u> <u>29</u> (1979) 249.

15. D. W. Tedder, U. S. Patent No. 4,399,000 (August 16,
    1983).

CHAPTER 5

ISOBARIC VAPOR-LIQUID EQUILIBRIUM DATA FOR
BINARY SYSTEMS:

H_2O/Ethanol/Isopar-M/Tri-n-butyl-phosphate

(Steven Babb and W. Y. Tawfik)

5.1 Summary

Vapor-liquid equilibrium data was obtained for various binary systems involving H_2O, Ethanol, Isopar-M, and tri-n-butyl-phosphate (TBP). These binary systems are important for any distillation processes (i.e. solvent regeneration) which might accompany liquid-liquid extraction during ethanol recovery from beer or other dilute aqueous streams.

Two types of data were the object of this study: vapor pressures of pure components, and binary vapor/liquid equilibrium (VLE) diagrams. Activity coefficients, furthermore, were obtained for the systems Ethanol/Isopar-M and TBP/Isopar-M. The Ethanol/TBP system was not studied.

The equipment was set up and checked out against the Ethanol/H_2O binary data of Larkin and Pemberton (1). The agreement is quite good, especially considering the experiment's accuracy to temperature of only $\pm 1^{\circ}C$. Based on vapor pressure data from this study, Isopar-M has an estimated average molecular weight between that of $C_{12}H_{26}$ and $C_{13}H_{28}$. The activity coefficients for the TBP/Isopar-M binary system indicate that TBP's activity is suppressed by moderate concentrations of Isopar-M and that in rich Isopar-M mixtures (weak TBP), Isopar-M behaves nearly ideally. The Ethanol/Isopar-M VLE data are not considered as reliable as the TBP/Isopar-M VLE data, yet ethanol and Isopar-M appear to mutually enhance each other's activities quite significantly.

5.2 Experimental

The liquid-vapor equilibrium chamber consisted of three principle devices: glassware for distilling under total reflux, an acetone/dry ice cooling system, and a pressure regulated vacuum system. Figure 5.1 illustrates the general layout of the apparatus. For a given liquid phase composition and system pressure, both the vapor phase composition and the system temperature are completely defined and do not represent independent degrees of freedom.

"A" = Condenser
"B" = Needle Valve

Thermometer

Acetone Pump

Dry Ice/Acetone Bath

Addition
Funnel

A

B

3-Way Valve

Cold Trap

Hg Trap

Manostat

Boiling
Flask

SEPTUM

To Rheostat

Heating Mantle

Sample Cow

Air Bleed

Manometer

Vacuum Pump

37
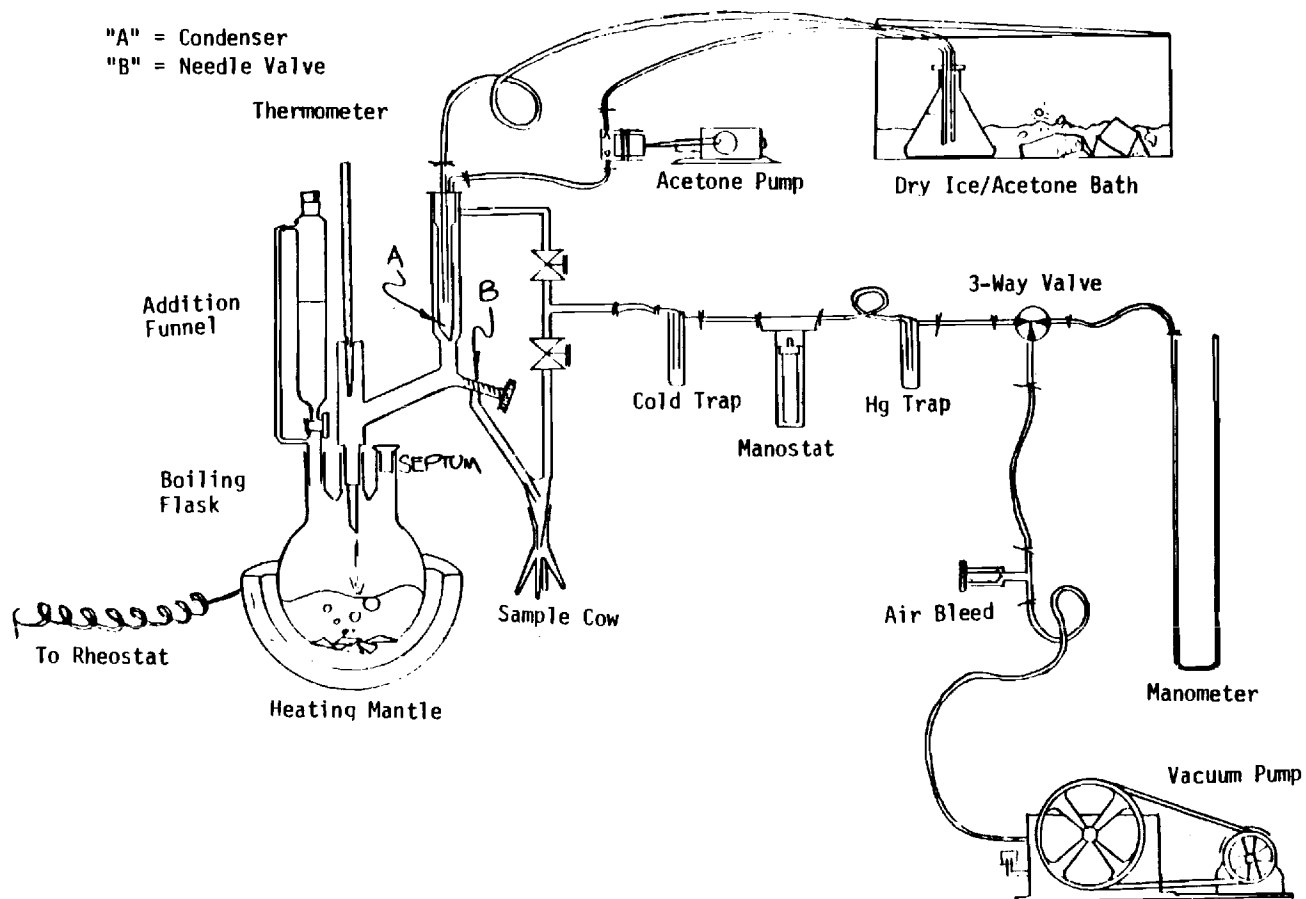
Figure 5.1   Simple Equilibrium Distillation Apparatus

The distillation glassware and heater consisted of a heating mantle with rheostat (0-110 V), 500 ml boiling flask, a distillation head with finger condenser, a side-mounted needle value for sampling refluxed condensate, a sampling cow with four 5 ml fingers, and vacuum attachments. A thermometer (typically $-10\,^{\circ}C$ to $250\,^{\circ}C$) was also used. Ideally, the 500 ml boiling flask should be three-necked, supporting the use of a septum for withdrawing liquid samples without breaking the vacuum, the thermometer, and an additional funnel for introducing the various components. More importantly, the system was insulated from the boiling flask to condenser to prevent premature condensation of the vapors.

The acetone cooling system included a positive displacement cooling pump (F.M.I.), a dry ice/acetone bath, and connections to the condenser.

The vacuum system included a cold trap, a Gilmont C-2200-D Manostat, a mercury trap, manometer, three way valve, air bleed needle valve, and a suitable high vacuum pump.

Two types of experiments are appropriate with the equipment described above. First vapor pressure curves can be generated, usually for pure components. In this case, temperature is treated as the dependent variable. Various pressures are set with the manostat to generate a given pure component curve. Vapor/liquid equilibrium diagrams can also be generated and are, perhaps, most useful. For a particular pressure setting, the liquid phase composition is gradually varied, producing changes in both the vapor composition and the system temperature. Figures 5.2 - 5.4 and Tables 5.1 - 5.4 summarize the various vapor pressure and VLE curves which have been generated thus far.

The most significant errors which may occur are due to leaks in the system, (allowing water to enter), pressure fluctuations, and the actual approach to true equilibrium between the liquid and vapor phases. Leaks in the system are especially damaging to the experimental results for those binaries which require the absence of water in the system, such as the system Ethanol/Isopar-M. However, experience has shown that water contamination can be reduced by at least an order of magnitude through methods described below and to quite acceptable levels. Pressure fluctuations, on the other hand, rendered temperature measurements accurate to only $\pm$ $2\,^{\circ}C$, even though the manostat is generally very reliable and stable.
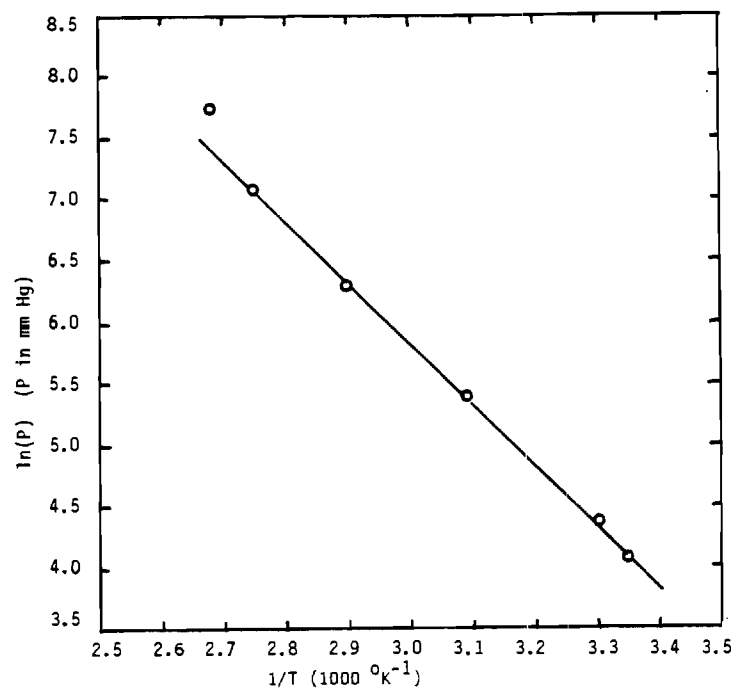
Figure 5.2   Vapor Pressure Versus Reciprocal Temperature for
              Ethanol

Table 5.1 Ethanol vapor presure data (from Ref. 1)

T (°C)	P (mm Hg)	1/T (10³K⁻)	ln P
25.0	59.20	3.353	4.081
30.0	78.62	3.298	4.365
50.0	221.3	3.094	5.400
70.0	542.3	2.914	6.296
90.0	1185	2.753	7.077
100.0	2346	2.680	7.760

Table 5.2 Experimentally measured TBP vapor pressures

T (°C)	P (mm Hg)	1/T (10³K⁻¹)	ln P
182 ± 2	44.5 ± 0.5	2.197	3.795
189.0	61.6	2.164	4.121
233.0	165.4	1.976	5.108
257.2	391.4	1.885	5.970
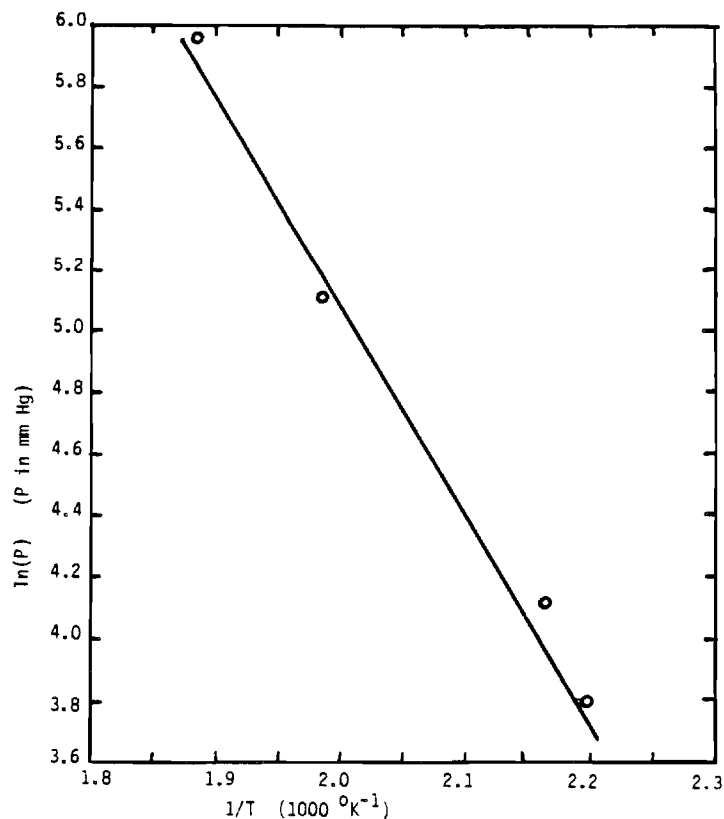
Figure 5.3   Vapor Pressure Versus Reciprocal Temperature for
TBP

Table 5.3   Experimentally measured ISOPAR-M vapor pressures

T ($^\circ$C)	P (mm Hg)	1/T (10^3K^{-1})	ln P
121.0 ± 2	40.7	2.537	3.706
158.6	134.3	2.316	4.900
175.4	208.3	2.229	5.339
187.2	280.3	2.172	5.636
200.7	391.4	2.110	5.970

Table 5.4   Experimentally measured pure component heats
of vaporization[a]

Component	ΔHv (cal/mol)
EtOH	10,450
TBP	13,500
ISOPAR-M	10,500

[a]   Based on the Classics-Clapyron equation
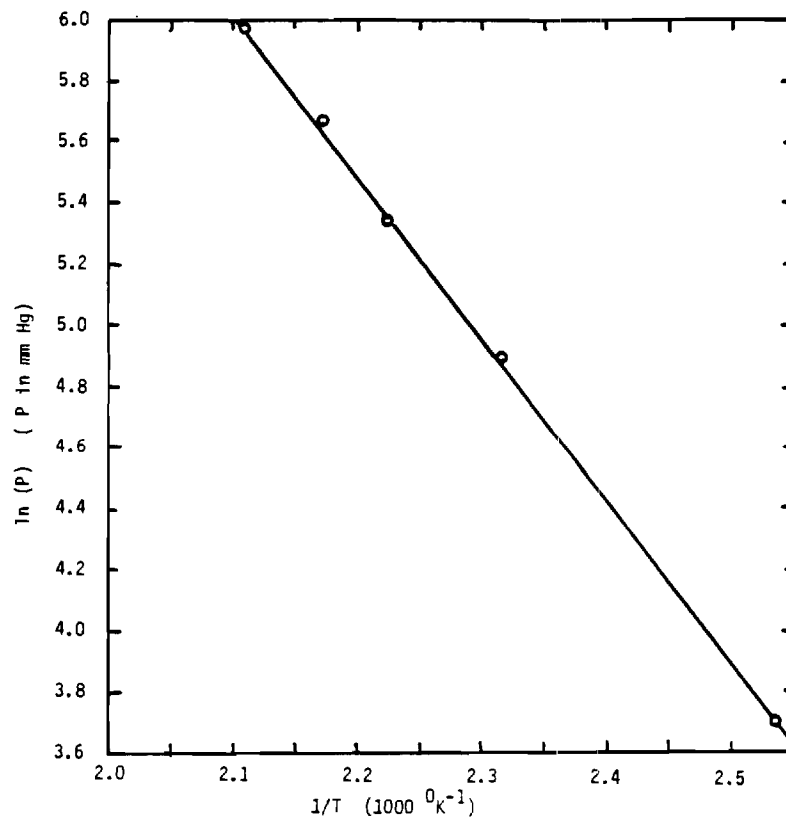
Figure 5.4   Vapor Pressure Versus Reciprocal Temperature for ISOPAR-M

The approach to equilibrium is generally time-consuming, requiring perhaps an hour for each "run". Each composition seems to have its own "time constant". That is, the Ethanol/H$_2$O system will approach equilibrium in about 30 min, but the ethanol/Isopar-M binary usually requires one full hour. Furthermore, the liquid and vapor phases are not truly in reversible equilibrium at all times. A small amount of condensate (~ 2 ml) is continually in transit, apart from the liquid.

Typical operation of the equipment, for either vapor pressure curves or VLE diagrams, started with cleaning the system. One of the components to be used was refluxed in the system for approximately 1/2 hour, the vapor needle valve was opened and flushed, and the boiling flask was finally removed and emptied.

Next, the sample cow was installed, and approximately 20 ml of a component was placed in the boiling flask, with several boiling chips. In the additional funnel the other component was placed (for a two-component system), or the funnel was replaced by a plug (if only a pure component was required for the system). For the binary systems Ethanol/TBP and Ethanol/ISOPAR-M, the organic is best placed in the flask and Ethanol placed in the addition funnel. In these systems, water contamination will tend to accumulate at the needle valve port near the condenser, and initial contamination can, therefore, be drained away.

Equilibrium is marked by an appropriate run time, on the order of one hour, steady temperatures, a constant drip rate, and moderate, smooth boiling. Thermal equilibrium appears to precede chemical equilibrium due to the limits of accuracy of the thermometer; it is not considered a solely reliable indication of vapor/liquid equilibrium (VLE). However, for vapor pressure readings, actual chemical equilibrium is not required and the temperature may be recorded from a run at constant pressure in as little as fifteen minutes.

Liquid samples were removed with a syringe, through the septum on the three-necked flask. On the other hand, vapor samples were drained through the needle valve (Figure 5.1, "B") as condensate. One finger of the cow may be used for purging water from the condensate and for purging the glassware of previous samples which have not drained completely into the cow's other fingers. Analysis of both liquid and vapor samples was by G.C.

5.3 Discussion

Vapor pressure measurements for TBP and Isopar-M were generally quite easy to complete and appeared to be fairly

accurate. One persistent problem, however, was TBP's unfortunate tendency to decompose at higher temperatures. Therefore, the TBP vapor pressure plot has much greater scatter than the Isopar-M plot, atlthough the degree of scatter is still quite acceptable.

Heats of vaporization obtained from the data (specifically, $-\Delta Hv/R$ = slope of ln P vs. 1/T) are approximately correct, since the heats of vaporization are not constant with temperature. It is interesting to note that ethanol and Isopar-M have similar heats of vaporization (~10.5 kcal/mol) and that for TBP, ΔHv is somewhat higher ($\sim$ 13.5 kcal/mol). While Isopar-M has a higher molecular weight than ethanol, ethanol hydrogen bonds, of course, accounting for the similarity in ΔHv.

Some experimental ethanol/water vapor-liquid equilibrium data were deleted from this report, compared to the original results. It was discovered that during initial runs, equilibrium was not properly approached during the 15 minutes allowed. The results presented are esentially those of later runs, allowing 30-40 minutes. Tie lines obtained from the experimental fall almost exactly on the curves of Larkin and Pemberton, although some temperature error is evident (see Fig. 5.5 and Table 5.5).

In general, the vapor-liquid equilibrium data for the ethanol/Isopar-M binary were difficult to obtain. Water contamination was a constant annoyance. Improved techniques, such as the use of the cow, addition funnel, and septum, reduced water contamination by at least an order of magnitude (see Table 5.6). The results, as plotted on Fig. 5.6, indicate relatively easy separation, without an azeotrope. The small hump around x = 0.9 - 1.0 ethanol was once mistakenly interpreted as an azeotrope, but closer inspection of the data reveals that the ethanol is 5.10). Moderate Isopar-M concentrations suppress TBP's activity coefficient, but at high concentrations of Isopar-M, the activity coefficinet appears to increase rapidly after some "break point". Of course, the apparent increase in the coefficient could actually be the result of calculations near x = 1, as discussed for the ethanol/Isopar-M system.
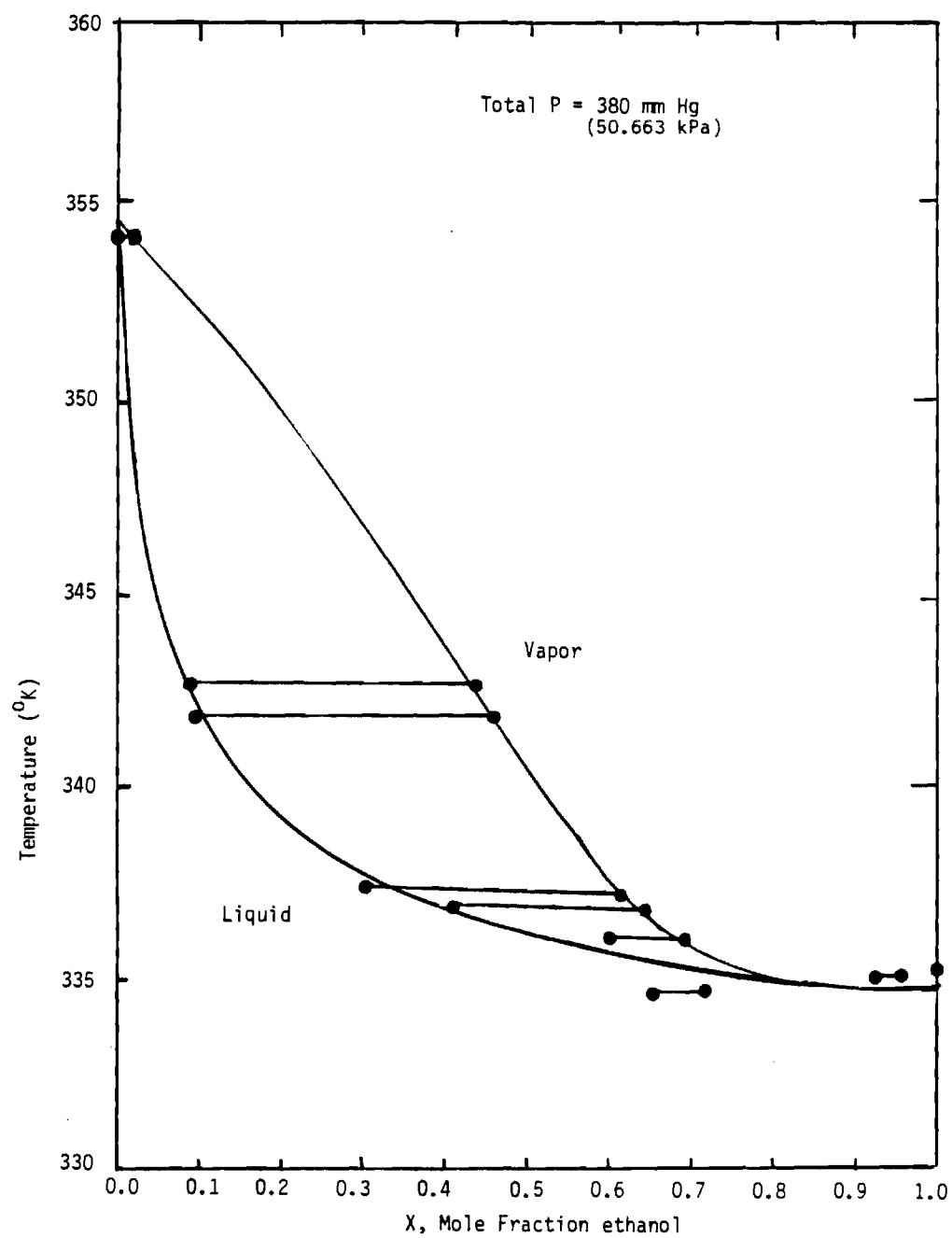
Figure 5.5   Ethanol Water Vapor/Liquid Equilibrium Diagram

Table 5.5   Experimental ethanol/water equilibrium data
at 380 mm Hg

x^a	y^b	$T(^{o}K)$
0.00	0.00	355.1 $\pm$ 1
0.0037	0.0029	354.3
0.0959	0.444	342.8
0.0976	0.47	341.9
0.3086	0.6211	337.4
0.4145	0.6674	337.2
0.6041	0.6889	336.8
0.6549	0.72	334.2
0.9410	0.960	335.7
1.000	1.000	335.6

[a] mole fraction ethanol in liquid

[b] mole fraction ethanol in vapor

Fig. 5.6   X-Y-T diagram for the ethanol/ISOPAR-M binary system.

Table 5.6 Experimental ethanol/Isopar-M
vapor/liquid equilibrium data

x^a	x^b_w	y^c	y^d_w	$T(^\circ C)$
0.00	0.00			196 ± 2
0.00219	-0-	0.2702	0.245	168
0.00624	-0-	0.5186	0.156	134
0.0059	-0-	0.2376	4.82^f	114
0.0120	-0-	0.796	7.6	93.0
0.0175	0.05	0.883	4.86	66.7
0.1836	-0-	0.970	9.8	63.0
0.4123	-0-	0.9468	2.18	61.1
0.4904	-0-	0.5984	0.77	61.9
0.5631	-0-	0.9443	3.02	60.3
0.5706	0.12	0.9540	0.34	63.5
0.6408	0.13	0.9512	1.43	60.0
0.7283	1.38	0.9798	12.74	62.0
0.8848	0.15	0.9836	0.38	63.0
0.9584	0.12	1.000	0.26	62.1
0.997	0.3	0.997	0.3	62.0

[a] Weight fraction ethanol and water in liquid phase

[b] Weight fraction water in liquid phase

[c] Weight fraction ethanol and water in vapor phase

[d] Weight fractionwater in vapor phase

[e] Improved technique is reflected by reduced water contamination in these five samples of liquid and five samples of vapor.

[f] Point deleted from plot.

See Figures VI, VII. Data oints reflecting greater than 5% H_2O contaminaton were not plotted.

Table 5.7   Experimental TBP/Isopar-M
vapor/liquid equilibrium data at 390 mm Hg

x^a	y^b	T (°C)
0.00	0.00	253.0 ± 1
	0.382	242.0
0.070	0.832^d	233.0
0.111	0.748	225.5
0.150	0.860	218.0
0.21	0.885	216.0
0.460	0.919	205.5
0.720	0.963	200.4

a   Weight fraction Isopar-M in liquid

b   Weight fraction Isopar-M in vapor

c   The sample was inadvertantly destroyed before analysis.

d   The data point is believed to be in error, and is deleted from Figs 5.8 and 5.9.
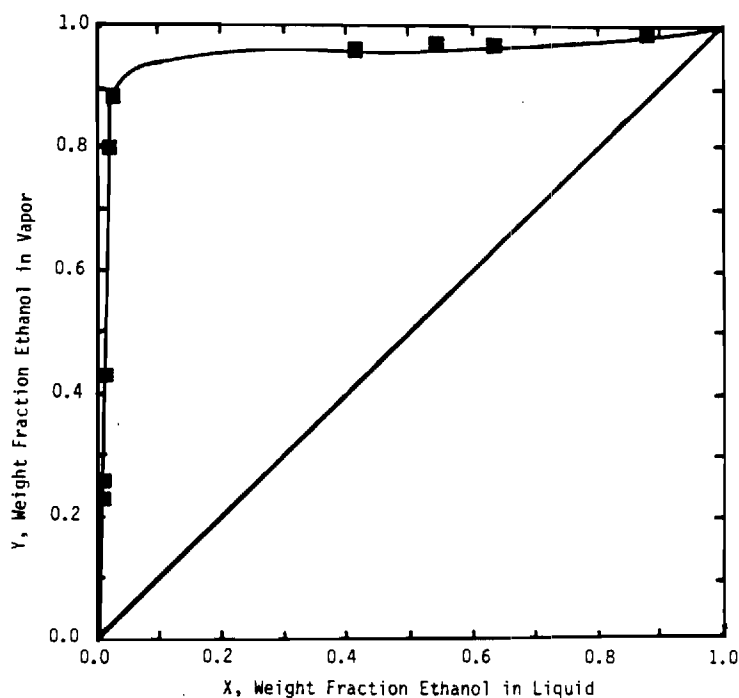
Fig. 5.7 X-Y Equilibrium diagram for the Ethanol/ISOPAR-M binary system.
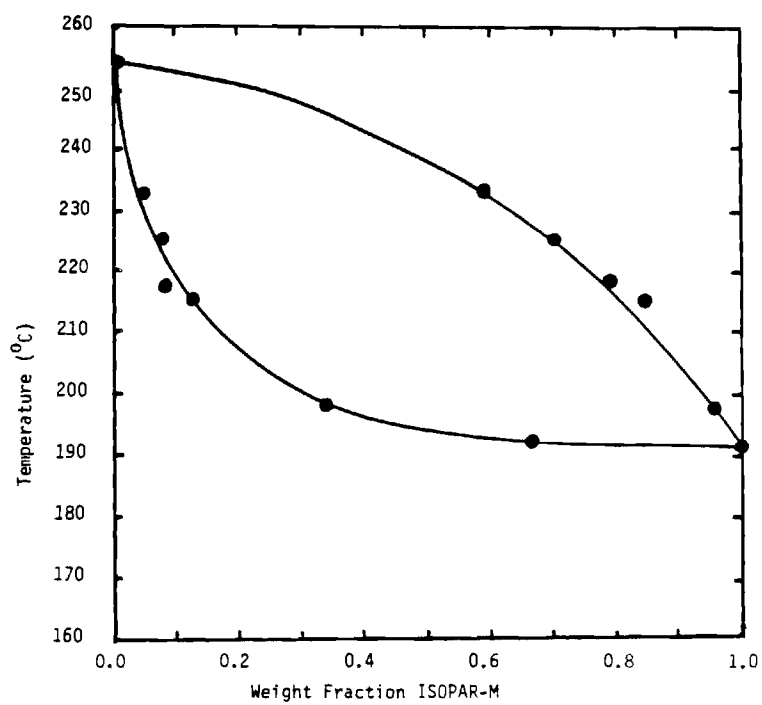
Fig. 5.8 X-Y-T diagram for the ISOPAR-M/TBP binary system.
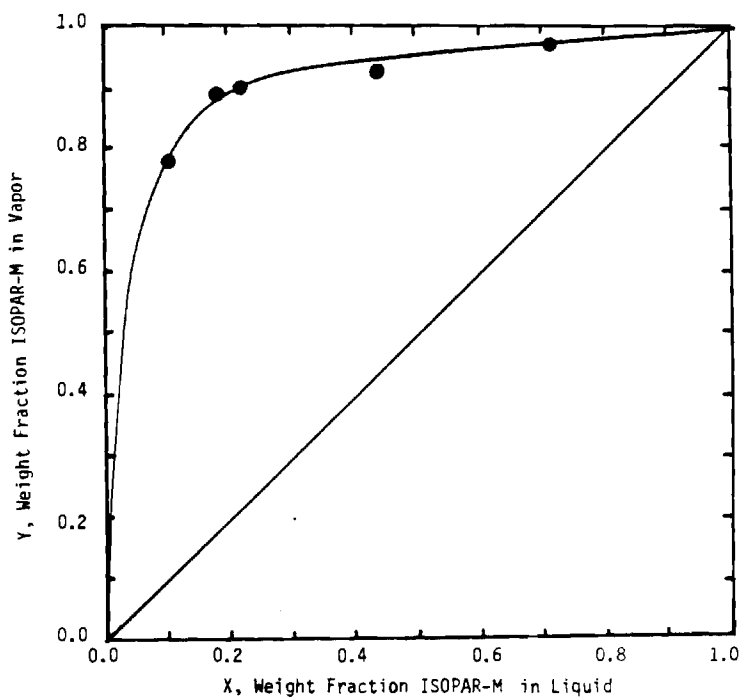
Fig. 5.9 X-Y diagram for the ISOPAR-M/TBP binary system.

Table 5.8   Activity coefficients[a] for ethanol/Isopar-M
at 390 mm Hg

vapor[c]P (mm HG)

T(°C)	x^b_1	Y_1	P_1^*	P_2^*	γ_1	γ_2^d
168	0.00219	0.2702	17,380	171.0	2.78	1.674
134	0.00624	0.5186	6,450	62.85	5.04	3.017
93	0.0120	0.796	1,517	14.68	17.1	5.51
66.7	0.0175	0.883	499	4.80	39.6	9.71
61.9	0.4904	0.9584	400	2.98	1.91	10.72
63.5	0.5706	0.9540	431	4.14	1.52	27.6
63.0	0.8848	0.9836	421	4.04	1.03	13.8

[a] Weight basis

[b] Ethanol weight fraction

[c] Pure component vapor pressures (estimated)

[d] Isopar-M activity coefficient
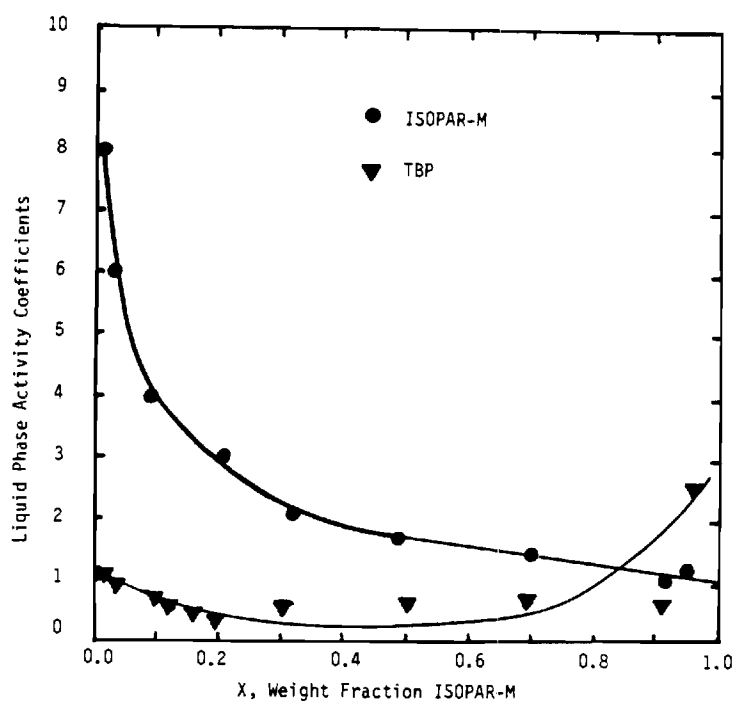
Fig. 5.10 Liquid Phase Activity Coefficients for the ISOPAR-M/TBP
binary system.

Table 5.9 Activity[a] coefficients for Isopar-M/TBP binary

T (°C)	x^b_1	y_1	Vapor[c]P (mm Hg)		γ_1	γ_2d
			p_1^*	p_2^*		
245	0.015	0.31	1017	261	7.93	1.05
240	0.032	0.455	921	230	6.02	0.95
230	0.085	0.655	750	177	4.01	0.83
225	0.11	0.74	675	154	3.89	0.74
220	0.16	0.825	606	135	3.32	0.60
215	0.21	0.89	543	117	3.04	0.46
210	0.305	0.905	485	101	2.39	0.53
205	0.48	0.925	403	87.4	1.86	0.64
200	0.69	0.96	385	75.2	1.41	0.67
199.2	0.9101	0.99	378	73.4	1.13	0.593
197.0	0.9562	0.982	358.7	68.7	1.12	2.34

[a] Weight basis

[b] Weight fraction Isopar-M in liquid

[c] Pure component vapor pressures

[d] TBP activty coefficient

Table 5.10 Vapor Pressures for a mixture of
4.38% TBP in Isopar-M

T(°C)	P (mm Hg)	γ_1 (est.)	γ_2 (est.)
121.9	43.0	1.12	*
146.0	95.2	1.12	*
171.1	199.5	1.12	3.67
185.5	294.6	1.12	2.35
197.0	391.4	1.12	2.34

* γ_2 was difficult to estimate in these instances

because of small errors in vapor pressure

measurements (P → p_2^*)

A vapor pressure table (Table 5.10) of a mixture of appreciately 5% TBP in Isopar-M was constructed to further investigate the TBP activty coefficient in weak solution (x → 1). For one point in the vapor pressure table (p = 391.4 mm Hg), liquid and vapor compositions were used to obtain an activty coefficiently for Isopar-M. The coefficient turned out to be 1.12. Using this coefficient, the TBP activty coefficienit was also determined for some of the other points along the mixture's vapor pressure curve. THe results were in reasonable agreement in that γ_2, the TBP activty coefficinet, is approximately 3 for a 5% TPB solution. To remove all doubt about the TBP activity coefficient, the usual VLE experiments should be run several more times.

5.4 Parameter Estimates for VLE Models

5.4.1 Antoin's Equation

The experimental data of vapor pressure are used to fit Antoin's equation parameters using nonlinear least square algorithm (NONLS2)

$$\ln P^0 = A + \frac{b}{C + T} \qquad (5.1)$$

where

P^0:   vapor pressure of pure component (Psi)

T: Temperature (^0F)

The objective function is to minimize the sum of the squares of the observed vapor pressure less the calculated values

$$\left(\Sigma \; (P^0_{os}{}^2 - P^0_{calc.}{}^2) \right)_{min}$$

The estimated parameters are tabulated for Ethanol, and Isopar M in table (5.11) in comparison with values obtained from reference (2).

Table 5.11.   Antoin's Vapor Pressure Parameters

Parameter	Ethanol	ISOPAR M
A	14.893[a] 14.264[b]	13.157[a] -----
B	-6170.91[a] -6162.36[b]	9524.86[a] -----
C	361.62[a] 359.38[b]	462.7769

[a]   This work

[b]   Values tabulated in Appendix A by Henley and Seader (2)

5.4.2. UNIQUAC Parameters

UNIQUAC Model proposed the following forms of the molar excess Gibbs energy

$$g^E = g^E \text{ (combinatorial)} + g^E \text{ (residual)}$$

For the binary mixtures:

$$\frac{g^E(\text{combinatorial})}{RT} = x_1 \ln \frac{\phi_1}{x_1} + x_2 \ln \frac{\phi_2}{x_2}$$

$$+ \left(\frac{Z}{2}\right) \left(q_1 x_1 \ln \frac{\phi_1}{\phi_1} + q_2 x_2 \ln \frac{\phi_2}{\phi_2}\right] \tag{5.2}$$

$$\frac{g^E \text{ (residual)}}{RT} = -q_1^1 x_1 \ln (\phi_1^1 + \phi_2^1 \Gamma_{21})$$

$$-q_2^1 x_2 \ln (\phi_2^1 + \phi_1^1 \Gamma_{12}) \tag{5.3}$$

where the coordination number Z is set equal to 10 and segment fraction, ϕ, area fraction, θ and θ^1, are given by

$$\phi_i = \frac{r_i x_i}{\Sigma r_i x_i} \tag{5.4}$$

$$\phi_i = \frac{q_i x_i}{\Sigma q_i x_i} \tag{5.5}$$

$$\phi_i^1 = \frac{q_i^1 x_i}{\Sigma q_i^1 x_i} \tag{5.6}$$

For each binary combination in a multicomponent mixture, there are two adjustable parameters, Γ_{12} and Γ_{21}. These in turn are given in terms of characteristic energies ΔU_{12} and ΔU_{21} by

$$\Gamma_{12} = \exp\left(-\frac{\Delta U_{12}}{RT}\right) = \exp\left(-\frac{q_{12}}{T}\right) \qquad (5.7)$$

$$\Gamma_{21} = \exp\left(-\frac{\Delta U_{21}}{RT}\right) = \exp\left(-\frac{a_{21}}{T}\right) \qquad (5.8)$$

The interaction parameters a_{12} and a_{21} are found to be a strong function of temperature

$$a_{12} = x_{12} + \frac{\beta_{12}}{T} \qquad (5.9)$$

$$a_{21} = x_{21} + \frac{\beta_{21}}{T} \qquad (5.10)$$

The experimental isobaric data for the ethanol, water and ethanol/Isopar-M binaries were used to fit the UNIQUAC interaction parameters α_{12}, β_{12}, and β_{21}. A non-linear least square routine to minimize the objective function

$$\Sigma\ (y^2_{1_{calc}} - y^2_{1_{obs}}) + \Sigma\ (y^2_{2_{calc}} - y^2_{2_{obs}})$$

The estimated values of the parameters are summarized in Table 5.12.

Table 5.12. Estimated UNIQUAC Interaction Parameters

Components	Temp $^{\circ}$K	α_{12}	α_{21}	β_{12}	β_{21}
Ethanol Water	335.0–354.3	137.47	-5.87×10^3	-6.833×10^4	21.38×10^5
Isopar M	335–469	-999.7 -499.7	502.42	29.1×10^4	21.67×10^4

The predicted equilibrium composition values for the binaries Ethanol/Water and Ethanol/Isopar M are plotted in Figures 5-11, and 5-12 and compared with the experimental values.
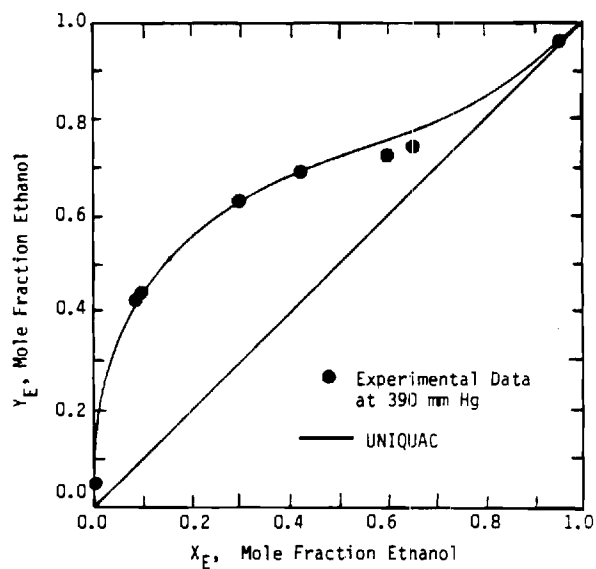
Figure 5.11 Binary VLE Estimation for Ethanol Water Using UNIQUAC
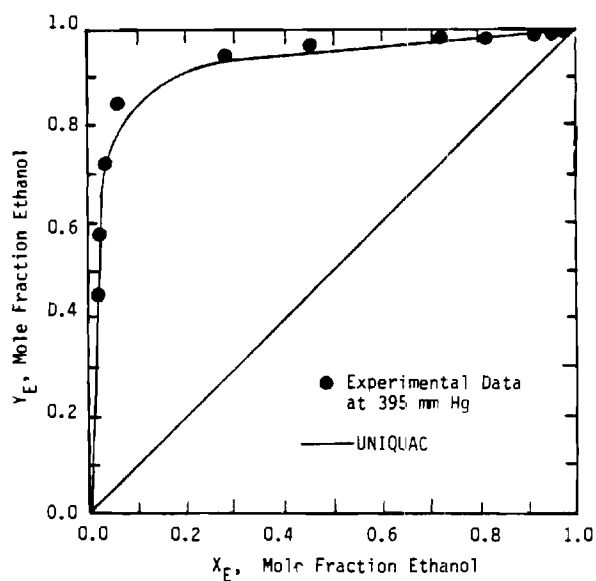
Figure 5.12 Binary VLE for Ethanol ISOPAR-M System Using UNIQUAC

The ethanol/water/VLE system has been widely studied by different investigators since it has a special importance for the ethanol dehydration. Furthermore, there is a good agreement among those who studied that system about the efficiency of UNIQUAC Model for predicting the equilibrium compositions for ethanol and water. Table 5.13 compares the values of the characteristic energies a_{ij} which were obtained by different investigators.

Table 5.13. UNIQUAC Characteristic Energy α_{ij} for Ethanol-Water System

Components					Data
1	2	Temp ^{O}K	α_{12}	α_{21}	References
Water	Ethanol	343	437.92	-81.94	MERTL, 1972[a]
	Ethanol	313	284.81	-27.36	MERTL, 1972
	Ethanol	351-372	387.38	-71.06	RIEDER, 1969
	Ethanol	333	561.82	-129.66	UDOVENKO, 1952
	Ethanol	328	380.68	-66.56	MERTL, 1972
	Ethanol	335.6-354.3	238.57	-57.76	W. TAWFIK[b],1984

Values Tabulated in Ref. (3), Appendix C.

5.5 Conclusions

The results of this experimental study seem quite encouraging for the feasibility of distillation in a scheme of ethanol recovery by solvent extraction:

1. No azeotropes were confirmed or found, except that of H_2O and ethanol.

2. TBP vapor pressure suppression hints at being promising. While TBP vapor pressure is already quite low at the temperatures which will probably be encountered, the material is expensive.

3. The latent heat of vaporization of Isopar-M is not exceptionally high. Isopar-M is expected to constitute most of the feed to the distillation, with lesser amounts of TBP, ethanol, and H_2O.

4. Separations were generally "easy", rather than "hard" (i.e., vastly different volatilities were typical among the various components).

If cooling water is available at 85°F, and an approach temperature for the condenser is assumed of 10°F, then distillation will probably proceed at approximately 125 mm Hg. This pressure corresponds to the ethanol saturation pressure at 95°F since the ethanol/Isopar-M system VLE has an essentially flat temperature profile over nearly the entire range.

At this juncture, a great deal of useful information can be obtained based only on the results in this report. In particular, various binary VLE diagrams can be predicted for any system pressure of choice, using activity coefficients already found. If the ethanol/TBP VLE system is measured in the future, every binary system of H_2O ethanol, TBP, and Isopar M will be complete. Equations to correlate the activity coefficients (Wilson, Van Larr, etc.) may be very useful in the distillation design, based on these binary systems.

5.6 Acknowledgments

Chris Sarzen, Tim Phan, and Steve Cox contributed in many ways too numerous to list, and deserve special acknowledgment.

5.7 References

1. J. A. Larkin and R. C. Pemberton, Thermodynamic Properties of Mixtures of Water and Ethanol, Division of Chemical Standards, England (January 1976).

2. E. J. Henley and J. D. Seader, Equilibrium Stage Separation Operations in Chemical Engineering, Wiley (1981).

3. J. Prausnitz et al., Computer Calculations for Multicomponent Vapor-Liquid and Liquid-Liquid Equilibria, Prentice-Hall.

CHAPTER 6

LIQUID/LIQUID EQUILIBRIA FOR SELECTED SOLVENT SYSTEMS

(W. Y. Tawfik)

6.1 Introduction

Traditionally, the problem of describing commercial extraction column performance has been one of defining the equilibrium curve and the operating line. A two model description of the equilibrium curve in the extraction system is proposed here. The first model predicts the distribution coefficients for the solute between the two phases in equilibrium. The same model can also predict the solvents selectivity for extracting the solute from the diluent. The second model utilizes the UNIQUAC equation to predict the mutual solubility (equilibrium) curve for the extraction system studied.

6.2 Past Research

Initial studies (1, 2) were concerned with gathering equilibrium data ethanol-water-organic solvent systems using different techniques such as tie-line measurements, solubility curve titrations, batch equibration and solvent stripping tests. The data obtained by these experiments classified the organic solvents into two broad categories: either drying solvents, or recovery solvents. Drying solvents have high selectivities for extracting ethanol from water, but their ethanol distribution coefficients are relatively low. Recovery solvents have higher ethanol distribution coefficients, but their selectivities for ethanol are much lower.

In this work, the effect of temperature on the equilibrium was examined using some of the systems which were studied earlier (21 - 2) at room temperature. These temperature studies resulted from a need to improve the equilibrium properties of some solvents by increasing the loading of the drying solvents and the selectivities of the recovery solvents. Such improvement was attempted by dissolving solids in the aqueous phase. Dextrose was chosen as the dissolved solid since it was insoluble in the organic solvent and present in the fermented liquor.

6.3 Experimental Techniques

Concentration measurements were carried out by gas chromatography. The GC used was a Hewlett Packard type 5710A with a 6 foot, Poropak Q 80/100 mesh packed column. Instrument grade helium was used as the carrier gas. The

gas chromatograph was operated at an oven temperature of 165°C and an injection port temperature of 250°C with a thermal conductivity detector at 250°C. The peaks were integrated using a Hewlett Packard 3390A peak integrator.

The output from the integrator was in the form of area percentages which were converted to weight percentages by calibration curves. Propanol spikes were used when all the components were not detectable to calculate weight percentages. The percent dissolved solids was determined by difference.

The calculation of the experimental distribution coefficients is described in detail by W. Y. Tawfik (16).

6.4 Experimental Results

The major effects of ethanol and dextrose concentrations, and temperatures upon the liquid/liquid equilibria of water and ethanol were evaluated through the use of factorial designs. These equilibration studies led to a data base which can be analyzed in several ways. Two alternative evaluation techniques are discussed below.

6.4.1 Distribution Coefficient Models

Simultaneous tests were made for the effect of temperature, the percentage of modifier, and the percentage of the dextrose on the distribution coefficients and the selectivities. The experimental results suggested an increase in the activity of the water in the aqueous phase occurs due to the presence of the dextrose. This effect was realized for the solvents, TBP in Isopar M and this increase resulted in an increase in ethanol distribution coefficients. However, no significant increase in the selectivity was noticed. On the other hand, the dextrose effect was insignificant for some of the dry solvents such as the methyl ester comparing to the temperature.

The effect of dextrose in the distribution coefficient is illustrated in Figs. 6.1-6.3 for the TBP/Isopar M solvent at different temperature and initial ethanol concentrations. The experimental values of the ethanol and water distribution coefficients are summarized in Tables 6.1-6.3. For the solvents TDOH/Isopar M, TBP/Isopar M, and Methyl Ester CE-1218, respectively. These values for ethanol exhibits a minimum behavior in the neighborhood of infinite dilution.

The basic model for the distribution coefficients of ethanol and water is proposed in the following form:

$$\ln D_i = f(X_e, X_D, \phi_m, \frac{1}{T}) \qquad (6.1)$$

For each solvent the non linear least square technique (NONLS2) (8) was used to fit the parameters of the models. The check on the statistical significance of the non linear model was the measure of omitting the variables interactions. The general form of the models is found to be:

$$\ln De = a_o + a_1 X_e^2 + a_2 X_e + a_3 X_D + a_4 X_D^2 + a_5 \phi_m + \frac{a_6}{RT} \qquad (6.2)$$

$$\ln D_w = a_o^1 + a_1^1 X_e + a_2^1 X_D + a_3^1 \phi_m + \frac{a_4^1}{RT} \qquad (6.3)$$

The parameters for equations 6.2 and 6.3 are summarized in Tables 6.4 and 6.5. For the solvents TDOH/Isopar M, TBP/Isopar, and Methyl ester, respectively. The variation of the parameter values can be explained by proposing different extraction mechanisms for ethanol and water, and the formation of different complexes. Although the model does not predict the plait point equilibrium composition, it can be used with reasonable accuracy in the practical range of extraction (low ethanol concentration).

Enough time was given to the two phases to achieve the equilbrium and to diminish any kinetic effect. However, the two phases compositions on a solvent free basis showed a competitive extraction over a range of time less than that required for equilibrium.

The weight fraction of ethanol and water was plotted versus the residence time (Fig 6.4) for the methyl Ester system. The calculated values of the distribution coefficients for ethanol and water are tabulated versus the observed values in Tables 6.6 through 6.11.
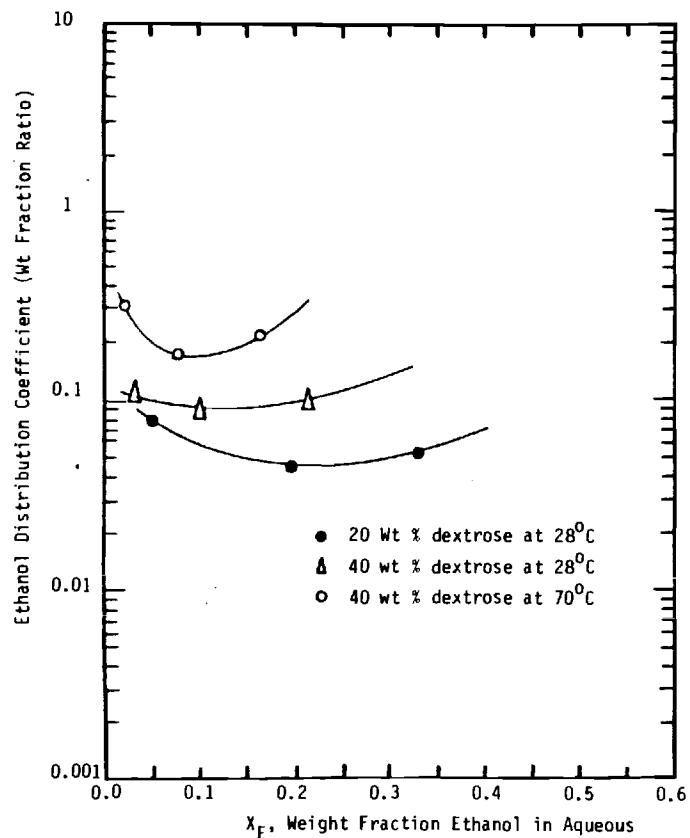
Fig. 6.1 The effect of dextrose on the ethanol distribution coefficient for the solvent 5 vol% TBP in ISOPAR-M
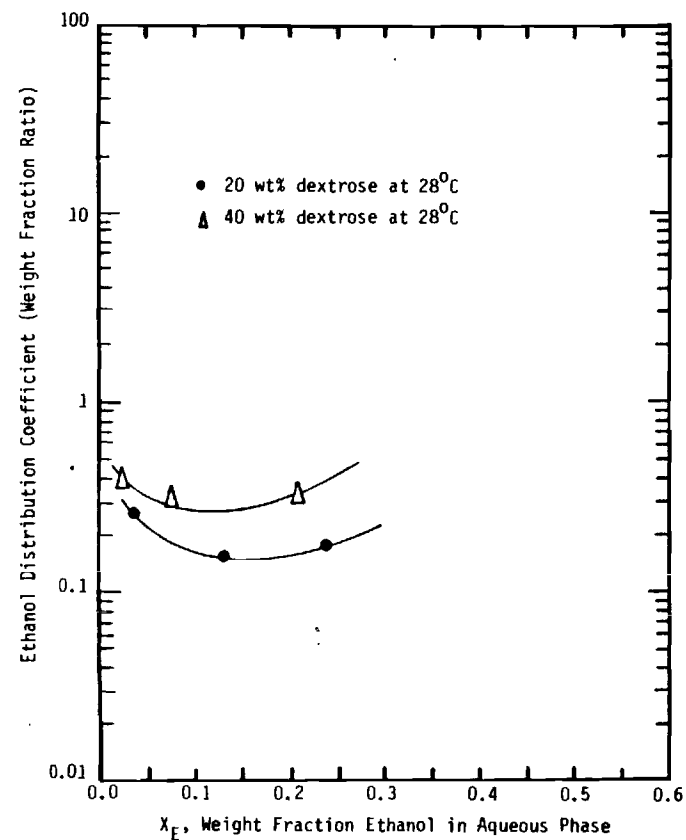
Fig. 6.2 The effect of dextrose on the ethanol distribution coefficient for ethanol with the solvent 20 vol% TBP in ISOPAR-M

61
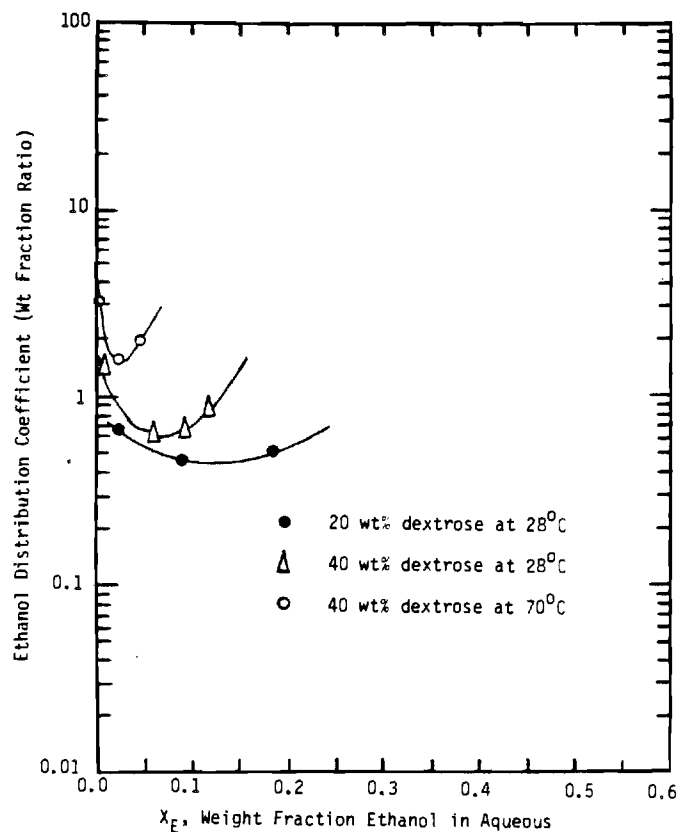
Fig. 6.3 The effect of dextrose on the ethanol distribution coefficient for the solvent 50 vol% TBP in ISOPAR-M
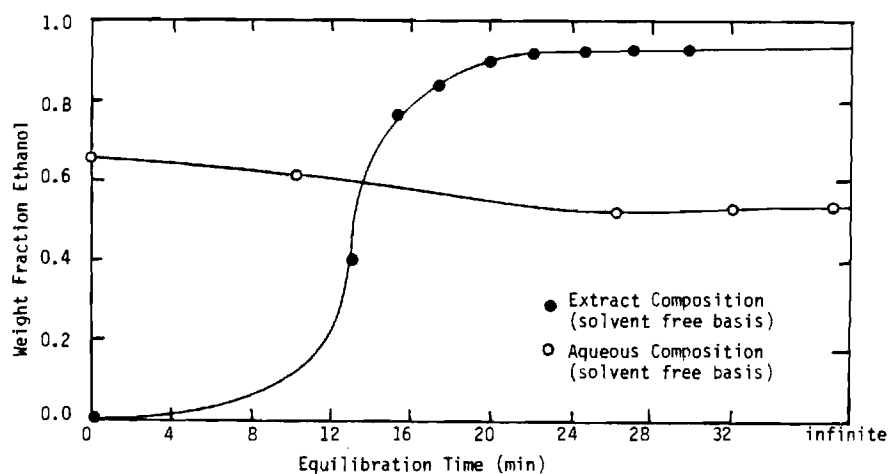
Fig. 6.4 The apparent change in extract composition (solvent free basis) with equilibration time. The ternary system consists of ethanol-water- and the methyl ester, CE-1218.

Table 6.1

The Experimental values of ethanol and water
distribution coefficients for TDOH/Isopar M
system in presence of dextrose

$D_e{}^a$	$D_w{}^a$	$X_e{}^b$	$X_D{}^b$	$\phi_T{}^c$	$100/T$ $(^oK^{-1})$
0.089	0.0016	0.072	0.205	0.1	0.342
0.061	0.0018	0.198	0.215	0.1	0.342
0.082	0.0034	0.354	0.212	0.1	0.342
0.781	0.0174	0.031	0.217	0.4	0.342
0.567	0.0183	0.098	0.234	0.4	0.342
0.648	0.0312	0.217	0.231	0.4	0.342
0.270	0.006	0.029	0.201	0.2	0.332
0.180	0.0052	0.105	0.226	0.2	0.332
0.210	0.0097	0.218	0.261	0.2	0.332
0.208	0.0029	0.032	0.214	0.1	0.291
0.21	0.0039	0.105	0.245	0.1	0.291
0.32	0.0058	0.195	0.240	0.1	0.291
0.378	0.0019	0.0091	0.491	0.1	0.291
0.188	0.0056	0.053	0.424	0.1	0.291
0.321	0.0088	0.146	0.474	0.1	0.291
1.98	0.031	0.003	0.225	0.4	0.291
0.97	0.058	0.032	0.244	0.4	0.291
1.54	0.062	0.141	0.235	0.4	0.291

a   Weight fraction ratio

b   Weight fraction

c   Volume fraction before mixing with diluent

Table 6.2

The experimental values of ethanol and water
distribution coefficients for TBP/Isopar M
system in presence of dextrose

D_e	D_w	X_e	X_D	ϕ_T	$100/T$
0.0791	0.0018	0.051	0.195	0.05	0.332
0.0442	0.0016	0.194	0.182	0.05	0.332
0.0524	0.0039	0.330	0.21	0.05	0.332
0.103	0.0023	0.0386	0.357	0.05	0.332
0.089	0.0031	0.1110	0.411	0.05	0.332
0.0982	0.0044	0.2153	0.396	0.05	0.332
0.1079	0.0048	0.206	0.421	0.05	0.332
0.175	0.0059	0.079	0.442	0.05	0.292
0.210	0.0022	0.158	0.474	0.05	0.292
0.314	0.0013	0.022	0.441	0.05	0.292
0.685	0.0202	0.0196	0.216	0.5	0.332
0.470	0.0224	0.085	0.225	0.5	0.332
0.505	0.0351	0.178	0.276	0.5	0.332
1.591	0.0236	0.0054	0.400	0.5	0.332
0.52	0.021	0.059	0.449	0.5	0.332
0.923	0.0409	0.1011	0.424	0.5	0.332
0.665	0.029	0.0932	0.503	0.5	0.332
0.264	0.0059	0.0329	0.203	0.2	0.332
0.153	0.00522	0.127	0.202	0.2	0.332
0.179	0.0102	0.236	0.245	0.2	0.332
0.374	0.00644	0.024	0.366	0.2	0.332
0.290	0.0067	0.0766	0.4301	0.2	0.332
0.251	0.0096	0.205	0.232	0.2	0.3332
0.291	0.0103	0.128	0.473	0.2	0.332
3.23	0.0222	0.0021	0.478	0.5	0.292
1.45	0.028	0.0168	0.519	0.5	0.292
1.868	0.039	0.0289	0.604	0.5	0.292

Table 6.3

The experimental values of ethanol and water
distribution coefficents for Methyl ester
system in presence of dextrose

D_e	D_w	X_e	X_D	$100/T$
0.1055	0.0024	0.07	0.0	0.3413
0.1075	0.0025	0.117	0.0	0.3413
0.2223	0.0034	0.147	0.0	0.3413
0.1663	0.0037	0.278	0.0	0.3413
0.1416	0.0049	0.30	0.0	0.3413
0.145	0.0023	0.062	0.0519	0.3413
0.164	0.0029	0.099	0.0536	0.3413
0,.2358	0.0041	0.1365	0.0593	0.3413
0.1944	0.0049	0.2119	0.063	0.3413
0.1345	0.0049	0.279	0.062	0.3413
0.1597	0.002	0.0828	0.2118	0.3413
0.175	0.0033	0.1401	0.2215	0.3413
0.169	0.0047	0.1997	0.233	0.3413
0.1001	0.0048	0.2681	0.233	0.3413
0.3118	0.00145	0.045	0.0	0.2915
0.5088	0.0023	0.087	0.0	0.2915
0.5529	0.0035	0.133	0.0	0.2915
0.1825	0.004	0.225	0.0	0.2915
0.339	0.0029	0.043	0.0534	0.2915
0.2128	0.0029	0.089	0.054	0.2915
0.273	0.0037	0.126	0.0667	0.2915
0.34	0.0038	0.154	0.0667	0.2915
0.248	0.0039	0.209	0.0669	0.2915
0.2754	0.0037	0.065	0.2164	0.2915
0.4045	0.0045	0.0919	0.2344	0.2915
0.265	0.0047	0.1629	0.2422	0.2915
0.677	0.0059	0.1035	0.276	0.2915

Table 6.4

The Parameter Values of Eqn. 6.2

Solvent Parameter	TDOH/Isopar M	TBP/Isopar M	Methyl Ester 1218
a_0	2.22	1.602	2.943
a_1	2.5	58.47	-34.137
a_2	-1.03	-19.29	8.144
a_3	1.2	0.985	-9.235
a_4	0.0	0.0	37.17
a_5	0.4	3.78	0.0
a_6	3198.4	1994.9	2863.9
Standard Error	0.282	0.248	0.08

Table 6.5

The parameters values of equation 6.3

Solvent Parameter	TDOH/Isopar M	TBP/Isopar M	Methyl Ester 1218
a_{0}^{1}	-1.28	-5.81	-5.131
a_{1}^{1}	3.53	3.88	2.78
a_{2}^{1}	-0.495	1.23	1.39
a_{3}^{1}	8.66	5.06	0.0
a_{4}^{1}	-3631.3	-652.3	651.42
Standard Error	0.0029	0.0034	0.0006

Table 6.6

The values of ethanol distribution
coefficient calculated from Eqn (2)
versus the observed values for
TDOH/Isopar M system

	$D_{e(OBS)}$	$D_{e(CALC)}$	O-C
1	.8900000D-01	.8374644D-01	.5253558D-02
2	.6100000D-01	.8103167D-01	-.2003167D-01
3	.8200000D-01	.8534347D-01	-.3343475D-02
4	.7810000D+00	.6067442D+00	.1742558D+00
5	.5670000D+00	.5902026D+00	-.2320258D-01
6	.6480000D+00	.5715123D+00	.7648770D-01
7	.2700000D+00	.1930645D+00	.7693551D-01
8	.1800000D+00	.1885370D+00	-.8536988D-02
9	.2100000D+00	.1915533D+00	.1844669D-01
10	.2080000D+00	.1989413D+00	.9058691D-02
11	.2100000D+00	.1961576D+00	.1384242D-01
12	.3200000D+00	.1901857D+00	.1298143D+00
13	.3780000D+00	.2807494D+00	.1725063D-01
14	.1880000D+00	.2498364D+00	-.6183643D-01
15	.3210000D+00	.2520449D+00	.6895519D-01
16	.1980000D+01	.1433432D+01	.5465681D+00
17	.9900000D+00	.1425948D+01	-.4359477D+00
18	.1540000D+01	.1322016D+01	.2179838D+00

Table 6.7

The values of water distribution coefficients
calculated from Eqn (3) versus theobserved
values for TDOH/Isopar M system

	$D_{w(OBS)}$	$D_{w(CALC)}$	O-C
1	.1600000D-02	.1428948D-02	.170522D-03
2	.1800000D-02	.2218059D-02	-.4180589D-03
3	.3400000D-02	.3852170D-02	-.4521695D-03
4	.1740000D-01	.1651186D-01	.8881445D-03
5	.1830000D-01	.2074065D-01	-.2440654D-02
6	.3120000D-01	.3161173D-01	-.4117321D-03
7	.6000000D-02	.3515150D-02	.2484850D-02
8	.5200000D-02	.4539860D-02	.6601398D-03
9	.9700000D-02	.6648071D-02	.3051929D-02
10	.2900000D-02	.3157034D-02	-.2570344D-03
11	.3900000D-02	.4022434D-02	-.1224341D-03
12	.5800000D-02	.5539870D-02	.2601305D-03
13	.1900000D-02	.2538496D-02	-.6384963D-03
14	.5600000D-02	.3063905D-02	.2536095D-02
15	.8800000D-02	.4150005D-02	.4649995D-02
16	.3100000D-01	.3807723D-01	-.7077226D-02
17	.5800000D-01	.4178519D-01	.1621481D-01
18	.6200000D-01	.6166139D-01	.3386132D-03

TABLE 6.8

The values of ethanol distribution coefficients
calculated from Eqn (2) versus the observant
values for TBP/Isopar M system

	D_e(OBS)	D_e(CALC)	O-C
1	.7910000D-01	.1115767D+00	-.3247667D-01
2	.4420000D-01	.5420410D-01	-.1000410D-01
3	.5240000D-01	.1557777D+00	-.2086701D+00
4	.1030000D+00	.7660509D-01	-.5277767D-01
5	.8900000D-01	.7660509D-01	.1239491D-01
6	.9820000D-01	.7389356D-01	.2430644D-01
7	.1079000D+00	.7205192D-01	.3584808D-01
8	.1750000D+00	.1535162D+00	.2148376D-01
9	.2100000D+00	.1031921D+00	.1068079D-01
10	.3140000D+00	.3288099D+00	-.1480993D-01
11	.6850000D+00	.1006794D+01	-.3217937D+00
12	.4700000D+00	.4292791D+00	.4072038D-01
13	.5050000D+00	.3138854D+00	.1911146D+00
14	.1591000D+01	.1563599D+01	.2740065D-01
15	.5700000D+00	.7099582D+00	-.1399582D+00
16	.9230000D+00	.4561351D+00	.4668649D+00
17	.6650000D+00	.5248899D+00	.1401101D+00
18	.2640000D+00	.2573905D+00	.6609459D-02
19	.1530000D+00	.1009544D+00	.5204556D-01
20	.1790000D+00	.1301412D+00	.4885884D-01
21	.3740000D+00	.3483309D+00	.2566910D-01
22	.2900000D+00	.1837048D+00	.1062952D+00
23	.2510000D+00	.1050290D+00	.1459710D+00
24	.2910000D+00	.1312599D+00	.1597401D+00
25	.3230000D+01	.2672715D+01	.5572852D+00
26	.1450000D+01	.2130189D+01	-.6801894D+00
27	.1868000D+01	.1894382D+01	-.2638235D-01

TABLE 6.9

The values of water distribution coefficient
calculated from Eqn (3) versus the observed
values for TBP/Isopar M system

	D_w(OBS)	D_w(CALC)	O-C
1	.1600000D-02	.2021335D-02	-.2213353D-03
2	.1600000D-02	.3466210D-02	-.1666210D-02
3	.3900000D-02	.6083911D-02	-.2183911D-02
4	.280000DD-02	.2351390D-02	0.5138985D-04
5	.3100000D-02	.3328829D-02	-.2288291D-03
6	.4400000D-02	.4900335D-02	-.5003349D-03
7	.4800000D-02	.4873625D-02	-.7362459D-04
8	.5900000D-02	.3483901D-02	.2416099D-02
9	.2200000D-02	.4924965D-02	-.2724965D-02
10	.1300000D-02	.2788708D-02	-.1488703D-02
11	.2020000D-01	.1792616D-01	.2273835D-02
12	.2240000D-01	.2336651D-01	-.9665061D-3
13	.3510000D-01	.3570247D-01	-.6024747D-03
14	.2360000D-01	.2143412D001	.2165880D-02
15	.2100000D-01	.2782830D-01	-.6828299D-02
16	.4090000D-01	.3177776D-01	.9122244D-02
17	.2900000D-01	.3396489D-01	-.4964692D-02
18	.5900000D-02	.4066766D-02	.1833234D-02
19	.5220000D-02	.5853448D-02	-.6334482D-03
20	.10200000D-01	.9423743D-02	.7762572D-03
21	.6440000D-02	.4301453D-02	.1638547D-02
22	.6700000D-02	.6368089D-04	.3319112D-02
23	.9600000D-02	.8222303D-02	.2997170D-02
24	.1030000D-01	.8202830D-02	.1377697D-02
25	.2200000D-01	.2637538D-01	-.4375379D-02
26	.2800000D-01	.2937019D-01	-.1370192D-02
27	.3900000D-01	.3417831D-01	.4821687D-02

TABLE 6.10

The values of Ethanol distribution coefficients
calculated from Eqn (2) versus the observed
values for Methyl Ester System

	$D_{e(OBS)}$	$D_{w(CALC)}$	O-C
1	.1-55000D+00	.1633723D+00	-.6257232d-01
2	.1075000D+00	.1802812D+00	-.7278118D-01
3	.2223000D+00	.1751999D+00	.4710006D-01
4	.1685000D+00	.7997983D-01	.8652012D-01
5	.1416000D+00	.6310899D-01	.7849101D-01
6	.1450000D+00	.1633502D+00	-.2335021D-01
7	.1640000D+00	.1835715D+00	-.1957147D-01
8	.2656000D+00	.1836004D+00	.5219959D-01
9	.1944000D+00	.1403124D+00	.5408759D-01
10	.1345000D+00	.8173440D-01	.5276560D-01
11	.1597000D+00	.1938624D+00	-.3416239D-01
12	.1750000D+00	.1985692D+00	-.2356923D-01
13	.1690005D+00	.1638606D+00	.2139415D-02
14	.1001000D+00	.9929204D-01	.6079569D-03
15	.3118000D+00	.3149435D+00	-.3146510D-02
16	.5065000D+00	.3595511D+00	.1469469D+00
17	.5529000D+00	.3659124D+00	.1659676D+00
18	.1625000D+00	.2564949D+00	-.7399467D-01
19	.3390000D+00	.3712957D+00	.1623425D-01
20	.2120000D+00	.3718937D+00	-.1564937D+00
21	.2730000D+00	.3318103D+00	-.1066103D+00
22	.3400000D+00	.3665863D+00	-.2658678D-01
23	.2430000D+00	.2934511D 00	-.4545107D-01
24	.2754000D+00	.3801879D+00	-.1047679D+00
25	.4045000D+00	.4092501D+00	-.4750032D-02
26	.2650000D+00	.3919307D+03	-.1269307D+00
27	.6770000D+00	.4238973D+03	.2531022D+00

TABLE 6.11

The values of water distribution coefficient
calculated from Eqn (3) using the observed
values for Methyl Ester System

	$D_{w(OBS)}$	$D_{w(CALC)}$	O-C
1	.2400000D-02	.2375970D-02	.2403033D-04
2	.2500000D-02	.2715343D-02	-.2053479D-03
3	.3400000D-02	.2939032D-02	.4609175D-03
4	.3700000D-02	.4220484D-02	-.520487D-03
6	.2300000D-02	.4414912D-02	.4150062D-03
6	.2300000D-02	.2428835D-02	-.1286358D-03
7	.4800000D--2	.8009799D-02	.1992254D-03
9	.4800000D-02	.8721161D-02	.1178639D-02
10	.4900000D-02	.4474180D-02	.4256200d-03
11	.2000000D-02	.3228473D-02	-.1228473D-02
12	.3300000D-02	.3850532D-02	-.5565317D-03
13	.4700000d-02	.4640014D-02	.5998579D-04
14	.4800000d-02	.5604972D-02	-.6049719D-03
15	.1400000D-02	.2606157d-02	-.1156157D-02
16	.2300000D-02	.2925744D-02	-.6257435D-03
17	.3500000D-02	.3303233D-02	.1737171D-03
18	.4000000D-02	.4284812D-02	-.2846193D-03
19	.2900000D-02	.2715764D-02	.1842362D-03
20	.2900000D-02	.8085593D-02	-.1855929D-03
21	.3700000D-02	.8453333D-02	.2365119D-03
22	.0900000D-02	.3741886D-02	.5611308D-04
23	.3900000D-02	.4356760D-02	-.45675970D-03
24	.3700000D-02	.3643007D-02	.5699324D-04
25	.4500000D-02	.4060010D-02	.4399902D-03
26	.4700000D-02	.5015754D-02	-.3157543D-03
27	.5900000D-02	.4554551D-06	.1335439D-02

6.4.2 Prediction of the Mutual Solubility Curve Using the UNIQUAC Model

Since all the liquid liquid systems which are included in this work contain water/ethanol mixtures in addition to different organic solvents, there are very few models available which can predict the equilibrium composition with an acceptable range of accuracy. In general, a good model should describe the nonideality caused by the presence of the polar components (eg. ethanol and water) and their degree of association. The liquid phase activty coefficient for component i directly related to the molar excess Gibbs free energy g_E by:

$$RT \ln \gamma_i = \left(\frac{\partial gE}{\partial x_i}\right)_{T,P,n_j \neq i} \tag{6.4}$$

The molar excess Gibbs free energy gE was defined in UNIQUAC Model of Abrams (1975) as slightly modified by Anderson (1978)

$$gE = gE \text{ (combinatorial)} + gE \text{ (residual)}$$

For a liquid mixture

$$\frac{gE \text{ (combinatorial)}}{RT} = \sum_i x_i \ln \frac{\phi_i}{x_i} + \frac{z}{2} \sum_i q_i x_i \ln \frac{\theta_i}{\theta_i} \tag{6.5}$$

$$\frac{gE(\text{residual})}{RT} = - \sum_i q_i^1 x_i \ln \left(\sum_j (\theta_j^1 \Gamma_{ji}) \right) \tag{6.6}$$

where

$$\phi_i = \frac{r_i x_i}{\sum_j r_j x_j}$$

$$\phi_i = \frac{q_i x_i}{\sum_j q_j x_j}$$

$$\phi_i^l = \frac{q_i^l x_i}{\Sigma q_j^l x_j}$$

For any component i, the UNIQUAC activity coefficient is given by:

$$\ln \gamma_i = \ln \frac{\phi_i}{x_i} + \left(\frac{z}{2}\right) q_i \ln \frac{\phi_i}{\phi_i} + l_i - \frac{\phi_i}{x_i} \sum_j x_j l_j$$

$$- q_i^l \ln \left(\sum_j \theta_j^l \Gamma_{ji}\right) + q_i^l - q_i^l \sum_j \frac{\theta_i^l \Gamma_{ij}}{\sum_k \theta_k^l \Gamma_{kj}} \tag{6.7}$$

where

$$l_j = \frac{z}{2} (v_j - q_j) - (r_j - 1)$$

Equation 6.7 requires only the pure component segment and area fractions (ϕ_i, θ_i) and the binary parameters which is gven by:

$$\Gamma_{ij} = \exp \left(- \Delta \frac{U_{ij}}{RT}\right) \tag{6.8}$$

The data sources for the interaction binary parameter G_{ij} as cited by J. M. Prausnitz (21) are

1. Vapor-liquid Isotherms (P, y, x)
2. Vapor-liquid Isobars (T, y, x)
3. Total Pressure data (P, x or y)
4. Boiling or dew point data
5. Mutual solubilities
6. Azeotropic data
7. Activty coefficients at infinite dilution

In this work mutual solubities and isobaric vapor liquid experimental data were used to estimate the binary interaction parameters Γ_{ij}.

The experimental weight fractions of the two liquid phases in equilibrium are summarized in Tables 6.12 through 6.14 for the systems 2 ethyl hexanol, methyl ester and Isopar M respectively.

For a multicomponent liquid-liquid system:

$$x_i \gamma_{xi} = y_i \gamma_{yi} \tag{6.9}$$

where

x_i = mole fraction of component i in x-phase

γ_{xi} = activity coefficient of component i in x-phase

y_i = mole fraction of component in y-phase

γ_{yi} = activity coefficient of component in y-phase

Then
$$\sum_j x_j \gamma_{xj}/\gamma_{yj} = 1 \qquad (6.10)$$

For a three component system, there are always two independent relations and the third dependent one is given by:

$$x_3 \gamma_{x3}/\gamma_{y3} = 1 - x_1 \gamma_x/\gamma_{y1} - x_2 \gamma_{x2}/\gamma_{y2} \qquad (6.11)$$

The non linear least square algorithm (NONLS2) (8) was used to fit the UNIQUAC binary interaction parameters Γ_{iu} in eqn. 6.8. THe objective function was to minimize the sum of squares of the two independent relations in eqn. 6.10.

$$\text{Min} \left(\sum_{N_{pts}} \left(\left(\frac{x_1 \gamma_{x1}}{Y_1} \right)^2_{calc} - \left(\frac{x_1 \gamma_{x1}}{Y_1} \right)^2_{obs} \right) + \right.$$

$$\left. + \sum_{N_{pts}} \left(\left(\frac{x_2 \gamma_{x2}}{Y_2} \right)^2_{calc} - \left(\frac{x_2 \gamma_{x2}}{Y_2} \right)^2_{obs} \right) \right) \qquad (6.12)$$

Table 6.12

Mutual solubility data for
Ethanol/water/2 ethyl hexanol system

* X_e	X_w	X_s	Y_e	Y_w	Y_s	T
0.024	0.9755	0.005	0.0169	0.0261	0.9570	293
0.0500	0.9490	0.0010	0.0350	0.0280	0.9370	293
0.097	0.9000	0.0030	0.0520	0.0295	0.9185	293
0.232	0.760	0.008	0.166	0.0516	0.7824	293
0.283	0.706	0.011	0.217	0.0652	0.7178	293
0.408	0.499	0.093	0.414	0.271	0.315	293
0.053	0.945	0.002	0.048	0.029	0.923	343
0.060	0.935	0.005	0.051	0.039	0.910	343
0.067	0.923	0.010	0.061	0.044	0.895	343
0.072	0.9080	0.020	0.071	0.049	0.880	343
0.205	0.735	0.06	0.195	0.141	0.664	343

* X_i, Y_i are mass fractions.

Table 6.13

Mutual solubility data for
Ethanol/water/Methyl Ester System

* X_e	X_w	X_s	Y_e	Y_w	Y_s	T
0.070	0.9292	0.0008	0.0073	0.0017	0.991	294
0.1170	0.8811	0.0009	0.0120	0.0018	0.9862	294
0.147	0.8517	0.0013	0.0216	0.0023	0.9761	294
0.276	0.721	0.003	0.0297	0.0026	0.9677	294
0.310	0.6885	0.005	0.0425	0.0034	0.9541	294
0.045	0.9542	0.0008	0.0145	0.0012	0.9843	338
0.095	0.9045	0.0015	0.0189	0.0014	0.9797	338
0.136	0.8620	0.002	0.0417	0.0021	0.9562	338
0.220	0.7760	0.004	0.0437	0.0028	0.9535	338
0.233	0.762	0.005	0.0635	0.0031	0.9334	338

* X_i, Y_i are mass fractions

Table 6.14

Mutual solubility data for
Ethanol/Water/Isopar M system at $298^\circ K$

* X_e	X_w	X_s	Y_e	Y_w	Y_s
0.320	0.6798	0.0002	0.0093	0.0004	0.9903
0.435	0.5645	0.0005	0.0113	0.0009	0.9878
0.664	0.331	0.005	0.0130	0.0010	0.9850
0.775	0.204	0.021	0.0208	0.0011	0.9781
0.787	0.1854	0.0276	0.0252	0.0012	0.9736
0.830	0.115	0.055	0.0341	0.0013	0.9646

The estimated binary interaction parameters obtained from the mutual solubility data are summarized in Table 6.15. There were no values obtained from the same source (mutual solubility) in the literature available for comparison. However, the calculated equilibrium molar compositions were plotted versus the experimental values in Figures 6.5 through 6.9.

The UNIQUAC interaction parameters (Γ_{iu}) are strong functions of temperature. The relation is given by:

$$\Gamma_{ij} = \exp\left(- \frac{\alpha_{ij}}{T} - \frac{\beta_{ij}}{T^2}\right) \qquad (6.12)$$

The parameters α_{ij}, and β_{ij} are difficult to be estimated from mutual solubility data, since isothermal experimental data are available for liquid liquid systems. The isobar binary vapor liquid experimental data (Tables 6.16 and 6.17) were used to estimate the temperature dependent parameter α_{ij}, and β_{ij} for Isopar M/Ethanol/Water system, which was studied earlier using the mutual solubility data. The estimated parameters are summarized in Table 6.18.

The predicted two phase invelop for Isopar M system using VLE binary interaction parameters was plotted in Fig. 6.10 versus the experimental data.

Table 6.15

UNIQVAC Parameters

System Parameter	Methyl Ester 20°C	Methyl Ester 65°C	2EHOH 20°C	2EHOH 70°C	Isopar M 25°C
Γ_{12}	1.66894	0.073023	0.1876	0.15057	0.6916
Γ_{13}	2.08981	0.76398	1.5677	0.70781	1.40359
Γ_{21}	0.024711	0.027557	1.28686	2.48834	0.17337
Γ_{23}	0.9732 x 10⁻¹¹	1.49449	0.39089	0.91765	0.37363
Γ_{31}	0.7184 x 10⁻³	0.0021565	0.318617	2.80112	0.39321 x 10⁻¹⁹
Γ_{32}	0.023036	0.0014876	0.189968	0.061667	0.002912
Standard Error	0.001843	0.00587	0.00791	0.00776	0.00150

Component

1: ETOH
2: H₂O
3: Solvent

Table 6.16

Experimental ethanol/water equilibrium

data[*] at 380 mm Hg

x[a]	y[b]	T (°K)
0.00	0.00	355.1 ± 1
0.0037	0.0029	354.3
0.0959	0.444	342.8
0.0976	0.47	341.9
0.3086	0.6211	337.4
0.4145	0.6674	337.2
0.6041	0.6889	336.8
0.6549	0.72	334.2
0.9410	0.960	335.7
1.000	1.000	335.6

[a]   Mole fraction ethanol in liquid

[b]   Mole fraction ethanol in vapor

[*]   Data obtained by S. Babb (1983)

Table 6.17

Experimental ethanol/Isopar-M
vapor/liquid equilibrium data[*]

x[a]	y°	T (°C)
0.00	0.00	196 ± 2
0.00219	0.2702	168
0.00624	0.5186	134
0.0059	0.2376	114
0.0120	0.796	93.0
0.0175	0.883	66.7
0.1836	0.970	63.0
0.4123	0.9468	61.1
0.4904	0.5984	61.9
0.5631	0.9443	60.3
0.5706	0.9540	63.5
0.6408	0.9512	60.0
0.7283	0.9798	62.0
0.8848	0.9836	63.0
0.9584	1.000	62.1
0.997	0.997	62.0

[a]   Weight fraction ethanol and water in liquid phase

[*]   Data obtained by S. Babb (1983)

6.5 Discussion and Conclusion

Tables 6.6 through 6.11 showed a good agreement between the experimental values of the distribution coefficients and the values predicted from Eqns. 6.2 and 6.3. The model could be useful at low to intermediate ethanol concentration. A big deviation was expected at high solute concentration. Therefore, the plate point could not be predicted. The variation on the coefficients values suggests that different extraction mechanisms predominate in different solvents. Mechanistic studies should also consider the degree of association between the solute and the diluent.

The ternary diagrams plotted in Fig. 6.5 - 6.9 show a good prediction of the ternary equilibria using the UNIQUAC model for three different organic solvents. On the other hand, Table 6.15 exhibited different fitted values for the same binary parameters. This variation was due to using the ternary mutual solubility data to fit binary parameters. The investigator recommeded using the VLE binary data to obtain the binary parameters. An additional ternary parameters (Γ_{ijk}) is recommended, to be obtained from the ternary LLE data.

Table 6.18

Estimated UNIQUAC temperature
dependent parameters

Parameter	Ethanol[1]/Water[2]	Ethanol[1]/Isopar M[2]
α_{12}	137.47	-999.7
α_{21}	-5870	502.42
β_{12}	-68330	29.1×10^4
β_{2k}	21.38×10^5	21.67×10^4
Temp., $^\circ K$	335 - 355	335 - 460
Standard Error	0.0047	0.0132
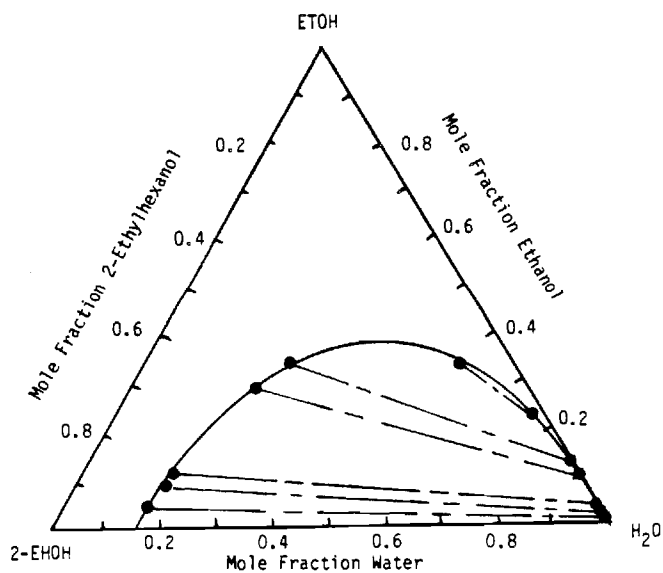
Fig. 6.5 Ternary Liquid/Liquid equilibria representation using UNIQUAC for the system water-ethanol-2-ethylhexanol at 20°C.
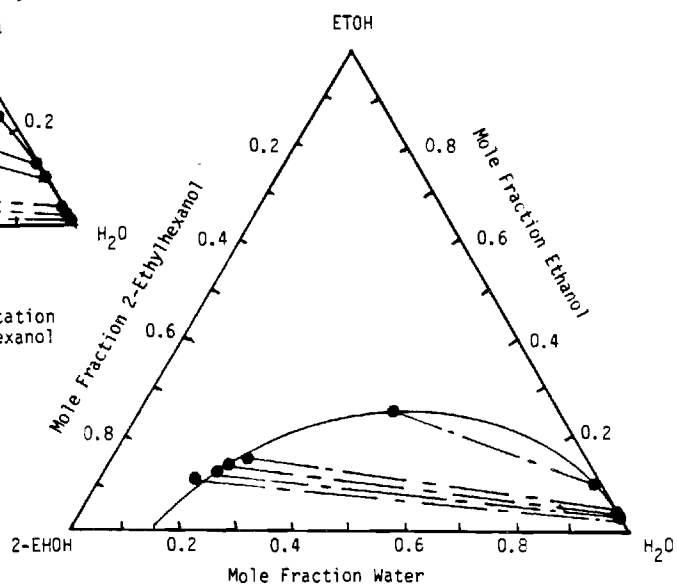
Fig. 6.6 Ternary Liquid/Liquid Equilibria representation with UNIQUAC for the system water-ethanol-2-ethylhexanol at 70°C. Tie lines are experimental.
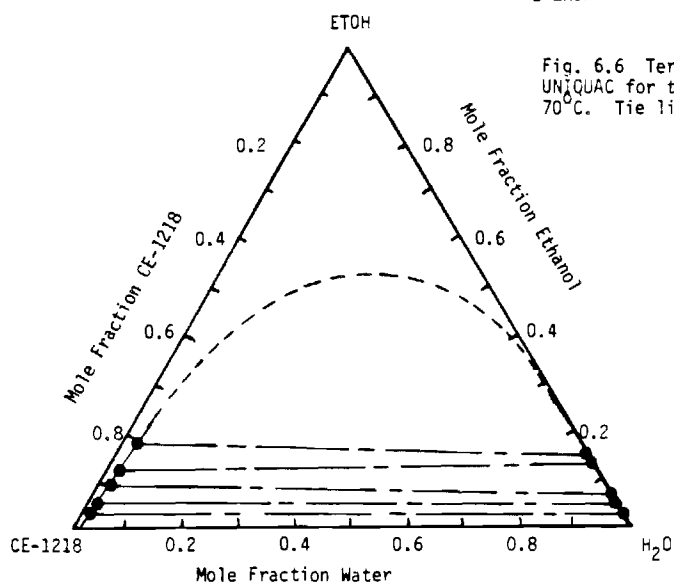
Fig. 6.7 Ternary Liquid/Liquid Equilibria representation using UNIQUAC to model the system: water-ethanol-CE-1218 (a methyl ester) at 20°C.

ETOH

Mole Fraction CE-1218

Mole Fraction Ethanol

0.2   0.8

0.4   0.6

0.6   0.4

0.8   0.2

CE-1218   0.2   0.4   0.6   0.8   H₂O

Mole Fraction Water
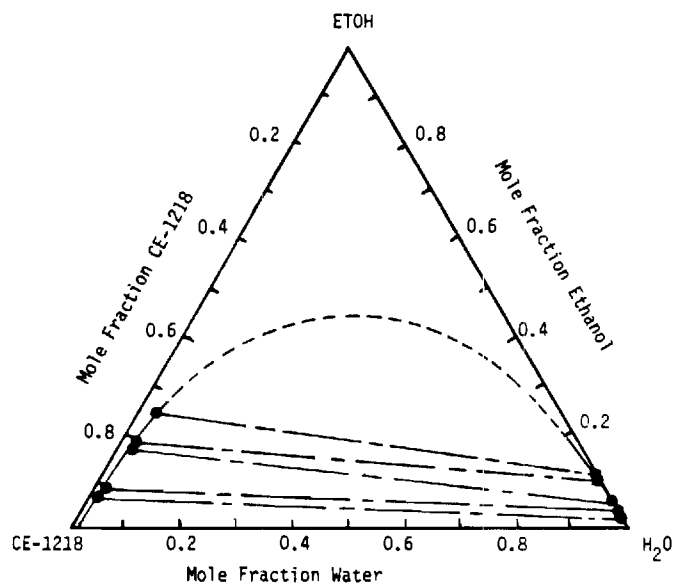
Fig. 6.8 Ternary Liquid/Liquid Equilibria representation using
UNIQUAC to model the system: water-ethanol-CE-1218 (a methyl
ester) at 65°C. Tie lies are experimental. Part of the mutual
solubility curve (dotted line) is a UNIQUAC prediction.

ETOH

Mole Fraction ISOPAR-M

Mole Fraction Ethanol

0.2   0.8

0.4   0.6

0.6   0.4

0.8   0.2

ISOPAR-M   0.2   0.4   0.6   0.8   H₂O

Mole Fraction Water
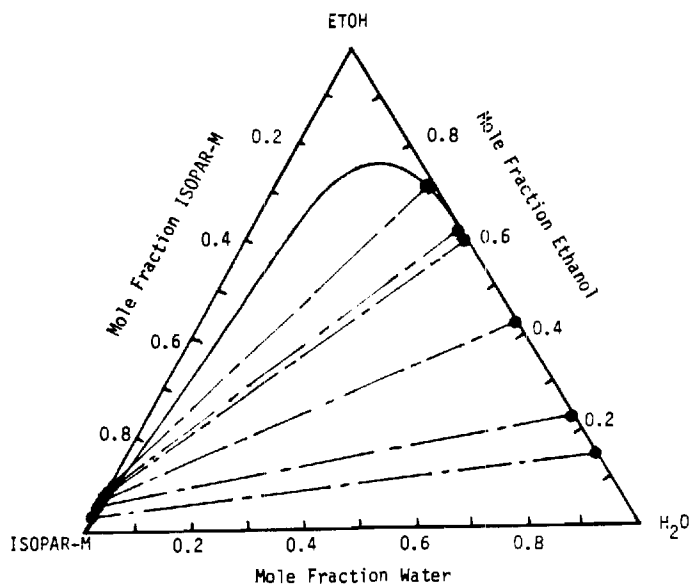
Fig. 6.9 Ternary Liquid/Liquid Equilibria Model for the
system water-ethanol-ISOPAR-M at 20°C using UNIQUAC. Tie
lies are experimental.

Fig. 6.10 Representation of ternary Liquid/Liquid equilibria for the system: water-ethanol and ISOPAR-M using the UNIQUAC equation and the binary interaction parameters from the vapor/liquid equilibrium data.

6.6 References

1. Alder, L., Liquid-Liquid Extraction, Elsevier, 1955.

2. Anderson, E. V., "Gasohol: Energy Mountain or Mole Hill?" C & E News (July 31, 1978).

3. Bachman, I., "Tie Lines in Ternary Liquid Systems", Ind. and Eng. Chemistry, Jan., 1940.

4. Brancker, A. V., T. G. Hunter, "Tie Lines in Two-Liquid Phase Systems", Ind. & Eng. Chemistry, Jan. 1940.

5. Chao, K. C. and T. Nitta et al., "A Group Contribution Molecular Model of Liquids and Solutions", AIChE J (Vol. 23, No. 2) March, 1977.

6. Hyskens, P. L., M. Cl. Itqulalt, and J. Mullens, "Water Absorption by Alcohols in Organic Solvents", The Journal of Physical Chemistry, vol. 84, no. 1, 1980.

7. Marion, Larry, "In the Spotlight: Ethanol", Chem. Eng. (Feb. 26, 1979) 78.

8. Marquardt, D. W., "An Algorithm for least-Squares Estimation of Nonlilnear Parameters", J. Soc. Ind. Appl. Math. 11 (2) 431 (June 1963).

9. Othmer, D. F., R. F. White, and E. Trueger, "Liquid-Liquid Extraction Data", Industrial and Engineering Chemistry, Oct., 1941.

10. Othmer, D. F., and P. E. Tobias, "Liquid-Liquid Extraction Data", Ind. and Eng. Chemistry, vol. 34, no. 6.

11. Oualline, C. M. and Van Winkle, "Ternary Liquid Systems", Ind. and Eng. Chemistry, July, 1952.

12. Roddy, J. W. and C. F. Coleman, "Distribution and Miscibility Limits in the System Ethanol-Water-TBP", Oak Ridge National Laboratory, 1981.

13. Roddy, J. W., "Distribution of Ethanol-Water-Mixtures To Normal Alkanes", A.I.C.H.E.J., 1981.

14. Schweitzer, P. A. (ed), Handbook of Separation Techniques for Chemical Engineers, McGraw-Hill (1979).

15. Schweppe, J. L. and J. R. Lorah, "Ternary System Ethyl Alcohol-n-Heptane-Water at 30°", Ind. and Eng. Chemistry, vol. 46, no. 11.

16. Tawfik, W. Y., "Efficiency of Ethanol Extraction from Aqueous Mixtures", Master's Thesis, Georgia Institute of Technology, 1982.

17. Tedder, D. W., C. L. Liotta, F. M. Williams and M. Spanbauer, Fuel-Grade Ethanol Recovery by Solvent Extraction: Technical Progress Report for the Period, September 15, 1980 through March 31, 1981, School of Chemical Engineering, Georgia Institute of Technology, Atlanta, Georgia (April, 1981).

18. Tedder, D. W. and C. L. Liotta, Fuel-Grade Ethanol Recovery by Solvent Extraction, Schools of Chemical Engineering and Chemistry, Georgia Institute of Technology, Atlanta, Georgia (June 30, 1979).

19. Tedder, D. W., et al., Fuel-Grade Ethanol Recovery by Solvent Extraction Technical Progress Report for the Period September 15, 1981, Georgia Institue of Technology, Atlanta, Georgia (October 1981).

20. Tuker, Edwin and S. D. Christian, "Alcohol Association Studies", The Journal of Phys. Chemistry, vol. 81, no. 13, 1977.

21. Prasnitz, J., et al.,"Computer Calculation for Multicomponent Vapor-Liquid and Liquid-Liquid", Prentice Hall International Series in Physical and Chemical Science.

CHAPTER 7

PILOT SCALE DRYING CYCLE TESTS AND MODELING STUDIES

(A. J. Eckles)

7.1 Summary

This work focused on demonstrating that the "drying cycle" concept is feasible. That is, processing a 50 wt % ethanol in water feed to recover a product whose composition is dryer than that of the ethanol-water azeotrope. These results suggest that this approach is technically feasible.

7.2 Introduction

The ability to model or predict the performance of a separation system is of key importance during process design and scale up. The purpose of the present work is to develop a model for the solvent extraction of ethanol in a Karr Reciprocating Plate Extraction Column.

This model is specifically for extraction of ethanol from medium concentration aqueous solutions (40 to 75%) to a relative dryness (ethanol concentration on a solvent-free basis) past the azeotrope (95.5% at 1 atm.) using Isopar L, a narrow cut, branched paraffin solvent. Experimental data was obtained using Isopar L in a one inch Karr Column, but the modeling was performed in such a manner as to allow fitting of the data from larger diameter columns and different solvents later.

This system is the second step of a possible solvent extraction method for drying ethanol past the azeotrope without use of the more energy intensive process of distillation. The first step would be the initial separation of ethanol from the dilute fermentation liquors by some method such as distillation, solvent extraction, or membrane permeation.

Initial solvent selection for the drying cycle was made by considering several major factors. The first such factor was the ethanol selectivity, (i.e. the ratio of the distribution coefficient of ethanol to that of water). Isopar L achieved ethanol drynesses past the azeotrope over a wide range of aqueous equilibrium concentrations and system temperatures. This solvent also showed good phase separation with aqueous phases and is easily stripped of ethanol due to its high molecular weight and low volatility. In addition, this solvent is relatively inexpensive (1) and is available in large quantities from Exxon Corporation.

To model the system it was first necessary to have a continuous extraction system with solvent recycle. Several drying cycle configurations were constructed in the laboratory. Subsequently, the latter model was used to complete over seventy extraction and solvent regeneration runs to gather data. Operating conditions were varied in a mixed order, similar to statistical design methods suggested by Murphy (19). One key point is that the variation of operating conditions were severely limited by the experimental equipment and conditions required for operation. Often a run was considered successful if no mechanical failures occured during a one hour period.

The modeling of the extraction column is based on dimensional analysis. Dimensional analysis was used because of its versatility in handling problems of complex character and where analytical solutions are impractical. This method also facilitates scaling up from pilot plant size systems to industrial scales. Further, it is often possible to treat problems of a more general nature with dimensional analysis than analytically (4).

A dimensional analysis of the operational parameters yielded seven dimensionless groups. Determination of the exponents on these dimensionless groups showed them to be qualitatively consistent with those values which were expected. The best computer model using these dimensionless groups showed a reasonable agreement with the experimental results.

Due to the similar effects of temperature and concentrations on many of the physical and equilibrium properties of Isopar L and aqueous ethanol, five of the dimensionless groups were highly correlated. A non-linear least squares fit to three dimensionless groups showed almost as good a fit as seven did. This high correlation may be reduced by expanding the data base to include different solvents.

7.3 Literature Survey

7.3.1. Introduction to the Literature Survey

This section consists of a general introduction and a survey of representative articles that the author feels are directly related to the present research.

7.3.2. General Extraction Column Studies

Higher extraction column efficiencies can often be achieved through the application of mechanical energy to the liquid/liquid mixture. Three common classes of

mechanically-aided extraction columns in the process industries are: (1) rotating impellers, (2) pulse columns, and (3) reciprocating internals or plates.

Henley and Seader (3) state that in the absence of experimental data, a crude correlation for estimating the height equivalent of a theoretical stage (HETS) for pulse and reciprocating plate columns can be used. This correlation is only applicable when the viscosities of both phases are less than or equal to one centipoise:

$$HETS/D^{1/3} = 0.14\,\sigma + 2.0 \quad (1)$$

where HETS = height of an equivalent stage (inches)

D = column diameter (feet)*
σ = interfacial tension (dynes/cm)*

This approximation represents values of HETS from a low of six inches for a three inch laboratory-sized column with a low interfacial tension-low viscosity system to as high as twenty five inches for a thirty-six inch commercial column operating with a high interfacial tension and one phase of high viscosity (greater than one centipoise). Values of HETS can be twenty-four inches or more for a small laboratory-sized column.

Selection of the continuous phase in a column can often be a significant design factor in column efficiency. Skelland and Chadha (4) established criteria for selecting the phase to be dispersed in perforated plate or spray extraction columns. The conventional criterion in this regard has been to disperse the phase present in larger volume, so as to provide the greater total interface. However Skelland (4) suggests that where comparable amounts of each phase are present, it may be better to disperse the phase such that offering the maximum to mass transfer occurs as indicated by the magnitude of the distribution coefficient. This way, even if trace quantities of surface active impurities should reduce the mass transfer rate, this will have a less serious effect on the rate of mass transfer. Trace amounts of surface active impurities will, in fact, frequently be present n a commercial scale extraction column.

In his work with rotating disc columns, Kung et al (5)

indicated that the size of the droplet was independent of the phase flowrates. He formulated an empirical relation for the characteristic column velocity (velocity of the dispersed phase) using dimensional analysis and least squares, but did not relate this to column efficiencies. Viscosity and interfacial tensions were used in his models as well as densities and various characteristic lengths.

Leonard et al (6) based centrifugal contactor efficiencies on a dimensionless dispersion number as did Tawfik (7). The dispersion number relates the settling time to the residence time. Neither author attempted to relate this to known or measured physical properties although Leonard speculated that the continuous phase viscosity and surface charge at the interface had a large effect upon the dispersion number.

H. R. C. Pratt (8) wrote a highly complex generalization for determining the actual column height or number or non-ideal backmixed contactors in terms of both diffusion and backflow models, assuming a linear equilibrium line. This model involves the use of numerous mathematically derived expressions obtained from the height of a transfer unit, Peclet numbers for both phases, and other physical properties and characteristic lengths. This might be useful for standard systems where the column and solvent system characteristics are well known, but of minimal value in predicting the performance of "non-standard" solvents and columns.

7.3.3. Pulse Columns

The operating principles of pulse columns are very similar to reciprocating plate columns. In the pulse column, the liquid is pulsed through perforated plates to provide dispersion and mixing of the two phases while a reciprocating-plate column moves the plates through the liquid. Examination of work with pulse columns can provide useful information in modeling reciprocating plate columns.

Hiromichi et al (9) indicated that pulse columns were used for light water reactor fuel reprocessing because they have a larger capacity and shorter contact time than a mixer-settler. Observing the droplets in photographs, Hiromichi determined that there was not much difference in drop diameters observed in aqueous continuous and organic continuous columns. If the drop diameters are the same, the specific contact surface area is proportional to the holdup. This agrees with calculations that show that the

aqueous continuous column had smaller heights of transfer units when the organic to aqueous ratio was greater than one. Hiromichi determined that the flooding velocity of the pulse-column depends mainly on the pulse intensity. He also determined that, with either phase continuous, the flooding velocity is dependent on the organic to aqueous ratio.

Smoot and Babb (10) used a last squares fit to determine a relationship for the methyl-isobutyl ketone-acetic acid-water system, with the aqueous phase continuous. The relation was:

$$HTU = 504 \ (S) \ \left[\frac{f \ A \ d \ \rho_d}{\mu_d}\right]^{-0.4} \left[\frac{V_c}{fA}\right]^{0.42} \left[\frac{O}{A}\right]^{-.56} \left[\frac{d}{s}\right]^{0.62} \quad (7.2)$$

where S = plate spacing

f = frequency of pulse

A = pulse amplitude

d = superficial eddy diffusivity

ρ_d = density of discontinuous phase

μ_d = viscosity of discontinuous phase

V_c = superficial velocity of continuous phase

O/A = organic to aqueous flow rate ratio (volumetric)

The average deviation for this relation was 27%.

Later Smoot et al (11) correlated flooding characteristics and mass transfer data on pulse columns from numerous literature sources. Dimensional analysis and multiple regression techniques were used to give generalized correlations for column flooding and height of a transfer unit. The form of the equation from both correlations was:

$$F = b_o \left[\frac{V_c}{V_d}\right]^{b_1} \left[\frac{\Delta\rho}{\rho_d}\right]^{b_2} \left[\frac{F \ \mu_c}{\rho_c \ \sigma^4}\right]^{b_3} \left[\frac{d\sigma\rho_c}{\mu_c^2}\right]^{b_4} \left[\frac{D}{d}\right]^{b_5} \left[\frac{g \ \mu_c^4}{\rho_c \ \sigma^3}\right]^{b_6} \left[\frac{\mu d}{\mu_c}\right]^{b_7} \quad (7.3)$$

where V   =   pulse amplitude multiplied by frequency

$\Delta\rho$ =   density difference of the two phases

ρ =   density

F   =   % free space in the plates

μ =   viscosity

D   =   column diameter

d   =   sieve hole diameter

g   =   acceleration of gravity

σ =   interfacial tension

d   =   discontinuous phase

c   =   continuos phase

D_r =   diffusivity of solute in dispersed phase

The following coefficients and exponents for the flooding velocity $(V_d + V_c)$ are:

b_0 =   0.527 b_4 =   0.458

b_1 =   -0.014 b_5 =   0

b_2 =   0.63 b_6 =   0.81

b_3 =   -0.207 b_7 =   -0.20

The flooding velocity allows the column diameter to be determined by

$$D = \left[\frac{4W}{\pi F(V_c + V_d)} \right]^{1/2} \qquad (7.4)$$

where D   =   column diameter

W   =   design capacity

F   =   fraction of flooding velocity

The third dimensionless group in the function is replaced by

$$\left(\frac{\mu_d}{\rho_d \, D_v} \right)^{b_3}$$

for the height of a transfer unit calculation. The coefficients and exponents for th eheight of a transfer unit divided by the plate spacing are:

b_o = 0.20 b_4 = 0.096

b_1 = -0.434 b_5 = -0.636

b_2 = 1.04 b_6 = 0.317

b_3 = 0.865 b_7 = 4.57

Which can be simplified to the following relation:

$$\text{HTU} = \frac{K \, \Delta\rho^{1.04} \, \sigma^{.097} \, V_c^{.539} \, D^{.319} \, \ell^{.683}}{V_o^{.434} \, d^{.434} \, \rho_d^{2.342} \, \mu_d^{3.27} \, D_r^{.865} \, V_d^{.636}} \qquad (7.5)$$

Mar and Babb (12) demonstrated that the logitudinal concentration gradients in a continuous countercurrent extraction are related to four dimensionless groups. These are the Peclet number, the number of transfer units, the concentration ratio, and a length ratio. They used dimensionless analysis, logarithmic transformation, and multiple regression to determine a correlation for the longitudinal eddy diffusivity, (which is used in the Peclet number). A smaller Peclet number indicates increased backmixing and decreased column performance. They found that the phase density difference, viscosity, and pulse amplitude had little effect upon eddy diffusivity.

Bell et al. (13) concluded, for columns under the conditions they tested, (with fewer than twenty-three cells), that holdup was highest in the center. On the other hand, for those with twenty-six or more cells, the holdup was uniform throughout.

Bell (14) studied the effect of interfacial tension on the overall holdup by varying a non-transferring solute which changed the interfacial tension without affecting the density or viscosity. An immediate and significant effect

on holdup for small changes in interfacial tension was found. This effect would have a large influence over mass transfer in the column.

Logsdale (15) correlated the performance of a pulsed plate column with several solvents to obtain the general correlation of:

$$
HTU = K \left[\frac{u_c g}{v_0^{-3}(1-x)^3 \rho_c} \right]^{2m/3} \left[\frac{\Delta\rho}{\rho_c} \right]^{2/3 \, (m-1)} \left[\frac{v_c^3 \rho_c}{g \mu_c x^3} \right] \left[\frac{vd}{vc} \right]^{1/2}
$$

$$
\left[\frac{g \rho_c^2}{\mu_c^2} \right]^{1/3} \quad exp \, (D/2) \tag{7.6}
$$

where x = fractional holdup of dispersed phase

$\bar{V}_D$ = mean droplet velocity

K = constant

m = 0.45 - 0.20 dp

dp = diameter of plate

D = column diameter

Vd = velocity of dispersed phase

V_c = velocity of continuous phase.

7.3.4. Reciprocating Plate Column

Karr (16) recommends the reciprocating plate column for its high extraction efficiency, high capacity, rugged construction, and versatility in extraction process studies. Karr (2) also indicates that the height of a theoretical stage and thoroughput per unit area should be independent of the diameter of; however, his later studies (10) indicated that an increase did occur. Studies done with various solvents as continuous and dispersed phases

demonstrated that roughly the same minimum height of a theoretical stage could be obtained with various stroke length and stroke speed combinations as long as the velocity terms resulting from the product of the strokes per minute and the strokelength are the same (i.e., a higher stroke speed would be required with a shorter stroke length).

Teh and Karr (16) discuss scale up procedures from one, three inch columns to sizes of twelve to thirty-six inches in diameter. Karr and Lo (17) observed that in scaling up laboratory-scale columns (one and three inches) to commercial-scale columns (twelve to thirty-six inches), that the height of an equivalent theoretical stage increases with increasing column diameter because of axial mixing effects. They report the following empirical relationships:

$$(HETS)_{D_2}/(HETS)_{D_1} = (D_2/D_1)^{0.38} \qquad (7.7)$$

and for the optimal reciprocating speed:

$$(SPM)_{D_2}/(SPM)_{D_1} = (D_1/D_2)^{0.14} \qquad (7.8)$$

where SPM is in strokes/min. However, no mathematical models for mass transfer in reciprocating plate columns were found in the literature.

7.4 Experimental Equipment and Materials

7.4.1. Karr Reciprocating Plate Extraction Column

The column used consists of 49 stainless steel perforated plates mounted on a central shaft which is reciprocated by means of a simple drive mechanism located above the column. The main portion of the column is a borosilicate glass pipe. The plate spacing is 2 inches and the perforated plates (1/4 inch diameter holes) have 62.8% free space. The frequency can be varied from 0 to 400 strokes per minute and the stroke amplitude is variable from 0 to 1 3/4 inches.

The Model used is KCl-8 purchased from Chem Pro Corporation in New Jersey. It has an overall height of 152 inches, a plate stack height of 96 inches, and base size of 24 by 15 inches. A schematic diagram of the column is given in Figure 7.1.

7.4.2. Solvent Temperature Control

The solvent feed to the column was preheated by a 3 ft (1/4" dia) coiled copper tubing heat exchanger in a hot stirred mineral oil bath mounted on a Model 210 stirring Hotplate from Fisher. Column heat loss was limited by use of Fisher "Heat by the Yard" heating tape connected to a variable autotransformer.

7.4.3. Temperature Measurements

Temperature measurements were made at three points in the column using Type K (Chromel/Constantan) thermocouples with a $0°C$ reference junction obtained from Omega Engineering, Inc. The thermocouples were connected to a digital multimeter, Simpson 460 Series 4, made by the Simpson Electronic Company with an accuracy of ± 0.5 degrees centigrade.

7.4.4. Solvent Stripper

The stripping section consisted of three major sections: a coalescer, a preheator, and a stripper. The water droplet removal section consisted of a modified separatory funnel with solvent added in the center and removed from the top, and a custom fabricated "Y" tube coalescer assembly packed with glass wool. The preheat section consisted of 3 feet of 1/8 inch copper tubing wrapped in Fisher "Heat by the Yard" heating tape controlled with a variable auto transformer. The heating tape is capable of operating up to $300°C$. The stripper was constructed of Pyrex by Mr. Don Lillie of the Georgia Tech Glass Shop. The flash section was 2 inches in diameter and 18 inches tall with a stainless steel mesh and glass wool demister pad at the top and an outlet for removal of solvent from the bottom. The inlet for the flash was in the center of the column. The bottom 8 inches were packed with 1/2 inch ceramic raschig rings. The stripper was also wrapped with Fisher heating tape, and temperature and pressure were monitored prior to, and in the stripper. Operating temperatures and pressures were varied from 25 to $60°C$ and 20 to 70 mm.Hg to produce stripped solvent with various concentrations of ethanol.
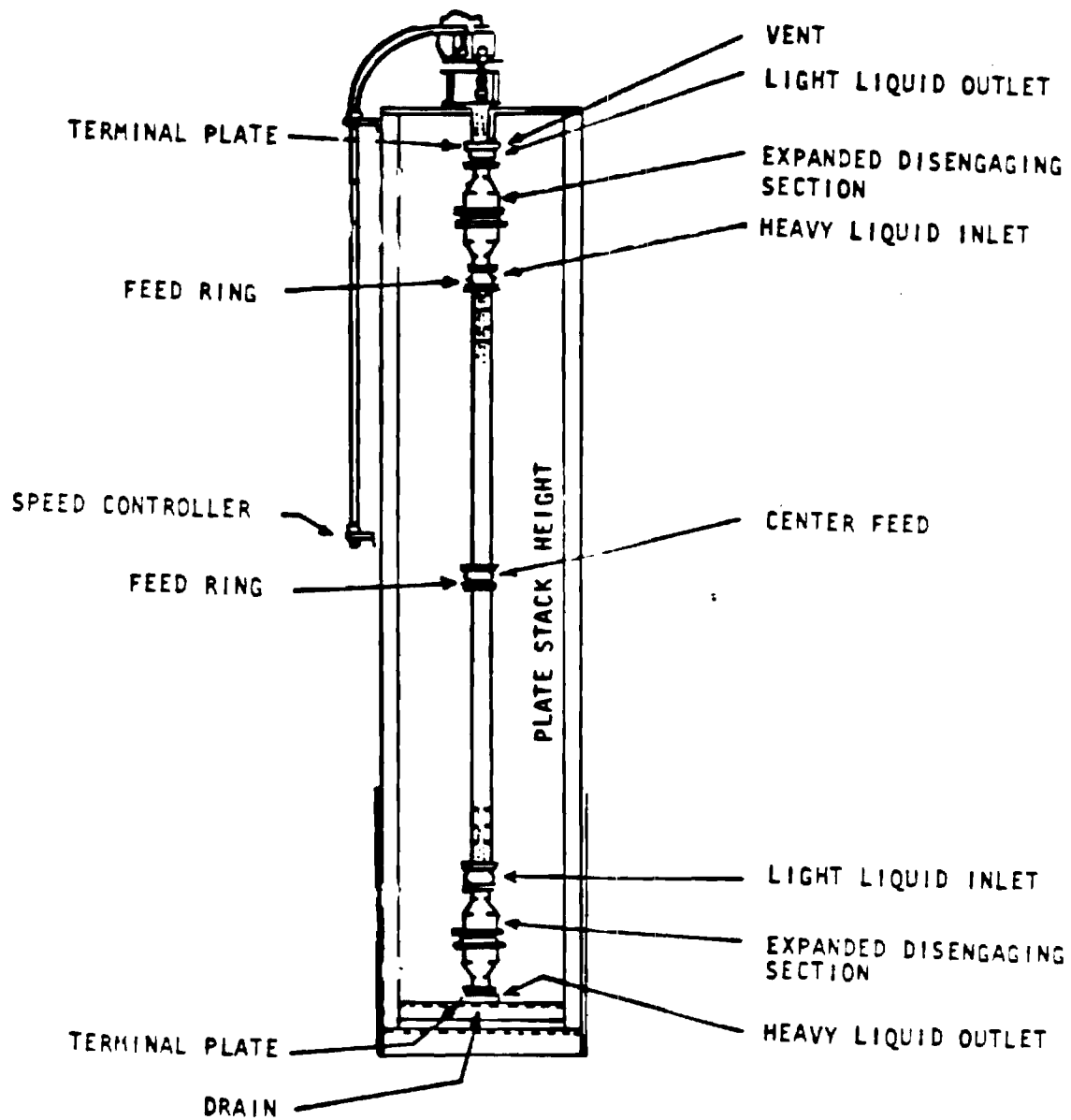
Fig. 7.1   Karr Reciprocating-Plate Column

7.4.5. Pressure Control in Stripper

Pressure was maintained in the stripping section by the use of a Welch 1400 two-stage vacuum pump, from Fisher Scientific. Pressure was controlled by means of a Cartesian Manostat, also purchased from Fisher Scientific. Pressure was measured with a closed end Bennet manometer constructed in the Georgia Tech Glass Shop.

7.4.6. Concentration Measurements

The concentration measurements were made using gas/liquid chromatography. A type 5710A gas chromatograph from Hewlett Packard was used. The column was 4 feet of 1/8 inch diameter tube packed with "Poropak Q" 80/100 mesh from Supelco, Inc., Bellafonte, Pennsylvania. The helium carrier gas was obtained from the Alabama Oxygen Co., Inc. The oven temperature was maintained at $165^{\circ}C$, the injection port at $250^{\circ}C$ and the thermal conductivity detector was also kept at $250^{\circ}C$. The peaks were integrated using a Hewlett Packard 3390A peak integrator which gave area percentages. Area percentages of aqueous ethanol samples were converted to mass percentages by correlations obtained from known mass percentages. The mass fractions of ethanol in the organic phases were obtained by calibrations comparing the area of the ethanol peak with the area of the propanol peak from a known amount of added propanol. This was necessary due to the difficulty of quantitatively analyzing Isopar L on the gas chromatograph (Isopar L remained in the column until the higher temperature cleaning cycle was run).

7.4.7. Pumps

Positive displacement pumps were used to provide a uniform flow of solvent and aqueous feed to the column. The organic pumps used were RPG 400's with 3/8 inch pistons and the aqueous feed pump was the RH 434 Lab Pump Jr., both from Fluid Metering, Inc. At a negligible pressure difference the RPG 400 is capable of 0 to 400 milliliters per minute flowrate and the Lab Pump Jr of 0 to 10 milliliters per minute.

7.4.8. Density Measurements

Density measurements for the Isopar L at various temperatures were made with a Mettler/Paar Calculating Digital Density Meter model DMA 45. A constant temperature

bath for the density measurements was provided by using a Haake D. 1 model.

7.4.9. Viscosity Measurements

Kinematic viscosity was determined using a calibrated Cannon-Fenske type kinematic viscometer, ASTM size 50. Viscosity measurements were made while using the Haake bath to control the temperature in a large pyrex water bath. These viscosity values were verified using a Brookfield Sycro-lectric Viscometer Model LVC. The Cannon-Fenske viscometer yielded results consistent to ±0.05 centipoise while the Brookfield viscometer give results consistent to ±0.5 centipoise.

7.4.10. Solvents

The solvent used for this system was Isopar L. Isopar L is a heavy narrow cut isoparaffinic solvent composed of mostly C_{10} to C_{12} mixtures of branched alkanes. It has a specific gravity of 0.767 at 15.6°C, and a viscosity of 2.20 cP at 25°C. The initial boiling point is 188°C, the 50% point is reached at 194°C and the dry point at 206°C. This solvent is a refinery product obtained from Exxon Refining.

Ultra dry ethanol was made by refluxing 99.5% ethanol for 4 hours over magnesium metal using the methodology of Lund and Bjerrum.[18] Reagent grade Propanol was purchased from Fisher for use in propanol spiking.

7.4.11. Interfacial Tension Measurements

Interfacial Tension measurements were made with a Model 21 Tensomat from Fisher Scientific. The accuracy of the apparent interfacial tensions were ±0.05 dynes per centimeter.

7.4.12. Non-Linear Least Squares Software

The software used for correlating various data sets was RUNLS2. RUNLS2 is an unconstrained, weighted nonlinear least squares program consisting of 3 subprograms, NONLS2, NEWLAM, and PARLIN. This program can minimize the sum of either

$$[y_i(obs) - F_i(x_{1,i} \ x_{2,i} \cdots x_{n,i})]^2$$

or

$$[(Y_i(obs) - F(Xi,1, Xi,2...Xi,n))/Y_i(obs)]^2$$

and allows for variable weighting of these. The author of this program was G. W. Westley, Computing Technology Center, Union Carbide Corporation, Oak Ridge, Tennessee.

7.5. Experimental Procedures

7.5.1. System Development

Equilibrium studies indicated that Isopar L should be a potential solvent for the production of a dry ethanol product. A first trial run was made in April, 1982, using a 50 weight percent ethanol feed and pure Isopar L counter-current flow through a 16 stage mini-mixer settler. The extract was then pumped into a simple stripper/condenser assembly constructed from standard 24/40 glassware. An extract of 97 wt% relative dryness and a product of 98% relative dryness (ethanol concentration on a solvent-free basis) were obtained from this initial run. The stripped solvent was discarded. This indicated the feasibility of the concept.

A 1 inch Karr Reciprocating Plate Column was then purchased and installed in May, 1982. The first operation of this column was as part of a 2 cycle solvent extraction system where ethanol was extracted from a 9% aqueous solution with a 50/50 volume mixture of Norpar 12 and Tridecyl alcohol in the mini mixer-settler. Then the stripped ethanol from this extract was pumped continuously from the condenser of the first system's stripper to the top of the Karr column as approximately a 50% ethanol feed to the column with Isopar L. The extract overflow was then stripped of most of its ethanol and returned to the bottom of the column. This system yielded ethanol of 98% dryness although solvent carryover gave a product of 74% ethanol and 26% Isopar L.

Once this concept was established, continuous stripping studies were carried out. Several runs with Isopar L were again made in July and August of 1982 but stripping and pumping problems necessitated low flow rates of approximately 60 ml/min. These low flow rates caused the

column to take longer to reach steady-state (e.g., from 45 min to 1 1/2 hrs.).

An adequate solvent regeneration system is a necessity for continuous column operation. The column and stripper were operated in August, 1982 with 2,6-dimethyl-6 heptanone, but solvent regeneration (stripping problems) prevented continuous runs with this solvent.

A larger and better solvent stripping (regeneration) system was constructed and larger pumps were installed in the Fall of 1982 allowing more runs with higher flow rates and a more rapid approach to steady-state to be obtained. At this point operation of the column, and the solvent regeneration system, were considered reliable enough to generate data for modeling of the Reciprocating Plate Extraction Column and for possible later use in the scale-up of ethanol drying systems.

7.5.2. Karr Reciprocating Plate Column Operation

The column was first connected to the appropriate pumps and valves with the solvent feed line into the bottom inlet (S_{in}), (see Fig 7.2) the raffinate outlet, (A out), connected to a valved line in the bottom, and the feed inlet (A_{in}) and solvent overflow or outlet (S_{out}) are connected at the top of the column. Once the column is properly connected, it is filled with solvent.

The flow of solvent is started and the reciprocating plates are turned on and adjusted to an intermediate value. Then the aqueous feed is started at the top of the column. The valve on the aqueous outlet line is adjusted to maintain a constant level interface in the lower disengaging section. At this point the stroke rate is adjusted to some point below the flooding point of the column.

The flooding point of the column is the point where the agitation and flowrates produce droplet sizes sufficiently small such that the droplets rise instead of falling through the column and form a layer in the upper disengaging section. Optimum operation is at a point just below the flooding point.

Unfortunately, the closer to the flooding point the tower is operated, the more droplets of aqueous feed are carried over with the extract. This necessitates that a settling container and droplet separator be used before the
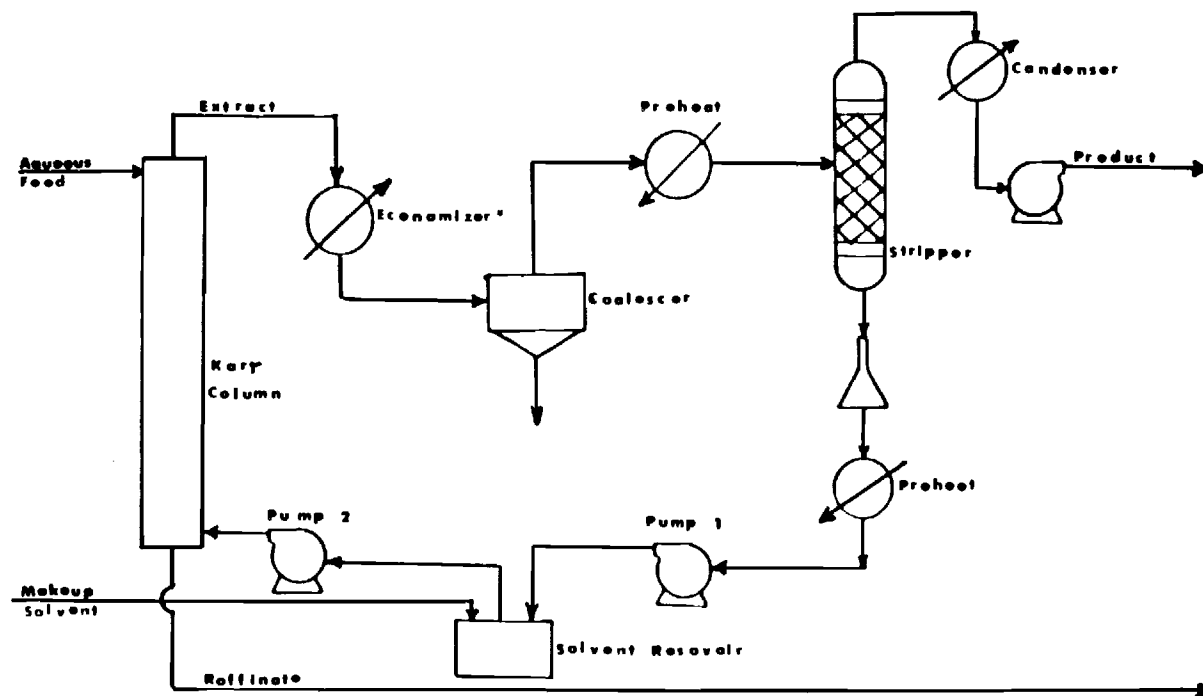
Fig. 7.2 Solvent Extraction System

solvent stripping is accomplished. Many runs were made, however, at well below flooding conditions to determine the effect of varying stroke rates on extraction.

7.5.3. System Operation

Due to the time requirements for steady-state conditions to be reached, solvent recycle is a necessity for proper operation. Thus, the solvent flowrate could not exceed the rate of solvent regeneration. The rate of solvent regernation is highly dependent on the concentration of ethanol allowable in the stripped (regenerated) solvent. Higher solvent flowrates are possible with the milder conditions and shorter residence time. On the other hand, more complete stripping required lower stripper pressures, higher temperatures, and longer residence times. Lower pressures and higher temperatures lead to considerable pumping problems due to cavitation.

The following general procedure was always followed to ensure proper system operation. First, the hot oil bath preheat was turned on and the heating tapes were turned to half of their normal operating settings. Then the stripper pressure was set by means of a vacuum pump and manostat and solvent was started through the stripper. The Karr column was then turned on and the solvent flow was started. The heating tapes were then adjusted to operating values and the aqueous feed to the column was begun. After the system was in operation, adjustments were made in various operating conditions to reach those desired for that run. The system was operated at a given set of conditions for 30 minutes until samples were taken. Often the run conditions were changed slightly and other samples were taken 30 minutes later after a new steady-state had been reached.

7.5.4. Data Acquisition

Experimental data was gathered in the following manner. Temperatures were monitored at short intervals and the heating input was adjusted accordingly. Temperatures were monitored at the inlet, outlet, and center of the column with bare thermocouples projecting into the center of the column. Temperatures were also obtained just prior to the solvent feed to the stripper and at two points inside the stripper.

Aqueous feed flowrates were determined by pump calibrations against setting of the Lab Pump Jr. Solvent

flowrates were determined by measuring the solvent overflow rate from the Karr Column just prior to taking each set of samples (due to cavitation problems affecting the accuracy of the large solvent pump, solvent flow rates were measured directly). Feed, raffinate, extract, stripped solvent, and condenser product samples were taken 30 minutes after steady operating conditions were obtained for each run (temperatures and flowrates were maintained constant within ± 5°C degrees and ±20 percent). Runs in which mechanical difficulties prevented proper operation were not included in the data table.

7.5.5. Variation of Experimental Parameters

At the onset of an experimental series, it is necessary to determine which variables are significant and how to vary them throughout the runs. The major variables decided on for analysis were total flowrates (combined organic and aqueous), organic to aqueous ratio, mean solvent temperature in the column, the stroke rate and the ethanol concentration in the stripped solvent. The ethanol concentration in the stripped solvent was varied for two reasons. First, this variable allows for the possibility of incomplete solvent stripping in the parameter models. Secondly, it allowed for the evaluation of various stripping conditions while performing the liquid/liquid extraction testing.

Solvent flowrates were varied from 80 to 310 ml/min and the aqueous flowrates from 2 to 9 ml/min. The solvent pump cavitated with the reduced stripper pressure at higher than 310 ml/min (lower rates at the higher temperature and lower pressure) and operation below 80 ml/min required a long a time to obtain steady state (approximately one hour or more). Also, the flowrates from the aqueous feed pump were not reproducible below 2 or above 9 ml/min.

Temperatures of the solvent in the column varied from 24°C to 74°C from run to run. Column temperatures below 40°C were difficult to control due to heating of the solvent in the stripper and temperatures above 73°C resulted in local "hot spots" where the ethanol began boiling inside the column.

The stroke rate was varied from settings of 3.5 to 4.2 which was 113 to 142 strokes per minute. Lower stroke rates led to uneven mixing and droplet dispersion and higher stroke rates led to excessive carryover of aqueous droplets with the extract. The stroke length was not varied because Karr (2) indicated that the column characteristics varied with the product of the stroke length and stroke rate. The

stroke rate was also easily adjusted. The stroke length was maintained at a constant valve of 1.905 cm.

The high, low, and intermediate values for each run variable were randomly assigned for various runs to prevent systematic errors from entering the analysis. The variables were altered (as much as operating conditions allowed) in accordance with statistical design methods outlined by Murphy (19) to make more efficient use of each data run. This method also simplified operation of the system because it would be very difficult to accurately reproduce run variables such as organic flowrate, and column temperatures, while changing just one operating variable.

7.5.6. Concentration Determinations

All concentration determinations were made using gas chromatography. Calibration curves and correlations were prepared to relate the area percent to the weight percent of the sample analyzed with the g.c. Since the quality (dryness) of the commercial absolute ethanol was unknown, a reliable standard was desired to properly correlate the dry end of the Area of Weight Percent of ethanol and water. Extremely dry (99.9 + %) ethyl alcohol was used. This extremely dry ethanol was used to make up dry standards for calibration and to verify the quality of the "absolute" ethanol.

The data used in both ethanol/H_2O and ethanol/propanol correlations is given elsewhere (34). When the data was graphed, however, the plot appeared linear from 99.9% to approximately 18 wt%. The ethanol-water data was then correlated in a linear form above 20% and to a quadratic form below 20%. The correlations used were:

For Ethanol > 20%

$$wt.\% = .92165 \ X(A\%) + 9.5270 \qquad (7.9)$$

with a correlation coefficient of .9979 and

For Ethanol

$$wt.\% = .003152 \ X(A\%)^2 + 1.12335(A\%) + .2548 \qquad (7.10)$$

With a correlation coefficient of .9968.

The ethanol-propanol data was not linear on normal graph paper, but was linear on Log/Log paper (see Ref 34). The ethanol to propanol weight ratio was correlated by eqn. 11:

$$\ell n\ W = .96466\ \ell n\ A - .079466 \tag{7.11}$$

$$\text{where } w = \frac{\text{wt EtoH}}{\text{wt. Propanol}}$$

$$A = \frac{\text{Area \% EtOH}}{\text{Area \% Propanol}}$$

and the correlation coefficient for this was .9988.

Aqueous samples could be injected with no prior preparation (no propanol spike was needed), and the weight percent ethanol could be determined directly due to the low solubility of Isopar L in water. For the organic samples, a tared amount of solvent and propanol were mixed and injected. Since the mass of propanol was known and the area ratios of propanol to ethanol are correlated, the ethanol and water concentrations could be obtained.

7.5.7. Density Determinations

Since the range of temperature was small (25 to 75°C) the density of Isopar L was measured at several temperatures and fitted to the linear equation

$$\rho_{I.L.} = 1.036764 - .000925\ T \tag{7.12}$$

where T = degrees Kelvin

with a correlation coefficient of .99823

The reason for using this correlation is that density for the ethanol/water mixtures is more strongly dependent upon ethanol concentration than temperatures so the density data in Lang's Handbook (3) from 75% to 15% at 25 degrees centigrade was fit to the equation

$$\rho = 1.00699 + .19459\ X_E \tag{7.13}$$

where X_E = mass fraction ethanol

the correlation coefficient was .9978

7.5.8. Viscosity Determination

The kinematic viscosity of Isopar L (34) was converted to viscosity using the density correlation and then fit to the exponential form recommended by Reid, Prausnitz, and Sherwood (19). The resulting equation for the viscosity in centipoise is:

$$\mu = \exp(1573. \; x \; (\tfrac{1}{T} - \tfrac{1}{329.154}) \tag{7.14}$$

where T = degrees Kelvin.

where the standard deviation = 0.050

7.5.9. Distribution Coefficient Determinations

The distribution coefficients in Isopar L were obtained from the correlations of Wahid Tawfik (7).

For Ethanol:

$$\ln DE = 1.86 + 1.44 \; (XE) - 1922/T \tag{7.15}$$

and for water

$$\ln DW = -5.18 + 4.86(XE) - 1321/T \tag{7.16}$$

where X_E = mass fraction Ethanol

D_E = distribution coefficient of ethanol

D_W = distribution coefficient of water

T = degrees Kelvin

7.5.10. Interfacial Tension Correlations

Treybal (20) indicates that Antoine's approximation cannot be relied upon, but found a linear relationship in ternary organic/aqueous systems between the interfacial tension and the $N = \ln[X_{AB} + X_{BA} + (X_{CA} + X_{CB})/2]$ where the concentrations in mole fractions are:

X_{AB} = water concentration in organic phase

X_{BA} = organic concentration in aqueous phase

X_{CA} = third component concentration in aqueous phase

X_{CB} = third component concentration in organic phase

Treybal found this relation successfully represented ternary organic/aqueous systems in equilibrium. A correlation obtained from his results is

$$\sigma = -7.409(N) - 5.374 \qquad (7.17)$$

where   in dynes per centimeter

N = the natural log of the mole fraction terms described earlier.

For industrial systems and/or those with more than three pure components, Treybal recommends that these systems be measured and correlated individually.

Interfacial tensions were measured for various mixtures of ethanol, water and Isopar L at equilibrium and non-equilibrium concentrations. These values were correlated with the relation

$$\sigma = \exp (3.78663 - 2.7893 \, XA - 10.353 \, XO) \qquad (7.18)$$

to allow for zero ethanol concentrations in both phases.
Where

XA = mass fraction ethanol in aqueous phase

XO = mass fraction ethanol in organic phase.

The actual values versus the calculated values can be seen elsewhere (34) both correlations are compared. All calculations, however, were done with the exponential relation be..iuse the Treybal equation is for equilibrium mixtures only.

7.5.11. Column Stroke Rate Determination

Calibration marks were inscribed on the speed indicator plate and the strokes per minute were counted at each even numbered setting. The strokes per minute were correlated linearly with the equation

$$\text{Strokes per minute} = 41.519(SK) - 32.61 \qquad (7.19)$$

where SK = speed setting

with a correlation coefficient of .9958.

The calibration data is shown elsewhere (34).

7.6 Experimental Results and Discussion

7.6.1. Solvent Extraction Data

The experimental data from the operation of the Karr column is given in ref. 34. The solvent flow rates were measured immediately before samples were taken for each run. These values, however, were not always representative of the average solvent flow rate during the run due to intermittent problems with pump cavitation. On the other hand, the feed rate data is considered reliable with the possible exception of the flow rates below 2.0 milliliters per minute. The feed and raffinate concentrations are considered very reliable, while most of the extract concentrations are considered accurate to ±0.1 percent ethanol. The ethanol concentrations in the stripped solvent are considered "most suspect" since their concentrations were approximately in the range of the error in our measurement techniques.

The temperatures are considered accurate to ±0.5 degrees Celsius, while linear temperature profiles are considered a good approximation between thermocouples. The temperatures were taken throughout the run and recorded at the time of the samples were taken. Sometimes there were significant temperature drifts during a run (±5°C). The stroke speed was adjusted initially and remained constant throughout each run. The complete solvent extraction data is also on elsewhere (34).

7.6.2. Dimensional Analysis

Dimensional analysis was used for fitting the data, instead of a simple polynomial fit, in hopes of providing generalized correlations of value in modeling other

systems. Hughs (21) confirms the fact that systems such as pulse columns where bubbles and drops are constantly being reformed are extremely complex mathematically. This method is especially useful in systems that are too complex for an analytic solution, such as solvent extraction, in a pulse or reciprocating plate extraction column.

The choice of parameters is important in obtaining a generalized relationship for the fitted function. Over-specifying the parameters can lead to analysis problems and underspecification can lead to a poor fit of the results.

The major parameters chosen were those of easily measured physical properties, dimensions, flowrates, and column settings that would be necessary to uniquely define the system. Some initial modifications were made of the input parameters to give parameters of a desired form to aid analysis. One modification was that total volumetric flowrate and organic aqueous ratios were used instead of organic flowrate and aqueous flowrate. Also, the density of the continuous phase and density difference between the continuous and dispersed phases were used rather than both densities. The parameters used in forming the dimensionless groups are shown below in Table 7.1.

The fitted function should be a dimensionless efficiency function or ratio of the input and output concentrations. In the case of this system, there is considerable choice as to the possible column performance or efficiency functions that could be used. Henley and Seader (3) state that despite compartmentalization, mechanically assisted liquid-liquid extraction columns operate more like differential contact devices than stage contactors. Therefore, it is more common to consider stage efficiency in such terms as height equivalent to a theoretical stage (HETS) or some function of mass transfer parameters such as height of a transfer unit (HTU). Although not on as sound a theoretical basis as the HTU, the HETS is preferred because it can be applied directly to determine column height from the number of equilibrium stages.

Table 7.1
Parameters Used in Dimensionless Groups

Parameter Description	Symbol Used	Dimensions (Power)		
		M	L	T
Density of Continuous phase		1	-3	0
Density of Difference of Dispersed and Continuous Phases		1	-3	0
Viscosity of Continuous Phase*		1	-1	-1
Total Volumetric Flowrate	V_t	0	3	-1
Interfacial Tension		1	0	-2
Column Diameter	D	0	1	0
Stroke Rate	S.R.	0	0	-1
Stroke Length	SL	0	1	0
Gravitational Acceleration	g	0	1	-2
Organic to Aqueous Ratio (Mass)	OA	0	0	0
Void Fraction		0	0	0
Distribution Coefficient	DE	0	0	0

*The continuous phase was Isopar L.

Smoot and Babb (10) define three different transfer units (NTU). By the original definition, the "true" number of transfer units is given by:

$$NTU = K_z \, ah/V_z \qquad (7.20)$$

where K_2 = overall mass transfer coefficient

a = interfacial area

h = column height in feet

V_z = superficial velocity of the given phase

The "measured" number of transfer units has been defined as:

$$NTU_m = \int_{Z_1}^{Z_2} \frac{dz}{Z_e - Z} \qquad (7.21)$$

where Z_i = concentration at point i

Z_e = equilibrium concentration with other phase at point i

This can be obtained graphically if the concentration profiles are known (which is not the case with the present study). The third method is termed the "apparent" number of transfer units. This equation assumes both a straight equilibrium line and a straight operating line, and is given by:

$$(NTU)_{Ap} = \frac{1}{[(X_i - X_o)/(D_e(Y_o - Y_i)] - 1} \ln \frac{x_i - (D_e)Y_o}{x_o - (D_e)Y_i} \qquad (7.22)$$

where X_i = mass fraction solute in feed stream

X_o = mass fraction solute in raffinate stream

Y_i = mass fraction solute in incoming solvent

Y_o = mass fraction solute in extract

D_e = distribution coefficient of solute

The "apparent" number of transfer units could be either higher or lower than the "actual" number of transfer units depending upon the system Peclet numbers and the magnitude of the number of transfer units. The "apparent" number of transfer units was calculated for forty-two runs (see Table 7.2).

The traditionally useful values to fit would be the number of transfer units NTU or the number of theoretical stages. Unfortunately these functions are extraordinarily sensitive to "noise" when the extraction factor is close to unity and when the solute concentration in the incoming extractant stream is significant in relation to the equilibrium concentration in the extractant stream.

In the case of the system studied, both of these conditions exist. The significance of calculating these functions is illustrated in Table 3 where the number of theoretical stages (or number of theoretical plates, NTP), were calculated by 3 standard methods. the first method assumes that the solute concentration in the incoming extractant stream is insignificant, which yields fractions of a theoretical stage (22). This equation is:

$$NTP(A) = \frac{\ln\left[(E-1)/\phi + 1\right]}{\ln E} - 1 \tag{7.23}$$

where $E = D_e * O/A$

a simplified Kremser Equation. A more generalized form of the Kremser equation is presented by Treybal (20). This is the Kremser-Brown-Saunders equation and is as follows:

$$NTP(T) = \frac{\ln\left[(X_i - Y_i/D_e)/(X_o - Y_i/D_e)*(1 - 1/E) + 1/E\right]}{\ln(E)} \tag{7.24}$$

when   or

$$NTP(T1) = (X_i - Y_i/D_e)/(X_o - Y_i/D_e) \tag{7.25}$$

when $E = 1$.

Table 7.2   Apparent Number of Transfer Units

Run	NTU$_x^a$
2	2.094
4	0.854
6	1.617
9	1.646
10	1.880
11	1.192
12	3.000
13	1.902
14	3.834
22	1.874
23	2.624
24	2.335
25	2.716
26	6.414
27	1.339
30	*
31	2.3806
33	0.555
36	*
37	*
39	0.401
51	1.059
52	2.780
53	*
54	*
55	*
58	0.230
59	0.3447
60	0.388
62	0.247
63	0.236
69	0.7071
70	0.460
71	1.393

[1]   Identical values were obtained when "apparent" NTU's were calculated from organic equilibriums.

*   Indeterminate in Calculating Equation

This equation assumes linear equilibrium and operating lines. These values are also listed in Table 7.3. The fourth method used was a numerical simulation of the graphical method with the only assumption being that of a linear operating line.

All of these equations are sensitive to noise of either the organic flowrate, the ethanol conentration in the stripped solvent, or both. A mass balance was performed on the ethanol in the column and volumetric flowrate of the feed concentration was calculated. This was presented in Table 7.4 as a ratio of the difference of the actual and calculated feed rates divided by the actual feed rate. The cut-off point decided on for this ratio was 0.333 which included approximately half of the run data. Both initial parameter determinations and the final parameter fits were then compared to those of the forty-two runs which had "acceptable" mass balances.

In this analysis, the fitted parameter is dimensionless:

$$F = (X_i - Y_i/D_e)/(X_o - Y_i/D_e) \qquad (7.26)$$

and it takes into effect the ethanol concentration in the stripped solvent which is significant in this case, and is equal to the number of theoretical stages when the extraction factor E is equal to 1.0. Also, the function, F approaches infinity as the X_o approached the value of Y_i/D_e and approaches 1.0 as X_o approaches X_i.

Using the dimensions mass (M), length (L), and time (T), the Buckingham Pi Theorem (33) gives the number of parameters minus three, (NPAR-3) dimensionless groups (9 for the present case). The void fraction (ε), organic to aqueous-ratio (O/A), and distribution coefficient for Ethanol in Isopar L (DE) are already suitable dimensionless groups so three groups are already decided upon. Since the void fraction is constant, it is part of a constant coefficient on the parameter fit and will not be mentioned further. One can then choose any three core variables, as long as they contain L, M, and T, and do not in themselves form a dimensionless group. The three chosen were column diameter (D), the stroke rate (SK), and the density of the continuous phase. These were used in combination with the other variables to form the eight dimensionless groups indicated by the Buckingham Pi theorem. The groups are shown below in Table 7.5.

Table 7.3. Theoretical Stage Calculations

Run #	NTP (A)	NTP (T)	NTP(T1)	NTP (G)
1	.0079	.1064	.0936	.7671
2	.0514	.4797	.3348	1.7047
3	.0296	.2312	.2000	.1585
4	.0710	.5065	.4139	.1753
5	.0329	.2958	.2559	1.7303
6	.0963	.7677	.5427	1.6792
7	.1703	.9390	.6639	.0894
8	.2305	1.3004	.8136	.1405
9	.2226	1.0342	.9466	1.4248
10	.1298	.7605	.5645	1.5728
11	.1739	.7971	.7451	1.7884
12	.2222	1.6375	1.0979	2.7099
13	.1344	.7930	.8400	1.3484
14	.4939	2.5986	1.6061	2.3675
22	.2427	1.0591	1.3758	1.1049
23	.2206	.7568	1.0137	1.0124
24	.1969	.7078	.9200	1.1642
25	.2979	.89551	1.2127	2.9077
26	.2698	.9826	.9767	2.3121
27	.2414	.8676	.9163	1.6306
28	*	*	4.3863	*
29	.3375	2.2184	1.2970	1.4896
30	.3034	*	5.3642	5.8603
31	.2545	1.2519	1.3174	2.8864
32	.2343	.8919	1.1045	.1199
33	.1242	.5293	.5094	.2646
34	.2936	1.08341	.8665	.0116
35	*	*	3.5605	*
36	.2255	2.4550	1.8453	5.6564
37	.4043	13.2362	3.7506	3.7028
39	.0277	.2210	.2266	.5589
40	.0849	.6346	.6489	3.8682
41	.0948	.5623	.5775	2.4230
42	.1232	.6094	.6527	2.1856
43	.0811	.8718	1.2397	3.6288
44	.0993	.4207	.5574	2.7049
47	.3671	.9284	1.5949	.0368
48	.0020	.0764	.0684	.7541
49	.1664	.6904	.6291	.3796
50	.1445	.5676	.7057	.1993
51	.2288	.7832	.9453	1.7837
52	.3175	1.0485	1.2938	2.8317
53	.3841	1.2583	1.4760	3.4836
54	.2680	2.1200	1.9374	4.3521
55	.2302	4.1579	3.3942	5.7966
58	.1494	.5312	1.4183	.1241
59	.1564	.4770	1.2151	.1256
60	.1381	.3990	.9951	.1592
61	.0640	.2627	.5537	.2902
62	.1678	.4630	1.3451	.1496
63	.1873	.4587	1.3542	.1628
64	*		.4735	1.9351
65	*	.3530	1.0976	1.7819
66	*	.2852	.7683	.0941
67	.0394	.4365	1.0458	1.8163
68	.0248	.5134	1.7904	1.7295
69	.0689	.6513	2.3547	1.5464
70	*	.4937	1.4354	.0112
71	.2941	1.1781	5.7503	2.8235

*Indicates indeterminate in the calculating equation.

Table 7.4. Feed Mass Balance on Ethanol

Run #	(F-FC)/F	Run #	(F-FC)/F
1	.6068	40	1.0656
2	.2408	41	.5882
3	.9136	42	.6030
4	.2886	43	.4268
5	.8208	44	1.2443
6	.2447	47	.5436
7	.5698	48	2.4705
8	.7348	49	.8644
9	.2605	50	.4231
10	.1497	51	.1946
11	.2947	52	.0499
12	.2925	53	.2418
13	.0126	54	.1022
14	.3596	55	.1661
22	.1406	58	.4351
23	.2812	59	.0824
24	.3162	60	.2096
25	.2299	61	.5786
26	.2039	62	.1951
27	.1857	63	.2152
28	1.0000	64	.4739
29	.7798	65	1.0280
30	.1950	66	.4908
31	.1327	67	.5298
32	.6483	68	.4386
33	.3437	69	.1229
34	.4978	70	.0778
35	1.0023	71	.1477
36	.0555		
37	.0659		
39	.1139		

Table 7.5. Initial Dimensionless Groups

Number	Group	Label or Description
π_1	$\Delta\rho/\rho$	Relative density difference
π_2	$\mu_c D^4 \rho_c SK$	*
π_3	$V_t SK/D^3$	*
π_4	$\sigma \, SK^2 D^3/\rho_c$	Surface tension to inertial force
π_5	SL/D	Ratio of stroke length to Column diameter
π_6	$g \, SK^2/D$	*
π_7	O/A	Organic to Aqueous Ratio (by weight)
π_8	D_e	Distribution Coefficient

Here the dimensionless group, π_s, is a constant and three of the groups do not appear to resemble any of the classical groups. These groups can be combined, however, to form other dimensionless groups which resemble more traditional groups.

Quite often it is necessary to modify dimensionless groups to place certain parameters together. Here, for example, the stroke rate was used in conjunction with the stroke length in a velocity-like term because of the relation between strokes per unit time and length per stroke. Also, Karr (2) indicates that the column performance will be the same for any combination of stroke length and stroke rate where the product of the two is the same. These new groups are illustrated in Table 7.6.

Table 7.6. Modfified Dimensionless Groups

Number	Group	Label or Description
π_1	$\Delta\rho/\rho$	Relative Density Difference
π_2	$V_t \rho/D\mu$	Reynolds Number
π_3	$SL^2 SR^2 D\rho_c/\sigma$	Weber Number
π_4	$gSK^2 SL^2/D^2$	Backmixing Number*
π_5	O/A	Organic to Aqueous Ratio (by weight)
π_6	D_e	Distribution Coefficient
π_7	$V_t SK\ SL/D^4$	Suspension Number (higher number will result in longer column hold up)*

*Non-standard dimensional group.

The calculated values were then compared to the experimental values for the fits using both sets of dimensionless groups. The weak variables were discarded in accordance with Taylor (23) and the final fits of both sets was compared.

In a system as complex as this reciprocating plate column, the point at which the physical properties of the solvent are measured, and/or calculated is extremely significant. Viscosity of the continuous phase in the column, for example, has a very strong dependence on the temperature. Under the present operating conditions, the viscosity of Isopar L can vary from 2.0 to 0.86 centipoise. For this analysis, therefore, the viscosity taken at the average column temperature. However, this is not a generally correct assumption, if there is a large temperature difference between the top and the bottom the column, because the viscosity is an exponential function of temperature. In this system, however, the viscosity at the average temperature was found to be very close to the average viscosity.

The density is another easy to measure physical property, but can vary widely depending upon column conditions and where it is measured in the column. The density of the continuous phase, Isopar L, is a strong function of temperature, and not significantly affected by slight ethanol concentration changes. On the other hand, the aqueous density is a relatively strong function of the ethanol concentration and a much weaker function of temperature. To avoid iterative calculations by using average concentrations, the aqueous density is calculated at the feed conditions which gives us a minimum density for the aqueous phase. Since the continuous phase density is a linear function of temperatures, it is taken at the average column temperatures.

In the system, the interfacial tension changes radically from the top of the column to the bottom. It is also a relatively strong function of the ethanol concentration in both phases and a weaker function of temperature. The lowest value of the interfacial tension is at the top where the maximum ethanol conentration occurs in both the aqueous and organic phases. The maximum interfacial tension occurs at the bottom of the column where the aqueous raffinate and the stripped organic streams come into contact. Using an average of these, a minimum, or

Table 7.7
Calculated Interfacial Tension
(dynes per centimeter)

Run	Top of Column	Bottom of Column	Average of Top and Bottom	Calculated from Feed and Stripped Solvent Concentrat.
2	9.926	14.017	11.971	10.70568
4	10.115	14.996	12.556	10.63486
6	9.693	15.478	12,586	10.42762
9	9.870	19.359	14.615	10.57110
10	9.514	16.655	13.085	10.48475
11	9.534	18.255	13.894	10.46957
12	9.016	18.273	13.644	10.16622
13	8.716	17.441	13.078	9.81468
14	8.752	22.863	15.808	9.96520
22	9.321	20.435	14.878	10.34631
23	9.073	20.510	14.792	10.57700
24	9.111	19.855	14.483	10.57590
25	9.111	22.342	15.726	10.64401
26	8.760	20.591	14.675	10.61869
27	9.418	20.236	14.827	10.62969
30	8.863	19.368	14.115	9.92152
31	9.086	20.055	14.570	10.28762
33	10.350	17.097	13.723	11.10790
36	8.215	18.247	13.231	9.79581
37	7.931	20.937	14.434	9.79581
39	10.243	13.469	11.856	10.74803
51	9.531	20.458	14.995	10.57080
52	9.088	22.218	15.653	10.51731
53	8.801	23.190	15.995	10.52166
54	8.706	19.660	14.183	9.98130
55	8.445	18.595	13.520	9.83309
58	10.157	20.906	15.531	10.38255
59	10.157	21.391	15.774	10.54396
60	10.157	20.916	15.537	10.65479
62	10.400	22.467	16.434	10.70380
63	10.504	23.473	16.988	10.81183
69	5.599	22.339	13.969	6.06159
69	5.599	22.339	13.969	6.06159
69	5.599	22.339	13.969	6.06159
69	5.599	22.339	13.969	6.06159
69	5.599	22.339	13.969	6.06159
70	5.629	17.659	11.644	6.02137
70	5.629	17.659	11.644	6.02137
70	5.629	17.659	11.644	6.02137
71	5.442	29.463	17.453	6.01491
71	5.442	29.463	17.453	6.01491
71	5.442	29.463	17.453	6.01491

maximum value would involve an iterative procedure in a predictive equation.

Two other possibilities are using an interfacial tension values calculated at some equilibrium concentration, or calculated for a hypothetical mixture of the stripped solvent and the aqueous feed. This last choice was used for several reasons. First, it gives a value between the highest and lowest Interfacial tension in the column and it was simpler to measure one interfacial tension of the feed mixture and solvent and use that value. Table 7.7, for example, shows the calculated interfacial tensions at the top and bottom of the column and with the interfacial tension calculated with the aqueous feed and stripped solvent.

The distribution coefficient was calculated at the feed concentration and average column temperature. The organic to aqueous ratio (mass flowrates) was calculated from the incoming flowrates, and density correlations.

A non-linear least-squares fit of the form:

$$F = \Delta \pi_1^{B(2)} \pi_2^{B(3)} \ldots \pi_n^{B(n+1)}$$ was used to model the

results. Seven dimensionsless groups were used to model three major fitted functions. The first function tried was

$$\frac{(Y_i - X_o)}{(X_o - Y_i/D_e)}$$

as suggested by Alders (14). This function was not fitted well by any combination of the dimensionless groups. Iterations utilizing the Marquardt Algorithm (33) resulted in some powers as high as 31. The next combination used was the ratio X_o/X_i which gave reasonable results for data sets with low solvent concentrations, but not for those with significant ethanol concentrations in the stripped solvent feed.

The function fitted best was eqn. 7.27 which gave reasonable fits to most of the data. This group can be substituted into the Kemsor-Brown-Saunders equation (20,22,23) directly to obtain the number of theoretical

stages since the extraction factor E is known. Also, this form can be used to solve for X_o, which will allow the calculation of NTU's from this relation numerically, or any other method desired. Using the statistical analysis in the non-linear least squares program, none of the parameter values crossed over zero in the nonlinear confidence interval calculations.

The resulting fit obtained is given below:

$$\frac{(X_i - Y_i/D_e)}{(X_o - Y_i/D_e)} = B1 \, \pi_1^{B2} \, \pi_2^{B3} \, \pi_3^{B4} \, \pi_4^{B5} \, \pi_5^{B6} \, \pi_6^{B7} \, \pi_7^{B8} \tag{7.27}$$

where   B1 = .0118
        B2 = 4.50
        B3 = 1.43
        B4 = 3.08
        B5 = -1.27
        B6 = 0.56
        B7 = -2.31
        B8 = -2.71

and the dimensionless groups are as defined in Table 7.6. The fit of this function can be seen in Table 7.8. The average deviation of 24.9 percent was considered acceptable due to the errors present in several of the operating variables. The observed verses the calculated values for the function can be seen in Figure 4, page 64. Figure 4 indicates that there is no high or low bias to the correlation.

These groups were multiplied together to get a relationship of the various dimensional parameters to the fitted function instead of dimensionless groups. The F function is dependent upon the following variables to a power times a constant:

The simplified equation is:

$$F = K \Delta \rho^{4.50} \, \rho_c^{0.01} \, V_t^{-1.28} \, (SL \cdot SK)^{0.91} \, \sigma^{-3.08} \cdot \tag{7.28}$$

$$\mu^{-1.43} \, \left(\frac{O}{A}\right)^{0.56} \, (D_e)^{-2.31}$$

where K is a constant.

The consistency of these results can be determined by comparing the improved column efficiency, where a higher F value indicates better performance, and the coefficient on each variable. Column performance appears to be a strong function of the density difference of the two liquid phases $\Delta\rho$, the interfacial tension, , the viscosity μ, the distribution coefficient, D_e, the stroke rate times the stroke length, (SL·SK), the organic to aqueous ratio, (O/A), and the total volumetric flowrate in the column, V_t. The density of the continuous phase, ρ_c, appears to have only a slight effect on F.

In the system the density difference, $\Delta\rho$, determines how small the droplets of the dispersed phase can be while still maintaining countercurrent flow. A larger density difference will allow smaller droplets which would incrase F which agrees with the positive exponent. This is also consistent with correlations by Smoot (10,11), Loggdale (15) and Mar (12). The density of the continuous phase is not expected to significantly affect column performance which is consistent with its small exponent.

The interfacial tension has a strong influence on drop size of the dispersed phase and is a strong influence on column performance. A lower interfacial tension results in smaller droplets which increases column performance (within the limits of operation) and is consistent with its negative exponent. This observation is in agreement with Hiromichi (9) who found that the droplet size was significantly larger with larger interfacial tensions. This is also consistent with Henley and Seaders (3) correlation (equation 7.1).

The viscosity has a strong effect on the operating conditions as a lower viscosity will allow better dispersion and formation of smaller droplets of dispersed phase. This could be accomplished by allowing the stroke rate to be increased without carryover of the dispersed phase droplets. Thus, the negative exponent is consistent with these expectations. This is also consistent with correlations of Logsdale (15), Smoot (10,11), and Kung (109), where the viscosity of the continuous phase has a negative exponent.

The distribution coefficient, D_e, has a negative exponent for the function F. This is opposite the effect expected if the fitted function were X_i/X_o, but suggests that the ethanol concentration in the stripped solvent feed in our system was very significant to column performance. Also, D_e appears in the denominator of the Y_s/D_e in the fitted function. Otherwise the exponent of DE would be

expected to be positive. In the case of this system, the effects of the solute, ethanol, in the incoming extractant stream, Y_i, more than outweigh the effects of the distribution coefficient upon the function F. Increasing the D_e increases the extraction factor and decrease the raffinate concentration. Its effect upon the number of theoretical stages, however, depends upon YS.

The function F can easily be substituted into the modified Kremser-Brown-Saunders Equation (eqn. 7.24) to get the number of theoretical stages. If other forms of equation, are desired, all of the factors are known except X_o in the F function so X_o can be determined from the correlation. The extract composition, Y_o, can then be calculated · by a mass balance and the number of transfer units or number of theoretical stages can be calculated by any method desired. No direct fit of theoretical stages was done because of the large differences in the number of theoretical stages calculatd by various methods.

Optimum operating conditions predicted by these correlations and actual observations indicate that the higher the temperatures of the solvents, the more efficient the column would operate. This would be due to the decrease in viscosity which would allow smaller droplets to be used without carryover, and a decreased interfacial tension which would tend to make it easier to produce the smaller droplets with less energy input. The fit of this seven variable fit are shown in Table 7.8.

A correlation matrix of the exponents of the dimensionless groups π_1, π_2, π_4, π_6 and π_7 showed them to be correlated (either positive or negatively) between 0.97 and 0.99 with each other. This indicates a stronge dependence of one variable upon the other. These groups are the relative density difference, the Reynolds number, the backmixing number, the distribution coefficient, and the suspension number.

Since these dimensionless groups are highly correlated, a three group correlation should give almost as accurate a value as seven did. The distribution coefficient, D_e, was chosen because of its use in the extraction factor. The F function (eqn. 7.26) was fit with the three dimensionless groups the Weber Number, the organic to aqueous ratio, and the distribution coefficient. The form of the equation used was

$$F = B1 \; \pi_3^{B2} \; \pi_5^{B3} \; \pi_6^{B4} \qquad (7.29)$$

where   B1 = 1.732
          B2 = 0.911
          B3 = 0.245
          B4 = 0.550

The exponents on the three dimensionless groups fit are all positive. The sign and the relative magnitude between the Weber number W and the O/A ratio is the same but in this case the exponent on the distribution coefficient is positive instead of negative as with the seven dimensionless groups.

The positive sign on the exponent of the distribution coefficient would be expected with low solute (ethanol) concentrations in the incoming solvent feed, but this was rarely true with our system. Instead, this positive exponent can be explained by the high correlation of the distribution coefficient with the other dimensionless groups, the Reynolds number, the relative density difference, the backmixing number, and the suspension number. If all of the exponents of the highly correlated groups are added together with the sign of the inversely correlated groups multiplied by -1.0, a positive exponent is obtained. The high correlation of these groups can be explained in this system, because the densities, viscosities, and distribution coefficients are all strongly influenced by the temperatures and phase concentrations. These have a strong effect upon what stroke rate can be set with the column.

The results of the fit with three dimensionless groups can be seen in Table 7.9. These values are only slightly less accurate than the seven parameter fit with an average deviation of 27.7 percent.

7.6.5. Extract Dryness Prediction

Wahid Taufik (20) found that the distribution coefficients of both the water and ethanol in the solvent, Isopar L could be represented by correlations of the equilibrium ethanol concentration in the aqueous phase and the system temperature.

It is assumed that percent dryness (ethanol concentration on a solvent free basis) could be calculated as shown, although the column is not in equilibrium with the feed.

$$\text{Extract Dryness} = 100 \; \frac{D_e X_e}{D_e X_e + D_w X_w} \qquad (7.30)$$

Table 7.8.
Observed versus Calculated Function Values (8 Parameters)

Run	F Observed	F Calculated	F(obs.)-F(calc.)
2	1.335	1.342	-0.006
4	1.414	1.104	0.310
6	1.543	1.222	0.321
9	1.947	1.470	0.477
10	1.565	2.062	-0.497
11	1.745	2.074	-0.329
12	2.098	2.621	-0.524
13	1.840	2.046	-0.206
14	2.606	2.337	0.269
22	2.376	1.608	0.768
23	2.014	1.756	-.258
24	1.920	1.732	0.188
25	2.213	1.693	0.520
26	1.977	2.092	-0.115
27	1.916	2.011	-0.949
30	6.365	2.462	3.903
31	2.317	2.161	0.156
33	1.509	1.637	-0.128
36	2.845	2.255	0.590
37	4.751	2.314	2.437
39	1.227	1.497	-0.270
51	1.945	1.457	0.488
52	2.294	1.484	0.810
53	2.476	1.482	0.994
54	2.937	1.956	0.981
55	4.394	2.007	2.387
58	2.418	2.695	-0.277
59	2.215	2.620	-0.405
60	1.995	2.525	-0.530
62	2.345	2.600	-0.255
63	2.355	2.510	-0.156
69	3.355	4.210	-0.855
70	2.435	4.693	-2.258
71	6.750	4.710	2.040

Average Deviation 24.9%

Table 7.9. Measured and Calculated F Values Using the 4
Parameter Model

Run	F Observed	F Calculated	F(obs.)-F(calc.)
2	1.335	1.405	-0.070
4	1.414	1.440	-0.026
6	1.543	1.556	-0.013
9	1.947	1.628	-0.319
10	1.565	1.787	-0.222
11	1.745	2.004	-0.259
12	2.098	2.023	0.745
13	1.840	2.274	-0.434
14	2.606	2.000	0.605
22	2.376	1.808	0.568
23	2.014	2.276	-0.262
24	1.920	2.283	-0.363
25	2.213	2.283	-0.070
26	1.977	2.138	-0.161
27	1.916	2.168	-0.252
30	6.365	1.788	4.577
31	2.317	2.009	0.308
33	1.509	1.358	0.151
36	2.845	1.456	1.389
37	4.751	1.447	3.304
39	1.227	1.315	-0.088
51	1.945	1.485	0.459
52	2.294	1.463	0.831
53	2.476	1.443	1.033
54	2.937	1.473	1.464
55	4.394	1.522	2.871
58	2.418	1.997	0.421
59	2.215	1.978	2.366
60	1.995	1.985	0.010
62	2.345	2.088	0.257
63	2.354	2.068	0.286
69	3.355	4.305	-0.950
70	2.435	4.267	-1.832
71	6.750	4.300	2.450

Average Deviation is 27.7%

where X_e = concentration of ethanol in aqueous phase

X_w = mass fraction of water in the aqueous phase

D_e = distribution coefficient of ethanol (equation 13)

D_w = distribution coefficient of water (equation 14)

The results of these calculations are shown in Table 7.10.

The measured values indicate good agreement with the calculated values in dryness of the ethanol in the extract with an average deviation of less than one percent. Due to temperature variations within the column and the exponential effect of the distribution coefficients by the temperature changes, this approximation of the extract dryness is considered sufficiently accurate for the initial modeling of this extraction system.

7.6.6. Discussion of Results

Many problem areas became apparent while modeling this system. First, many of the operational parameters could not be changed over a large range and still maintain system operation. This situation reduced the variation necessary for statistically significant modeling of these parameters. Second, since only one solvent system was studied, it was not possible to change many parameters without altering others simultaneously. For example, a change in temperature will affect the densities, viscosities, concentrations, distribution coefficients, and interfacial tensions. Changes in concentration also affected many of these parameters also. Also, some significant factors were not changed during the runs such as plate spacing, plate void fractions and column diameter.

The fit of the model is reasonably good considering the variations in some of the parameters such as the organic to aqueous ratio and temperature variations. The model for determining the column efficiency fit the data to within 24 percent for the seven variables and 27 percent for three variables. This is well within the range of errors reported by other researchers in similar systems (111,112,118) where average deviations of 27 to 30 percent were reported. The extract dryness was correlated well with column temperatures and aqueous feed concentrations.

Table 7.10.   Extract Dryness Verses Calculated Dryness
(percent)

Run	Analyzed Dryness	Calculated Dryness	Actual Calculated Dryness
6	89.0	95.9	-6.9*
7	87.0	95.8	-8.8*
8	97.2	95.8	1.4
10	96.8	95.9	0.9
11	96.2	95.9	0.3
12	92.4	95.9	-3.4
13	98.1	95.8	2.3
28	96.4	95.9	0.5
32	94.2	95.8	-1.9*
33	93.6	95.8	-2.2*
34	97.0	95.8	1.2
35	96.8	95.8	1.0
39	93.7	95.8	-2.1
43	89.5	95.9	-6.4*
44	81.3	95.8	-14.5*
47	93.1	95.9	-2.8*
48	97.3	95.8	1.5
50	94.5	95.8	-1.3*
51	96.1	95.8·	0.3
52	93.9	95.8	-1.9
53	96.1	95.8	0.3
55	96.0	95.8	0.2
59	98.0	95.8	2.2
60	92.0	95.8	-3.0
61	94.0	95.8	-1.8*
62	84.0	95.8	-11.8*
63	88.9	95.8	-6.9*
64	89.6	96.5	-6.9*
65	98.0	96.5	1.5
66	97.8	96.2	1.6
67	98.9	96.0	2.9
68	79.6	96.4	-16.8*
69	94.3	96.4	-2.1
70	83.9	96.5	-12.6*
71	91.3	96.5	-5.2*

* Mass balance indicates aqueous phase contamination   of
sample.

The number of theoretical plates or stages (NTP's) and the "apparent" number of transfer units were calculated using the eight parameter correlation (eqn. 7.27). For the number of theoretical plates, the F function was substituted directly into the Kremser-Brown-Saunders equations. For the "apparent" number of transfer units, the raffinate concentration was calculated from the function F by the equation:

$$X_o = \frac{(X_i - Y_i/D_e)}{F} + Y_i/D_e \qquad (7.31)$$

The extract concentration, Y_o, was then calculated by a mass balance and the resembling values were substituted into eqn. 7.22 as suggested by Smoot and Babb (10) to calculate the apparent number of transfer units. The results are shown in Table 7.10.

This current model would be of use in a qualitative manner for modeling other systems but could easily be applied to other systems using the data from other systems to determine new exponents and coefficients. As a rough comparison to other models. Henley and Seader (3) give an approximation for the height of a theoretical stage base only on interfacial tension. This correlation (equation 1) yields a height of twenty-three inches, but it is only applicable to low viscosity systems while Isopar L is a high viscosity system. Thus, our average height of a theoretical stage of 90 inches (from graphical calculations) is not out of line with that predicted here (greater than 23 inches).

For future development of this model, other solvents of widely different physical characteristics and distribution characteristics should be modeled along with the use of different sized columns. These would allow large changes in one parameter without directly changing others simultaneously in the same direction.

Table 7.11 Comparison of Theoretical Stages vs Transfer
Units Using the 8 Parameter F Correlation

Run	NTP	NTU (App.)
2	.448	.454
4	.123	.047
6	.288	.275
9	.507	.672
10	1.694	3.709
11	1.240	1.899
12	2.582	3.138
13	.967	1.023
14	2.089	4.888
22	.517	.393
23	.613	.690
24	.588	.653
25	.555	.670
26	1.097	1.586
27	.960	1.337
30	1.971	.599
31	1.054	.966
33	.617	.838
36	1.462	.881
37	1.612	1.038
39	.499	.588
51	.395	.526
52	.428	.540
53	.435	.562
54	.950	.587
55	.9151	.000
58	.590	.037
59	.575	.175
60	.544	.242
62	.515	.127
63	.495	.193
69	.820	.307
70	.926	.332
71	.928	.373

7.7 Conclusion

The following conclusions are relevant to this work.

1. The drying cycle is technically feasible and can be operated successfully over a range of conditions.

2. Column extraction efficiency can be satisfactorily correlated from the physical properties and concentrations of the inlet streams.

3. The efficiency factor correlations are qualitatively consistent with earlier work in solvent extraction.

4. Further work is warranted to apply the dimensionless group models from solvent properties to other systems.

5. The HTU volumes are relatively high for this liquid/liquid system compared to other solvent extraction systems. This may be inherent to the system or a consequence of completing the experiments using an organic continuous phase in the contactor (vs an aqueous continuous operation).

7.8 References

1. Tedder, D. W., Fuel Grade Ethanol Recovery by Solvent Extraction. Technical Progress Report (for Period Sept. 15, 1981-Sept. 15, 1982,"Solar Energy Research Inst., under contract No. XK-0-9082-1, (1981).

2. Karr, Andrew E., "Performance of a Reciprocating-Plate Column." AIChE J., 15 (4), 446-452 (1959).

3. Henley, Ernest J., and J. D. Seader, Equilibrium Stage Separation Operations in Chemical Engineering, John Wiley and Sons, Inc., New York, N. Y., 516-522 (1981).

4. Skelland, A. H. P., and N. Chadha, "Selection of Dispersed Phase in Spray or Plate Extractions, Ind. Eng. Chem. Proc. Des. Dev., 20 (2), 232-239 (1981).

5. Kung, E. Y., and R. B. Beckman, "Dispersed-Phase Holdup in a Rotating Disk Extraction Column," AIChE J., 7 (2), 319-324 (June 1961).

6. Leonard, Ralph A., George J. Bernstein, Ralph H. Pelton and Alton A. Ziegler, "Liquid-Liquid Dispersion in Turbulent Couette Flow," AIChE J., 27 (3), (May 1981).

7. Tawfik, Wahid, Y. Efficiency of Ethanol Extraction from Aqueous Mixtures," Thesis, Georgia Inst. Tech., Atlanta, GA (1982).

8. Pratt, H. R. C., "Generalized Design Equations for Liquid-Liquid Contactors," Solv. Extr. and Ion Exch., (not yet published).

9. Hiromichi Fumoto, Eric Zimmer, Ryohei Kiyose and Erich R. Merz, "A Study of Pulse Columns for Thorium Fuel Reprocessing," Nuclear Tech., 58, 447-464, (Sept. 1982).

10. Smoot, L. D. and A. L. Babb, "Mass Transfer Studies in a Pulsed Extraction Column," I. & E. C. Fund., 1 (2), 93-103 (May 1962).

11. Smoot, L. D., B. W. Mar, and A. L. Babb, "Flooding Characteristics and Separation Efficiencies of Pulsed Sieve-Plate Extraction Columns," Ind. Eng. Chem., 51 (9), 1005-1009 (Sept. 1959).

12. Mar, B. W. and L. A. Babb, "Longitudinal Mixing in a Pulsed Sieve-Plate Extraction Column," Ind. Eng. Chem., 51 (9) 1009-1018 (Sept. 1959).

13. Bell, Richard H., and Albert L. Babb, "Holdup and Axial Distribution of Holdup in a Pulsed Sieve-Plate Solvent Extraction Column, "I.&E.C. Proc. Des. and Dev., 8 (3), 392-400 (July 1969).

14. Bell, Richard, L., The Effect of Interfacial Tension on the Holdup of Pulsed Sieve-Plate Solvent Extraction Columns, Ph.D. Dissertation, Univesity of Washington, Seattle, WA. (1964).

15. Logsdail, D. H., and J. D. Thornton, "Mass Transfer in a Pulsed Plate Column," Trans. Instn. Chem. Eng., 35, 331-335 (1957).

16. Teh, C. Lo and Andrew E. Karr, "Development of a Laboratory-Scale Reciprocating Plate Extraction Column," Ind. Eng. Chem. Proc. Des. Dev., 11 (4), 295-501 (1974).

17. Karr, Andrew E. and T. C. Lo, "Performance of a 36 Inch Diameter Reciprocating-Plate Extraction Column," paper presented at 82nd National Meeting of AIChE, Atlantic City, (Aug. 29-Sept. 1, 1976).

18. Lund, and Bjerem, "Practical Organic Chemistry," (1931).

19. Murphy, Thomas D., Jr., "Design and Analysis of Industrial Experiments," Chem. Eng., 84 (12) 180-186 (June 6, 1977).

20. Treybal, Robert E., Liquid Extraction, 2nd Ed#ort (for Period Sept. 15, 1980-Sept. 15, 1981,"Solar Energy Research Inst., under contract No. XK-D-9082-1, (1981).

21. Karr, Andrew E., "Performance of a Reciprocating-Plate Column." AIChE J., 15 (2), 232-239 (1959).

22. Henley, Ernest J., and J. D. Seader, Equilibrium Stage Separation Operations in Chemical Engineering, John Wiley and Sons, Inc., New York, N. Y., 516-522 (1981).

23. Taylor, Edward S., "Dimensional Analysis for Engineers" Clarendon Press, Oxford, (1974).

24. Skelland, A. H. P., and N. Chadha, "Selection of Dispersed Phase in Spray or Plate Extractions, Ind. Eng. Chem. Proc. Des. Dev., 20 (2), 232-239 (1981).

25. Kung, E. Y., and R. B. Beckman, "Dispersed-Phase Holdup in a Rotating Disk Extraction Column," AIChE J., 7 (2), 319-324 (June 1961).

26. Leonard, Ralph A., George J. Bernstein, Ralph H. Pelton and Alton A. Ziegler, "Liquid-Liquid Dispersion in Turbulent Couette Flow," AIChE J., 27 (3), (May 1981).

27. Tawfik, Wahid, Y. Efficiency of Ethanol Extraction from Aqueous Mixtures," Thesis, Georgia Inst. Tech., Atlanta, GA (1982).

28. Pratt, H. R. C., "Generalized Design Equations for Liquid-Liquid Contactors," Solv. Extr. and Ion Exch., (not yet published).

29. Hiromichi Fumoto, Eric Zimmer, Ryohei Kiyose and ⊔rich R. Merz, "A Study of Pulse Columns for Thorium Fuel Reprocessing," Nuclear Tech., 58, 447-464, (Sept. 1982).

30. Smoot, L. D. and A. L. Babb, "Mass Transfer Studies in a Pulsed Extraction Column," _I. & E. C. Fund._, 1 (2), 93-103 (May 1962).

31. Smoot, L. D., B. W. Mar, and A. L. Babb, "Flooding Characteristics and Separation Efficiencies of Pulsed Sieve-Plate Extraction Columns," _Ind. Eng. Chem._, 51 (9), 1005-1009 (Sept. 1959).

32. MAR, B. W. and L. A. Babb, "Longitudinal Mixing in a Pulsed Sieve-Plate Extraction Column," _Ind. Eng. Chem._, 51 (9) 1009-1018 (Sept. 1959).

33. Marguardt, D. W., "An Algorithm for Least-Squares Estimation of Non-linear Parameters," _J. SIAM._, 11.(2) 431 (1963).

34. Eckles, A. J., "Modeling of Ethanol Extraction in the Karr Reciprocating Plate Column", M.S. Thesis, School of Chemical Engineering, Georgia Institute of Technology (1984).

CHAPTER 8

LIQUID-PHASE DIFFUSION OF ETHANOL
IN ORGANIC SOLVENTS

(L. H. Krosnowski and C. W. Gorton)

8.1 Summary

The results of an experimental study using capillary cells to determine the diffusivity of ethanol in two solvents, Isopar L, and a twenty volume percent mixture of tridecyl alcohol in Norpar 12, are presented. Concentration and temperature dependent diffusivities determined from a preliminary data analysis and closed form expresssions determined by means of nonlinear least squares are given. At infinite dilution, ethanol appears to diffuse as a tetramer and this may be the predominate species in nonpolar mixtures.

8.2. Introduction

There were multiple objectives for performing the research. The first was to obtain diffusivities by the capillary tube method for ethanol in organic solvents. Secondly, a method was developed for analyzing the data which includes the concentration (to a certain extent) and temperature dependence of the diffusivity. Thirdly, it was hoped that the diffusivity measurements would lead to inferences concerning the mechanisms of transport. The results of the research are presented in greater detail by Krosnowski (1983). The present paper is a summary of this work.

8.3. Experimental Apparatus and Solvents

The capillary cells consisted of glass capillary tubing of uniform, precision bore of 0.5 mm. These were obtained from the Sargent Welch Scientific Company, in vials containing 250 capillary tubes of 13 cm length. The capillaries were then cut to nominal lengths of 2, 3, and 4 cm, with the aid of a fine steel file. One end of the capillary was then sealed with an acetylene torch. The other end of the capillary was ground flat and smooth so as to avoid having any rough open ends which might interfere with the diffusion process.

The capillary supports consisted of two different types of materials, depending on the temperature at which the experiment was conducted. For experiments performed at 25°C., styrofoam was found to be quite adequate. At temperatures of 45° and 65°C., however, teflon was chosen due to its resistance to organic solvents. In all cases, the supports were used to fix the capillary tube orientation in the bulk liquid. The capillary supports were placed in 400 ml beakers, so that the supports could be wedged in tightly. This avoided any shifting in position of the whole support after it was in the beaker.

To analyze the solution compositions, both before and after the experiments, a Hewlett Packard 5710A gas chromatograph, equipped with a HP 3390A peak integrator, was used. The column used in the gas chromatograph was packed with PORAPAK Q 80/100 mesh. The carrier gas used was helium. The oven temperature of the gas chromatograph was set at 140°C., and the injection port temperature was set at 250°C. The thermal conductivity detector was also operated at 250°C.

The water bath consisted of a circulating HAAKE-L heating element in a stainless steel reservoir. The temperature control of the bath was approximately $\pm$ 0.1°C.

The syringes used in the capillary cell experiments were of 10, 15 and 25 microliters. The syringes had an outside needle diameter just slightly smaller than the capillaries 0.5 mm inside diameter.

The reagents used in the research were ethanol, tridecyl alcohol, Norpar 12, and Isopar L. The ethanol used was absolute ethanol, obtained from the U. S. Industrial Chemical Company. Gas chromatography analyses showed that there was always some trace of water present, the driest being 99.9 percent ethanol.

Tridecyl alcohol is a distilled product, consisting of isomeric primary alcohols, mainly C_{13}. It has a specific gravity of 0.846 at 20°C., a viscosity of 42.3 cp at 20°C., and an initial boiling point of 253°C.

Norpar 12 is a narrow cut, normal parrafinic, Exxon Refinery solvent composed mainly of C_{11} and C_{12} mixtures of alkanes. It has a specific gravity of 0.751 at 15.6°C., a viscosity of 1.26 cp at 25°C., and an initial boiling point of 188°C.

Isopar L is a heavy narrow cut, isoparaffinic, Exxon Refinery solvent, composed of C_{12} mixtures of hydrocarbons. It has a specific gravity of 0.767 at 15.6°C., a viscosity of 1.99 cp at 15.5°C., and an initial boiling point of 188°C.

8.4. Experimental Procedure

The capillaries were filled with a solution of known concentration by means of the syringes. The syringe was inserted into the capillary until it reached the closed end and then the plunger was slowly pushed, forcing the solution in and the air out of the capillary. The filled capillary was then inserted into the capillary support which was in the beaker containing the solvent.

In all of the experiments, there was pure solvent surrounding the capillary tubes. The capillary cells were placed in the support as nearly vertical as possible. As a rule, if the solution was less dense than the solvent, the capillary was oriented with the closed end up and the open end facing downward. If the solution was denser than the solvent, the capillary was placed with the closed end down and the open end facing upward. When the capillaries were not placed in this manner, schlieren effects were observed at the open ends of the cells, and the apparent diffusion coefficients were approximately an order of magnitude greater than when such effects were not present. These effects indicated bulk flow due to density differences.

Diffusion was allowed to occur until the concentration of the ethanol in the capillary cell had changed by an amount sufficient to provide an accurately measurable change, (typically a 500% change). The capillary cell was then gently pulled out of the solvent, the diffusion time noted, and the capillary cell contents analyzed using the gas chromatograph. The entire contents of the capillary cell were then analyzed in the gas chromatograph to obtain a value for the average mass fraction at the end of the run.

To analyze the ethanol-water samples, the contents of the capillary tubes were removed with a syringe and placed directly into the gas chromatograph for analysis. The resulting ethanol and water GC area percentages were then converted to weight fractions using a calibration curve.

In ethanol-solvent systems, the solution was spiked with a known quantity of propanol in order to determine the mass fraction of ethanol in the original solution. Propanol

spiking was required because the solvents did not yield a measurable peak using the GC in this way. For the analysis of the organic solutions, therefore, a calibration curve was made using reagent grade propanol, obtained from Fischer Scientific. The propanol was diluted into reagent grade dodecane so as to maintain the proportion of propanol to ethanol at about 1:1. Dodecane was used because it also does not produce peaks in the gas chromatograph under the conditions which were used. Periodic temperature cycling of the GC was required to purge solvents from the column and control base line drift.

The procedure for use with the organic solvents was then as follows. A microliter hypodemic syringe was tared and then weighed with approximately 2 microliters of the propanol-dodecane spiking solution. The final contents of the capillary cell were then drawn into the syringe and it was reweighed. The whole contents of the syringe were then injected into the gas chromatograph.

8.5. Experimental Data

A total of twenty eight runs were made utilizing 370 capillaries which varied in length from approximately one to four centimeters. These runs are summarized in Table 8.1. The results of a typical run are given in Table 8.2. Note that sets of the data correspond to capillaries of about the same length and very nearly the same times. This is due to the fact that groups of capillaries were removed and the contents analyzed at selected time intervals.

8.6. Analysis of Data and Results

The one-dimensional unsteady binary diffusion equation with bulk flow is (see, for example, Bird et al, 1960):

$$\rho(\frac{\partial w}{\partial t} + u \frac{\partial w}{\partial x}) = \frac{\partial}{\partial x} (\rho D \frac{\partial w}{\partial x}) \tag{8.1}$$

where w is the mass fraction and u is the velocity.

The continuity equation for one-dimensional unsteady flow is:

$$\frac{\partial S}{\partial t} + \frac{\partial}{\partial x} (\rho u) = 0 \tag{8.2}$$

Equation (8.2) may be rearranged to give

$$\rho u = \int_X^L \frac{\partial S}{\partial t} \, dx \tag{8.3}$$

where use has been made of the fact that $u = o$ at the closed end of the tube $(x = L)$. If the density is constant (which implies no volume change on mixing, under isothermal conditions), equation (8.3) shows that $u = o$, and equation (8.1) may be written as:

$$\frac{\partial w}{\partial t} = \frac{\partial}{\partial x} \left(D \, \frac{\partial w}{\partial x} \right) \tag{8.4}$$

Further, if it is assumed that a constant "average" D can be used then:

$$\frac{\partial w}{\partial t} = D_{avg} \frac{\partial^2 w}{\partial x^2} \tag{8.5}$$

If the mass fraction at the open end of the capillary is assumed to be the same as the mass fraction in the bath, the boundary condition at $x = o$ becomes:

$$t > o, \quad x = o, \quad w = w_b$$

At the closed end of the capillary tube, the boundary condition is:

$$t > o, \quad x = L, \quad \frac{\partial w}{\partial x} = o$$

The initial condition is:

$$t = o, \quad o < x < L, \quad w = w_i$$

Table 8.1. Summary of Experimental Runs

Solvent	Temperature (°C)	Initial Mass Fraction of Ethanol	Number of Capillaries
Water[a]	25	.105	7
	25	.295	6
	25	.495	6
	25	.998	3
Isopar L	25	.247	18
	25	.485	16
	25	.710	16
	25	.999	11
	45	.256	16
	45	.499	15
	45	.731	17
	45	.999	16
	65	.256	15
	65	.499	14
	65	.731	13
	65	.999	16
TDOH/N12[b]	25	.250	15
	25	.490	15
	25	.753	14
	25	.999	11
	45	.241	11
	45	.489	14
	45	.724	16
	45	.999	17
	65	.241	11
	65	.489	13
	65	.724	12
	65	.999	16

[a] Some of the ethanol-water data was obtained at room temperature but the temperature was not measured. Thus, the 25°C represents a nominal value.

[b] This solvent is a 20 volume percent mixture of tridecyl alcohol in Norpar 12.

Table 8.2. Typical Experimental[a] Data

Capillary Length (cm)	Diffusion Time (hrs:min)	Final Mass Fraction of Ethanol
2.07	73:06	.539
2.06	73:08	.496
2.06	171:54	.259
2.13	171:59	.339
1.98	172:05	.246
2.01	172:09	.384
2.80	172:21	.345
2.90	172:25	.503
2.91	172:50	.451
2.83	194:22	.487
3.00	194:27	.459
2.86	310:58	.374
3.79	311:22	.455
3.82	334:52	.508
3.84	335:00	.465
3.87	335:14	.534

[a] This solvent was Isopar-L intially containing 71 wt % ethanol at 25°C

The solution to the partial differential equation (8.5) with the given initial and boundary conditions is (see, for example, Dunlop et al, 1972):

$$\frac{W_{avg} - W_b}{W_i - W_b} = \frac{8}{\pi^2} \sum_{n=0}^{\infty} \frac{1}{(2n + 1)} \exp [- (2n + 1)^2 \pi^2 D_{avg} t/4L^2] \quad (8.6)$$

It should be noted that a similar derivation utilizing the same assumptions, but using density rather than mass fraction would result in the same equation with densitites replacing the mass fractions. For systems in which there is a volume change on mixing, there will be a difference in the calculated diffusivities.

Equation 8.6 was used to determine D_{avg} from the experimental data. Since the diffusivity is a function of the mass fraction of ethanol (for a given system at a specified temperature), some "average" value of mass fraction should be associated with this diffusivity. One possibility would be to use the arithmetic mean of the initial and final average mass fraction. However, in the present work, the decision was made to use the following time average:

$$\bar{w}_{avg} = \frac{1}{t} \int_o^t w_{avg} dt \quad (8.7)$$

where w_{avg} is the spatial average mass fraction.

The results for the ethanol-water system are presented in Figure 8.1. Numerical integration using expression (8.6) was performed to determine W_{avg} after D_{avg} was found.

The diffusivities were obtained by using densities (grams ethanol/cm^3) and the time-average mole fractions were obtained from the time-average mass fractions. Mole fractions were used so that the results could be compared directly with the work of Hammond and Stokes (1953) and Smith and Storrow (1952). The curve drawn in Figure 8.1 for the results of the present study is based on a non-linear least squares fit (using a computer code which incorporates the algorithm developed by Marquardt (1963)) of the data with an equation of the form:
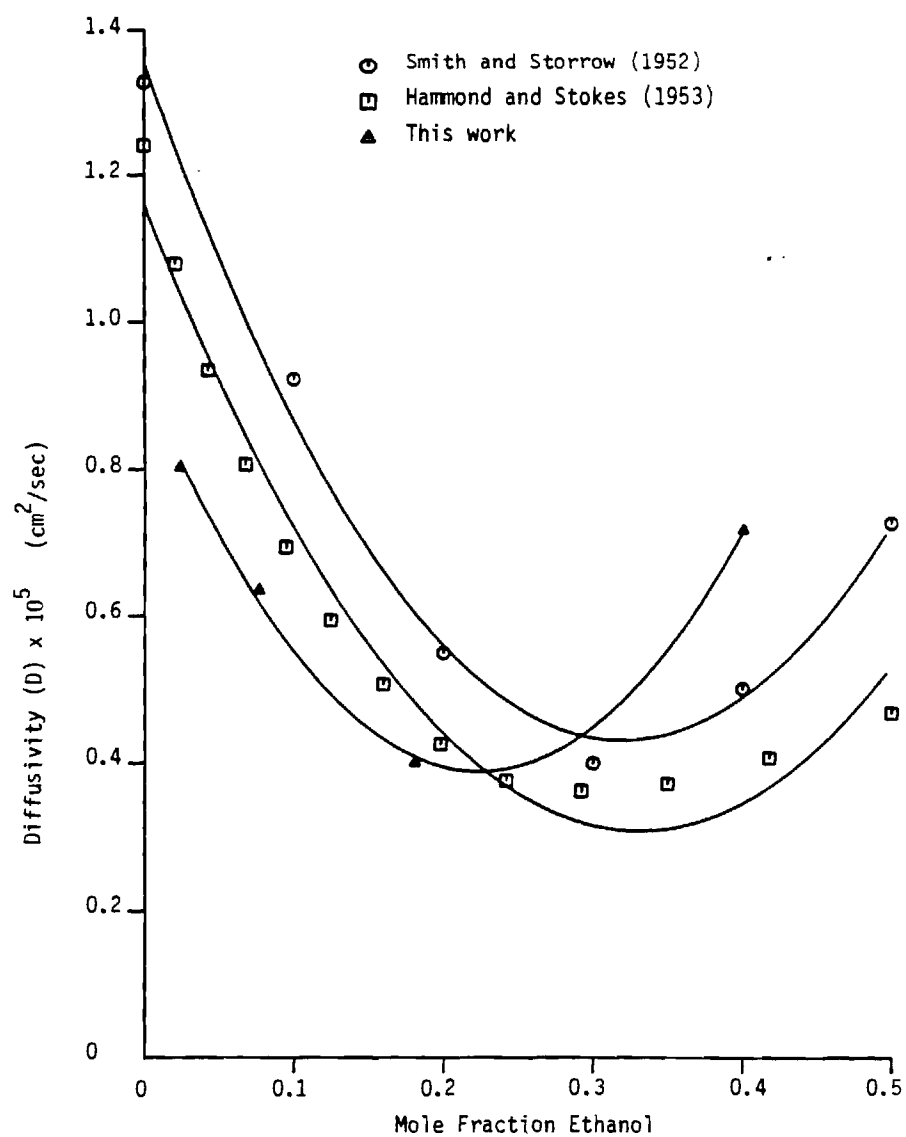
Fig. 8.1 Experimental diffusivity results for the ethanol-water binary system at 25°C.

$$D_{avg} = a_o + A_1 \bar{w}_{avg} + a_2 \bar{w}^2_{avg} \qquad (8.8)$$

where a_o, a_1, and a_2 are constants.

As can be seen from Figure 8.1, at high ethanol concentrations, the values of Hammond and Stokes (1953) are approximately one half of the values of Smith and Storrow (1952). In the present work, the diffusivity at the highest average ethanol concentration, 0.4 mole fraction ethanol, is greater than that obtained by either of the previous investigators.

At lower molar fractions of ethanol, the previous works mentioned both show a minimum diffusivity value, differing by approximately 10 percent from each other, at a mole fraction of 0.3. In the present investigation the diffusivity was not measured at an average concentration of 0.3 mole fraction ethanol; however, the minimum measured diffusivity does appear to occur in this region, as can be noted from the values obtained at a mole fraction of ethanol of 0.2.

The results for the ethanol-Isopar L system are presented in Figure 8.2. These results were determined using mass fractions. As can be seen from Figure 8.2, the ethanol-Isopar L system appears to follow the same pattern for all the temperatures studied, all going through a minimum diffusivity at a mass fraction range varying from 0.3 - 0.5. The curves drawn in Figure 8.2 are based on a non-linear least squares fit of the data with an equation of the form:

$$D_{avg} = (a_o + a_1 \bar{w}_{avg} + a_2 \bar{w}^2_{avg}) \, e^{-\frac{E}{RT}} \qquad (8.11)$$

where a_o, a_1, a_2, and E are constants.

The results for the ethanol-TDOH/N12 System are presented in Figure 8.3. The results were obtained using mass fractions. In the ethanol-TDOH/N12 system, the solvent used was a mixture of 20 percent by volume of tridecyl alcohol in Norpar 12. This solvent mixture has been treated as one component, and ethanol diffusivities into it have been calculated as if the ethanol and solvent were a binary mixture. No general characteristics of the data are evident. Part of the scatter in the data could be related to the fact that the system is a multicomponent one. As with the ethanol-Isopar L system, the curves drawn in Figure 3 are based on a nonlinear least squares fit of an equation
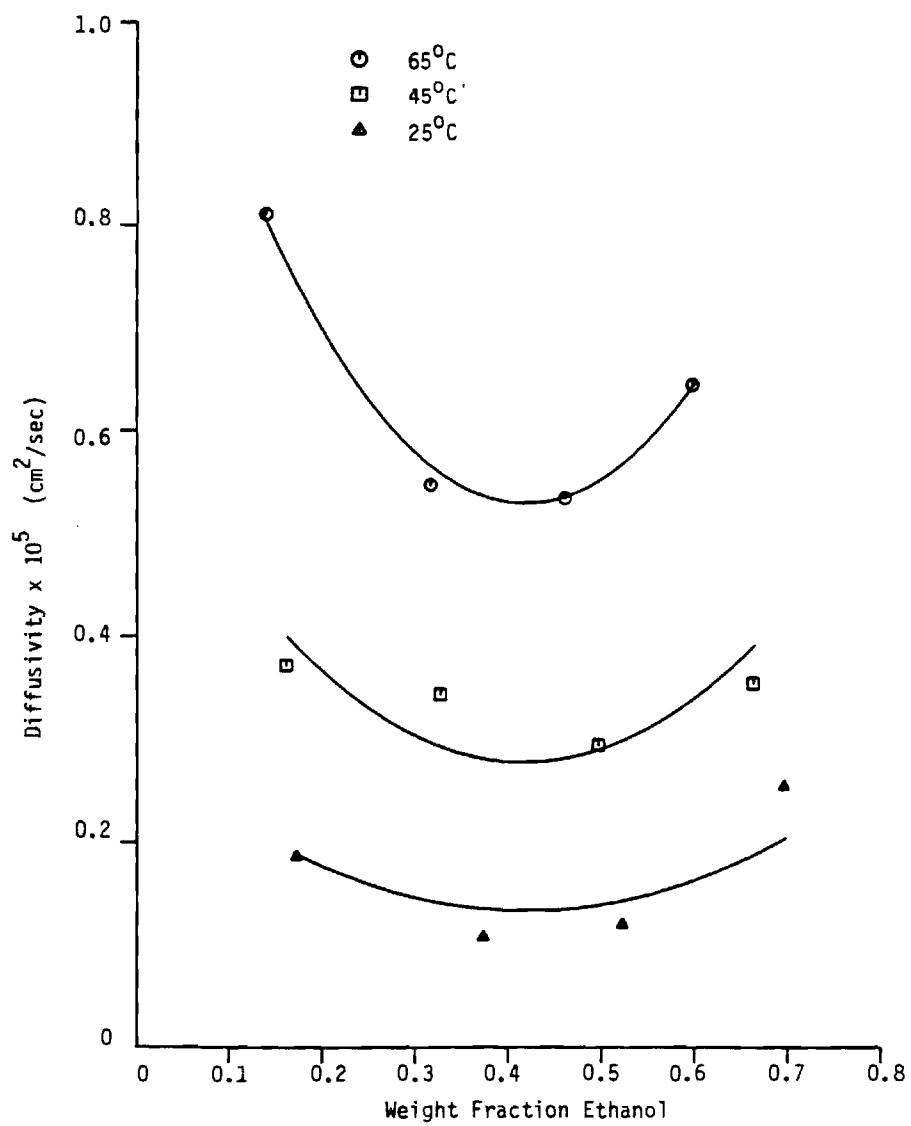
Fig. 8.2 Experimental diffusivity results for the binary system:
ethanol-ISOPAR-L

of the form of equation (8.11). The fact that the curves do not fit the data well is due, in part, to the fact that the data for all three temperatures are fitted with the same equation.

The nonlinear lest-squares results for both systems are presented in Table 8.3.

8.7. Discussion and Conclusions

The data analysis presented here represents an initial approach to data reduction. The one use of D_{avg} and w_{avg} are clearly approximations to the representation of diffusivity data which is concentration dependent.

In general, the prediction of liquid-phase binary diffusivities at a given temperature as a function of concentration involves the diffusivities at infinite dilution for each component, activity data, and the viscosity variation of the solution as a function of concentration. The diffusivities of infinite dilution may be obtained from experimental data or obtained by predictive methods. These predictive methods involve such quantities as the molecular weight and viscosity of the solvent, and the molar volume of the solute at its normal boiling point.

Both Isopar L and Norpar 12 are mixtures of various components. Since TDOH/N12 is a mixture of tridecyl alcohol and Norpar 12, it was decided to exclude this data from consideration using predictive equations. Also, because of the lack of available data on activities and viscosity of ethanol-Isopar L solutions, only predictive equations for diffusivities at infinite ethanol dilution were used for comparison with the data. The molar volume at the normal boiling point and the molecular weight of Isopar L were taken to be those of dodecane $(C_{12} H_{26})$. The results are summarized in Tables 8.4 and 8.5.

The results presented in Table 8.4 indicate reasonable agreement among the predicted results and the experimental

Table 8.3. Nonlinear Least Squares Parameters

System	a_o (cm^2/s)	a_1 (cm^2/s)	a_2 (cm^1/s)	E (cal/mol)
Ethanol-Isopar L	0.312	−0.804	0.962	6859
Ethanol-TDOH/N12	0.225×10^{-1}	$-.222 \times 10^{-2}$	$-.434 \times 10^{-2}$	5250
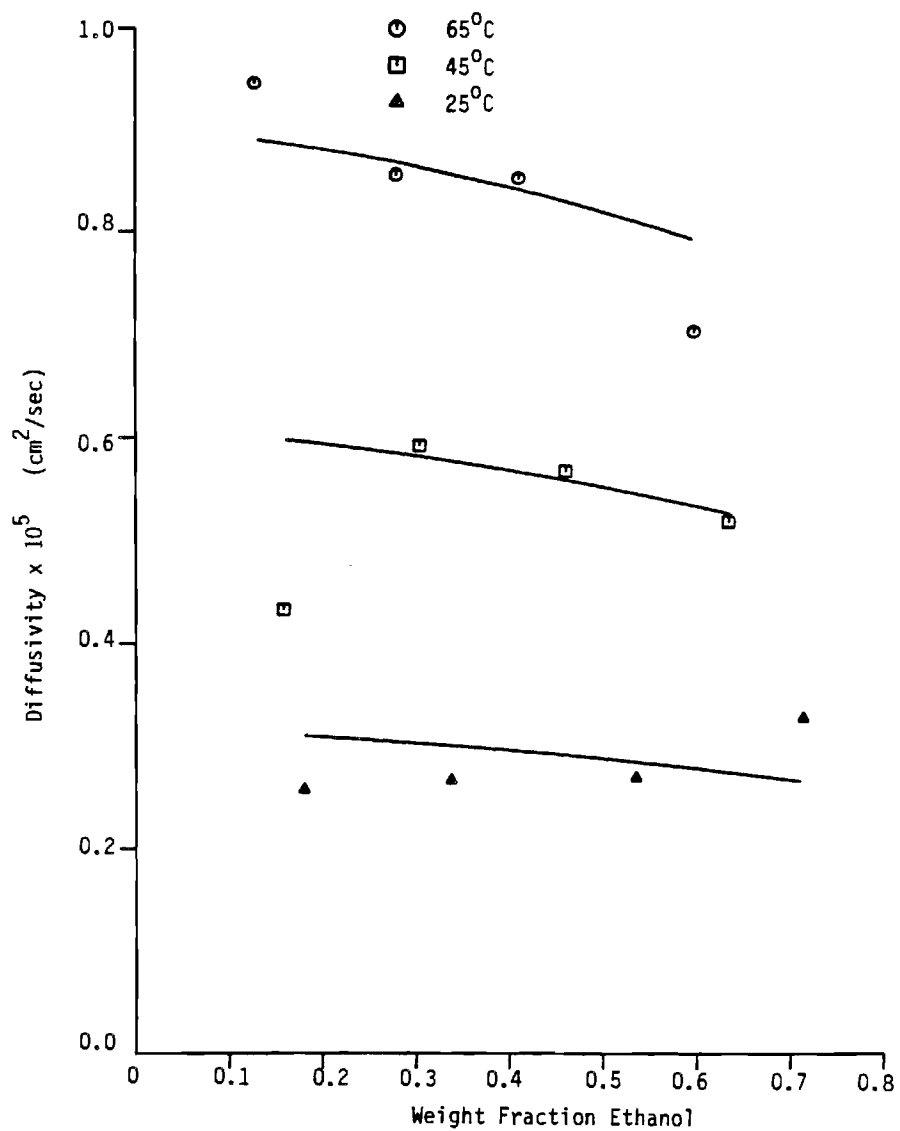
Fig. 8.3 Experimental diffusivity results for the system:
ethanol- tridecyl alcohol - NORPAR-12.

Table 8.4. Diffusion Coefficients at Infinite Dilution for Isopar L in Ethanol

Solute - Isopar L (A)
Solvent - Ethanol (B)

Temperature   Experimental

$$D \times 10^5$$

(°C)	(cm²/s)	Experimental	Wilke-Chang[c,d]	Scheibel[d]	Reddy and Doraiswamy[d]	Lusis and Ratcliff[d]
25	.44	1.6	2.8	2.2	2.6	2.3
45	.91	2.3	2.8	2.2	2.6	2.3
65	1.72	2.8	2.8	2.2	2.6	2.3

[a] Obtained from equation (11) for

[b]

[c] Using an association parameter of 1.5 (ethanol).

[d] See, for example, Reid et al., (1977).

Table 8.5. Diffusion Coefficients at Infinite Dilution for Ethanol in Isopar L

Solute - Ethanol (A)
Solvent - Isopar L (B)

Temperature   Experimental

$$D \times 10^5$$

(°C)	(cm²/s)	Experimental	Wilke-Chang[c,d]	Scheibel[d]	Reddy and Doraiswamy[d]	Lusis and Ratcliff[d]
25	.29	1.7	8.2 (3.0)[e]	4.4 (2.8)	4.3 (2.7)	9.1 (3.0)
45	.61	2.3	8.2 (3.0)	4.4 (2.8)	4.3 (2.7)	9.1 (3.0)
65	1.15	3.0	8.2 (3.0)	4.4 (2.8)	4.3 (2.7)	9.1 (3.0)

[a] Obtained from equation (11) for

[b]

[c] Using an associatin parameter of 0.7.

[d] See, for example, Rreid et al. (1977).

[e] See Discussion for an explanation of the values in parentheses.

data. As indicated, the experimental results have a stronger temperature dependence than the predicted results. The results presented in Table 8.5, however, suggests that a bias exists between the experimental and predicted results.

It is interesting to note that (for example) if four times the molal volume for ethanol is used in the predictive equation and if the association parameter in the Wilke-Chang equation is taken as 0.7, then the values indicated in the parentheses in Table 5 result. The agreement among the predicted results and the reasonably good agreeement of the experimental data suggests ethanol diffuses in Isopar L as molecular clusters rather than single molecules in this concentration range. It is interesting to note that water also appears to diffuse as a tetramer in organic solvents (Skelland, 1974).

Although these results suggest that the ethanol tetramer is important at ethanol infinite dilution, little can be said from these data concerning the existence of ethanol dimeric or trimeric species. We have been unable to obtain stability constants for these complexes from the data if, in fact, they exist. On the other hand, at infinite ISOPAR-L dilution, (i.e. high ethanol concentrations) we would expect the ethanol clusters to be loosely configured in solution and the experimental data seem to confirm this expectation. That is, clusters may exist in concentrated ethanol solution, but the diffusivity data suggest that rapid ethanol exchange occurs between them. Tetramers may still exist under these conditions, but they are probably configured more loosely due to the higher polarity of the bulk phase.

A qualitative argument, suggesting that the tetramer is particularly stable, can be obtained from geometric considerations. Such a cluster in a nonpolar hydrocarbon solvent, such as NORPAR 12 or ISOPAR L, should be stabilized by hydrogen bonding through the hydroxyl groups of the ethanol molecules. A tetramer would involve four hydroxyl groups which may be organized to comprise a tetrahedral cluster with one hydroxyl oxygen located approximately at each of the four tetrahedral corners.

In this environment, each of the hydroxyl hydrogen atoms is then able to associate simultaneously with three oxygens. That is, each hydrogen is located proximate to one of the tetrahedral planes which are defined by the oxygen atoms.

Such a cluster is symmetric with ethyl groups protruding uniformly into the solvent in all directions. It offers, therefore, maximum shielding of the polar hydroxyl groups from the solvent. It also enables the hydrogen atoms in the hydroxyl group to associate with the maximum number of oxygen atoms in a relatively tight structure.

Although these results do not prove conclusively that such tetramers exist, they do suggest their existence. Coupled with geometric consideration, it is not unreasonable to suppose that the tetramer predominates at low ethanol concentrations in nonpolar hydrocarbon diluents.

8.8   References

1.   Bird, R. B.; Stewart, W. E.; Lightfoot, E. M. "Transport Phenomena"; John Wiley and Sons, Inc.: New York, NY, 1960.

2.   Dunlop, P. J.; Steel, B. J.; Lane, J. E. "Physical Methods of Chemistry" Vol. 1; edited by Weissberger, A.; Rossiter, B. W.; John Wiley and Sons, Inc.: New York, NY, 1972.

3.   Hammond, B. R.; Stokes, R. H. Trans Faraday Soc. 1953, 49, 890-895.

4.   Krosnowski, L. "The Measurement of the Diffusion Coefficients of Ethanol in Organic Solvents"; M. S. Thesis, Georgia Institute of Technology, Atlanta, GA, 1983.

5.   Marquardt, D. W. J. Soc. Indust. Appl. Math 1963, 11, 431-441.

6.   Reid, R. C.; Prausnitz, J. M.; Sherwood, T. K. "The Properties of Gases and Liquids"; McGraw-Hill, Inc.: New York, NY, 1977.

7.   Skelland, A. H. P. "Diffusional Mass Transfer"; John Wiley and Sons, Inc.: New York, NY, 1974.

8.   Smith, I. E.; Storrow, J. A. Jnl. Applied Chemistry 1952, 2, 225-235.

CHAPTER 9

MEMBRANE USE IN ETHANOL RECOVERY PROCESSES

(L. M. Sroka)

9.1 Introduction

The membrane processes of ultrafiltration, reverse osmosis, and pervaporation are possible partial solutions to the problem of economically producing fuel-grade (anhydrous) ethanol from fermentation liquors. Although the phenomenon of osmosis has been known for over a century, the practical use of artificial membranes as separation media for reverse osmosis, ultrafiltration and pervaporation was not possible until the late 1950's (1). Then cellulose acetate was found to be an effective membrane material exhibiting high water fluxes, acceptable strength and selectivity with water and salt.

Asymmetric design of artificial membranes gave added improvment to their strength, flux and selectivity. Different chemical modifiers were added to increase cellulose acetate's selectivity and new membrane materials were also developed.

Research in membrane manufacture has now provided the consumer with tailor made pore size distribution, thickness, physical and chemical properties and configurations such as tubular or flat sheet in preassembled units. Most are proprietary. Vendors will generally indicate the permeabilty and chemical compatibility of their membranes, but not the materials of fabrication.

Permeation can be defined as mass transfer through a medium by a variety of transport mechanisms under various driving forces such as concentration gradient, pressure gradient, electrical potential and temperature gradient. (2). Since the actual mechanism of transport through the membrane is not well known, permeability is used to describe the flow of compounds through the membrane. However, the possible transport mechanisms include diffusion, membrane dissolution, and capillary flow through the membrane pores. All these mechanisms are probably present in varying degrees in membrane processes.

Membrane selectivity can be expressed in terms of a separation factor, defined as a concentration ratio of ethanol/water in the permeate divided by the ratio of ethanol/water in the concentrate.

Permeotropism is defined as the feed concentration for which no separation occurs through the membrane. Ultra filtration is based on the simple concept of the mechanism of "sieve-filitration" where separation is achieved by the differnce between the molecular sizes of the solvent and solute.

Surface forces also play a role in the separation process. Generally the particles retained are less than 1 micron and greaer than .02 microns. Larger molecules can be separated by conventional methods of filtration or sedimentation. A large size difference is needed, however, in order to perform an efficient separation. Generally a molecular weight difference of 10 times or of an atomic diameter difference of 2 times is sufficient ( ).

Pressure is one driving force which may push the solvent through the membrane pores. Typical pressure gradients are of the order of 1-10 atmospheres. Turbulence is also required to minimalize pore clogging and boundary layer formation due to build-up of the larger molecules. Limitations on maximum practical feed concentration are generally due to membrane fouling and to osmotic pressure gradients which occur whenever the larger molecules cannot pass through the membrane.

Reverse osmosis is similar to ultrafiltration except that the pressures are considerably higher and the pore sizes of the membrane are much smaller if they exist at all. The proposed mechanism of separation is not as simple as with ultrafiltration because separation of salt and water is possible and their atomic volumes are of similar size although the salt hydrates are much larger than water. The surface chemistry of the solution and the membrane may also affect the separation. If one component is preferentially sorbed at the surface, for example, then a boundary layer with a higher concentration of that component forms at the surface and can flow through the capillary pores. This is the Preferential Sorption - Capillary Flow model as proposed by Sourjoun (21).

Also, differences in diffusivity and solubility of the solutes in the membrane are important. However, there is very little flow of the average concentration solution through the pores because the average pore size is the order of the molecule's size. Consequently, the theoretical predicti<n of separation is very difficult. However, some theories for the transport of electrolytes and water through the membrane have been suggested (7).

Pervaporation is similar to reverse osmosis except that the presssure difference is not as great because a phase change occurs. This phase change creates the difference in chemical potential instead of just a pressure difference.

In this case, solubility and diffusivity play important roles in the separation factors and permeability of a particular membrane. Preferential sorption at the surface can also affect the separation although it is not believed that pore flow occurs in pervaporation membranes. It is more likely that the components of the liquid mixture will selectively dissolve into the membrane at the surface and diffuse through the membrane. The ratio's at which the molecules of the components can diffuse through the membrane are determined by the physical and chemical interactions between these molecules and the membrane substance. Since in distillation the partial pressures of the components govern the ratio at which these components leave the liquid, azeotropes, in principle, can be avoided by pervaporation.

G. D. Mehta (1) examined reverse osmosis as a replacement for distillation in the separation of ethanol and water. He found present reverse osmosis membranes could be used to increase the concentration of ethanol in fermentation beers. However, the osmotic pressures needed to obtain pure water as permeate limited the concentration of the ethanol and water solution. From the membranes tested, none were found to pass ethanol preferentially. An economic evaluation for the use of a hypothetical membrane as a concentration step and a dehydration step with a distillation column in the intermediate separation process was done. The flux and separation were specified and the osmotic pressure of the concentrate was used as the operating pressure. The replacement of the dehydration still with a reverse osmosis sunit was economically attractive, but the membrane is not available yet.

P. Schissel (2) tested a number of reverse osmosis membranes on ethanol and water solutions which covered the entire concentration range. The results showed low separations and the preferential passage of water also. Pervaporation experiments were performed with the reverse osmosis membranes. Most did not separate the ethanol/water solution appreciably. Two were found that showed a good separation and were tested at many concentrations. The Filmtec FT-30 membrane had a vapor-liquid curve similar in shape to a vacuum distillation of the solution exhibiting small separations or an azeotrope at high concentrations. The UOP RC-100 had a vapor-liquid curve which had a definite azeotrope near 50 wt. %. The economics for using these membranes as a separation process were not examined.

Hope that a perfect ethanol retaining membrane will be found has induced experimentation in reducing the osmotic pressure which would have to be overcome to obtain a pure substance on each side of the membrane. Lee, Babcock (15) examined a counter current reverse osmosis unit. Dry ethanol is to be recycled on the permeatic side of the

membrane to lower the effective osmotic pressure. Nichols (16) proposed to use a membrane to keep an ethanol selective solvent physically separated from the ethanol and water phase. Ethanol would pass through the membrane into the solvent phase whereas the water would remain in the other phase because it was insoluble in the solvent, not because the membrane retained it. As in normal extraction process, the ethanol has to be stripped from the solvent to obtain a pure product.

The research in pervaporation has been in the direction of modifying the membrane surface characteristics. Tealdo (10) made styrene-grafted PFTE films to improve the PFTE films selectivity. In doing so the permeation rate was decreased, and only slight improvements in separation were realized. The Southern Research Institute (12, 13) tried attaching water or ethanol insoluble compounds to the membrane to increase selectivity. This was temporarily successful. Coatings of styrene-divinylbenzene polymer were applied to porous support membranes in an another attempt to improve selectivity. They even tried incorporating three angstrom molecular sieve to retard the water flow and enrich the ethanol permeate.

In summary, it is desired to find a membrane which will separate ethanol from water or the extraction solvent. Pervaporation, reverse osmosis, ultrafiltration experiments were conducted on commercially available membrane looking for high flux, high selectivity, material compatability, low cost and easy handling and maintenance. The compatibility and durability were determined from visual observations once the solution had come in contact with the membrane and the noted handling problems that occurred during testing. The flux and the selectivity were determined from the experiments. The cost of the membrane and handling instructions were available from the vendor. This information was collected and the present feasibility of membrane in ethanol recovery was determined.

9.2 Experimental Techniques

The ultrafiltration, reverse osmosis and pervaporation experiments were performed in batches with the same equipment used in different ways. Feed solutions were mixed, sampled and pre-heated to the bath temperature, if necessary, before being poured into the membrane apparatus. The membrane apparatus was immersed in the constant temperature bath on the magnetic stirring table. To test a membrane's suitability for reverse osmosis or

A - Membrane Apparatus
B - Constant Temperature Bath
C - Magnetic Stirrer
D - Liquid Trap

E - Temperature Controller and Indicator
F1 - Pressurized Nitrogen
G1 - Pressure Regulator and Indicator
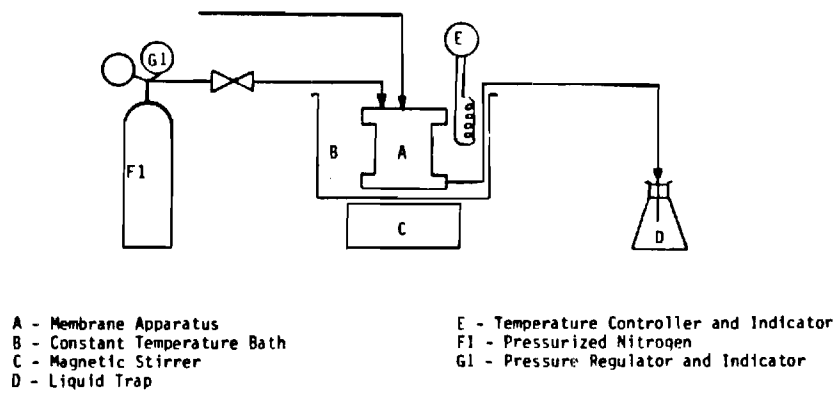
Figure 9.1 The Schematic Representation of the Reverse Osmosis and Ultrafiltration Experimental Apparatus

A - Membrane Apparatus
B - Constant Temperature Bath
C - Magnetic Stirrer
D - Liquid Trap

D2 - Condenser
E - Temperature Controller and Indicator
F2 - Vacuum Pump
G2 - Pressure Regulator and Indicator
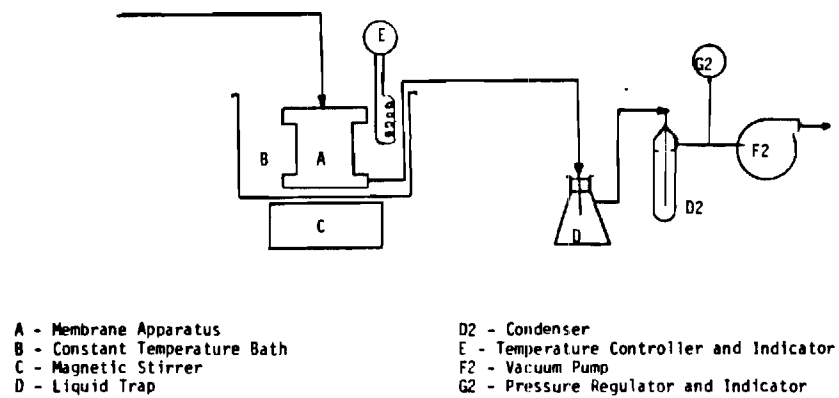
Figure 9.2 Schematic Representation for the Pervaporation Ultrafiltration Experimental Apparatus

ultrafillation, pressure was applied to the cell and the permeate collected in the liquid trap (see Figure 9.1).

To test a membrane's suitability for pervaporation a vaccum was drawn on the cell and the permeate collected in the liquid trap or the liquid nitrogen condenser (see Fig. 9.2). Temperature and pressure readings were taken during all runs. Samples of the concentrate and permeate were taken when the run were complete.

The selectivity and flux of the membranes were studied with an Amicon (401 S) pressure cell. Model 401 S is a heavy duty, magnetically-stirred ultrafitration cell which may be used at pressures up to 250 psi (17 atm.) and with corrosive chemicals or organic materials. All wetted parts are made of Type 304 stainless steel coated internally with Teflon, and sterilizable. Pressure is applied to the cell through the pressurized gas inlet assembly (see Figure 9.2) and permeate leaves through the outlet. The concentrate collects in the cell. The membrane is supported by a 3 inch (76 mm) diameter porous metal disc with an effective surface area of 6.08 square inches (39.2 cm). Leaks are prevented by oversized o-rings.

To keep the effects of temperature on membrane separation and flux to a minimum, a HAAKE D1 heating element and controller was used. The water bath could be operated within $\pm 0.1^{\circ}C$. The experiments were relatively long and the initial feed was preheated in the bath before it was placed in the pressure cell to ensure that the ethanol mixture was at the bath temperature.

The vacuum was supplied by a Cole-Parmer Air Cadet vacuum pressure pump. It is capable of pumping 900 cubic inches of air creating up to 20" hg vacuum or 18 psig of pressure. Corrosion problems were limited with a viton diaphram, teflon valves, and noryl wetted parts. The vacuum was regulated by a 30" hg maximum regulator with an adjustable spring-loaded air bleed valve.

The system was pressurized with instrument grade nitrogen which is inexpensive and inert to the solvents being used. The pressure was regulated by a Fisher nitrogen gas regulator capable of 0 to 400 psig.

The liquid trap was a standard 500 ml erlenmeyer vacuum flask. The condenser was a glass b bble trap immersed in a liquid nitrogen or dry ice and acetone bath.

Isopar L is a heavy narrow cut, isoparaffinic solvent mainly composed of a mixture of C_{12} branched alkanes. It has a specific gravity of 0.767 at 15.6 C, a viscosity of 1.99 cp at 25 C and a boiling range from 188 to 206 C. The solvent was a obtained from Exxon Refining. Reagent grade

ethanol and distilled water were used. The membranes were used according to instructions provided from their respective vendors (see Tables 9.1 and 9.2).

Membrane permeation data were collected from analyses of the initial feed, the permeate and the remaining concentrate. The concentration analyses were made by gas chromatograph. The GC used was a Hewlett Packard type 5710A with a 6 foot column, Poropak Q 80/100 mesh packed column. Instrument grade helium was used as the carrier gas. The gas chromatograph was operated at an oven temperature of 165°C and an injection port temperature of 250°C with a thermal conductivity detector at 250°C. The peaks were integrated using a Hewlett Packard 3390A peak integrator.

The output from the integrator was in the form of area percentages of those sample components which were detected by the thermal conductivity detector. The area percentages were converted to the corresponding weight percentages using calibration curves which were made by analyzing samples of known compositions and plotting the integrated area percentages versus the weight percentages. For samples containing undetected solvent, similar calibration curves were made by using reagent grade propanol as a reference peak. The sample and propanol spike weights were needed to find the weight of ethanol in the sample. The weight percent of ethanol and water on a solvent free basis was obtained and used to determine the weight of water in the sample. The solvent weight was calculated as the difference between the initial sample and the ethanol and water weights.

9.3 Experimental Results

All membranes performed well with ethanol and water feed solutions. The organic solvent (Isopar L) caused the GE Silicon, GE MEM-213, and the S&S AC-63 to swell when used. The swelling weakened the membrane structure enough that they ruptured when the pressure gradients were applied. If the ethanol, or solvent swelled the other membranes in Tables 9.1 and 9.2, it was not visually detectable.

The GE Silicon unbacked membrane was difficult to handle because of its gel-like form that needed to be held taut. The same membrane with single backing performed well when used in the pervaporation experiments. The S&S AC-63 membrane needed to be soaked in increasingly stronger solutions of ethanol before use with organic solvents and had to be kept wet to preserve its delicate pore structure. Since the ethanol evaporated very quickly, handling had to be done with a liquid cover and its gel-like form, which would not cut, made it difficult to handle. A

Table 9.1 . Commercial Membranes Studied.

Manufacturer, Trade Name	Product Description
Celanese Corp.	
Celgard 2400	Air-breathable and water repellent, 1 mil thick, 38% porosity with 0.02 micron effective pore size polypropylene film.
Celgard 2500	Air-breathable and water repellant, 1 mil thick, 45% porosity with 0.04 micron effective pore size polypropylene film.
Celgard K-442	Water repellant, embossed laminate of Celgard 2400 between layers of nonwoven polypropylene.
Ionics, Inc.	
Type 61 CZL 386	Modacrylic fiber-backed cation transfer membrane, 24 mils thick.
Type 103 QZL 386	Modacrylic fiber-backed anion transfer membrane, 25 mils thick.
Schleicher & Schuell, Inc.	
TE 30	Polytetrafluoroethylene film, 8 mils thick, hydrophobic with 0.02 micron pore size.
AC 63	Cellulose Acetate film with an 0.02 to 0.0015 micron effective pore size.
Gelman Sciences	
HT 200	0.2 micron effective pore size film.

Table 9.1 Commercial Membranes Studied.

Manufacture, Trade Name	Product Description
Millipore Corp.	
MF Millipore	Nitrocellulose film with 0.025 micron effective pore size.
ROW P00 800	Nitrocellulose
ROW P00 600	Nitrocellulose
Whatman Laboratory Products	
Type WPT	Polytetrafluoroethylene film with 1 to 0.2 micron pore sizes, backed with polypropylene.
Fluid Systems	
TFC	4 layer laminate.
General Electric	
MEM-100	Unbacked Dimethyl Silicone.
MEM-101	Single backed Dimethyl Silicone.
MEM-102	Double backed Dimethyl Silicone.
MEM-213	Single backed Silicone-Polycarbonate.
Abcor, Inc.	
HKF-131	Non-cellulosic UF, featuring a nominal molecular weight cut-off of 5,000.
HFM-180	Non-cellulosic UF, featuring a nominal molecular weight cut-off of 18,000.
NCA-RO	Non-cellulosic RO, featuring 95% NaCl rejection and water flux of 20 gfd at 700 psi, 25 ^{0}C with 0.5% NaCl.

152

few of the other membranes needed to be kept wet and or treated before use. These were not as difficult to handle because they were all backed and water was the only necessary solvent.

Most of the companies selling membranes and reverse osmosis units have the handling problems under control by providing the membrane in enclosed units which are not handled by the customer. A spiral wound sheet is available, for example, which can be placed in a pressure tubular reactor. Hollow fiber bundles are also available. These units can be used directly after washing without the operator ever handling the delicate membrane. Flat sheets of membrane material are not efficient for surface area optimization and handling .therfore many companies do not even produce them except for research orders.

The results are presented in Tables 9.3-9.9. The units of measure in all cases are the same. Time is in hours; amounts are in mls; pressures are in psig; temperatures are in ^{0}C; and fluxes, J, are in ml/cm^2-hr. The R values in the tables refer to the percent ethanol rejection. A value near zero implies poor selectivity. Negative R values indicate a preferential passage of ethanol through the membrane. The alpha values in the tables refer to the membrane selectivity defined in the usual fashion.

9.3.1. Ultrafiltration

Ultrafiltration was considered as a finishing process to recover solvent from the ethanol product in the solvent extraction process (19). A feed solution simulating the product from the final stripper was used in these experiments. There were no positive results for this application of ultrafiltration in this ethanol separation process (see Table 9.3).

The size difference between the ethanol and the solvent does not appear to be great enough or the pore size of the ultrafiltration membranes was too large for a separation to be realized. The minimal ultrafiltration membrane size tested was .02 microns (200 A) which is much larger than the estimated diameter of the Isopar L. (approximately 10 A (5).

The experimental values for the separation coefficient are different from unity when actually no separation has occurred because of measurement error.

The measurement error is in the analysis of feed and permeate. These values are not exact because when the solvent is present the samples must be weighted, spiked, and the results of the GC correlated graphically. The separation would need to be greater than what is observed in these results or be beyond the experimental error to be of any great importance.

Table 9.2.   Non-Porous Polymer Membranes Studied.

Membrane Material	Thickness
Cellulose Acetate (Rohm & Haas)	0.8 mil
Polypropylene (Rohm & Haas)	2.0 mil
Polyethylene (Dow)	2.0 mil
Polyethylene	1.0 mil
Cellophane	na
Plastic	na

na - not available

Table 9.3   Results of the Ultrafiltration Studies.

| Membrane | Feed | | Permeate | | Amount | Time | Pres. | Temp. | R | J |
	Etoh	H_2O	Etoh	H_2O						
Millipore MF	77.8	0	78.1	0	56	35	155	Amb	-0.4	12.66
S&S TE 30	74.5	0	75	0	20	20	115	Amb	-0.7	7.91
S&S TE 30	85.8	1.5	86.0	1.6	27	25	160	Amb	-0.5	8.54
Fluid Systems TFC	74.5	0	75.5	0	15	15	120	Amb	-1.3	7.91
Ionics 103 QZL 396	79.2	2.0	78.5	1.8	11	25	100	Amb	0.9	3.48
Ionics 61 CZL 386	79.6	1.8	77.0	1.9	13	40	100	Amb	3.3	2.57
Ionics 61 CZL 386	84.6	1.5	84.6	1.5	44	20	160	Amb	0.0	17.41
Celguard 2400	76.2	1.5	76.1	1.5	12	90	100	18.5	0.1	1.05
Celguard 2400 & Styrene	74.6	1.5	74.3	1.5	20	60	180	20	0.4	2.03

Table 9.3. Results of the Ultrafiltration Studies. (cont.)

| Membrane | Feed | | Permeate | | Amount | Time | Pres. | Temp. | R | J |
	Etoh	H_2O	Etoh	H_2O						
Gelman HT-200	84.1	1.8	84.3	1.9	200	10	10	Amb	-0.2	30.3
Celguard 2400	87.1	1.5	87.9	1.4	110	10	50	40	-0.9	16.7
Celgurad K-442	87.7	1.5	86.5	1.4	200	10	10	35	1.4	30.3
Celguard 2400	84.2	1.5	84.0	1.5	50	5	25	Amb	0.2	15.2
Whatman PTFE 0.2 micron	84.1	1.5	84.0	1.5	200	5	10	Amb	0.1	60.6
Celguard 2500 & Styrene	87.0	1.5	85.8	1.5	63	10	-3	Amb	-1.4	9.5
S&S AC-63	83.6	1.7	85.4	1.8	8	3	-3	23	-2.2	0.3

The ultrafiltration membranes which were tested have a possibility of performing the separation if appropriate modifications were made to their surface (10, 12, 13). It was attempted to reduce pore their size by coating the surface of the Celguard 2400, 2500 and Fluid Systems TFC membranes with styrene and then attaching functional groups to the styrene. Solutions of styrene monomer and hexane were used to coat the membrane. The results showed no better separation than before.

Many types of polymer films and plastics were tried such as polypropylene, polyethylene and cellophane. These films were tested under conditions of raised temperature and pressure in an attempt to create an ultrafiltration process with extremely small pores which separated atoms on a sieve-filtration basis (process).

The results of the severe condition ultrafiltration experiments are shown in Table 9.4. They also were not encouraging for the separation of ethanol and water from the solvent. At first, it appeared that two of the tested membranes exhibited a preference for passing water. This ws not actually the case. It was concluded that water was leaking into the permeate line from the constant temperature bath since a simple mass balance showed more water permeating the membrane than what was present in the initial feed. This condition was corrected and the membranes were tested again. This time they showed no appreciable separation.

There is also the possible use of ultrafiltration with commercial membranes in the separation of solids from the fermentation beer or as a pretreatment step before a reverse osmosis and pervaporation step. The excellent ethanol and water flows, and low pressure differentials required make this an attractive alternative. This pretreatment step might save on reverse osmosis and pervaporation membrane maintenance.

After the ultrafiltration experiments failed to separate the solvent from the ethanol, reverse osmosis with commercial membranes was tried. Feed solutions simulating the stripper product were used in these experiments also. The results are shown in Table 9.5.

As in the ultrafiltration results, the experimental technique for the three component analysis makes determination of small separations difficult. The GE membranes which were designed for gas phase separations did not allow any flow through them unless a vacuum was drawn on the one side. This was surprizing since the flux was noticeable when the pervaporation technique was used.

Pervaporation experiments were also tried with the simulated stripper product feed for use in the same

Table 9.4   Results of the Ultrafiltration Studies With the Non-porous Films.

Membrane	Feed Etoh	Feed H_2O	Permeate Etoh	Permeate H_2O	Amount	Time	Pres.	Temp.	R	J
Plastic	80.2	1.2	-	-	-	1	75	60	-	-
Polyethylene	76.0	1.5	-	-	-	8	75	60	-	-
Saran	88.2	1.5	86.6	1.5	30	12	50	55	1.8	0.06
Cellulose Acetate	82.3	1.5	-	-	-	6.5	100	50	-	-
Cellophane	82.3	1.5	-	-	-	7.5	120	60	-	-
Dow Polyethylene	86.0	1.5	70.1	30.0	2	7.5	80	60	18.6	0.0067
Dow Polyethylene	84.5	5.1	84.0	11.7	2	44	80	60	0.6	0.0011
Plastic	86.2	5.0	88.0	5.9	10	91	60	60	-2.1	0.0028
Cellophane	90.0	6.2	62.0	40.0	4	168	60	60	31.1	0.0006
Cellophane	89.7	5.2	84.9	14.0	3	20	60	80	5.7	0.0038

Table 9.5   Results of the Reverse Osmosis Studies.

Membrane	Feed Etoh	Feed H_2O	Permeate Etoh	Permeate H_2O	Amount	Time	Pres.	Temp.	R	J
Abcor HKF-131	84.3	15.6	82.2	17.8	50	8	200	60	2.5	0.16
Abcor NCA-RO	84.6	1.1	82.2	1.4	20	1.5	220	20	2.8	0.40
Millipore ROWP00800	85.2	1.7	84.2	1.9	20	2	150	60	1.2	0.25
Millipore ROWP00600	85.2	1.7	84.7	1.9	50	3	150	60	0.6	0.42
GE MEM-101	53.0	47.0	-	-	-	4	200	60	-	-
S&S AC-63	86.6	1.5	85.2	1.5	35	0.5	50	50	1.6	2.1
GF MEM-213	53.0	47.0	-	-	-	3	150	60	-	-

application. The results of the pervaporation experiments are shown in Table 9.6. The three component feed of ethanol, water and Isopar L showed no positive results. The solvent swelled some of the membranes and caused them to rupture or no flow occurred at all.

A binary feed of ethanol and water was tried to avoid the compatibility problem. The GE MEM-101 and GE MEM-213 exhibited no adverse effects with the ethanol and water solution. The GE MEM-101 even showed a preferential passing of ethanol, the results are shown in Table 9.6.

The efficiency of the separation by the GE MEM-101 membrane is compared to a vacuum distillation occurring at similar temperatures and presures in fig 9.3. The data were obtained from a National Laboratories Report for temperatures of $50^{\circ}C$ (92-220 mm Hg), $70^{\circ}C$ (233-542 mm Hg) and 50 kpa (80-60$^{\circ}C$) (9). The points for the membrane separations fall below this curve at low ethanol concentrations and near the curve at high or azeotropic concentrations. This represents a poorer separation than an ordinary vacuum distillation would produce.

Figure 9.4 shows the variation of flux with ethanol concentration. As the ethanol concentration increased, the flux also increases rapidly. The solubility and diffusivity of ethanol in the polymer appear to be concentration dependent.

Figure 9.5 shows the variation of flux with temperature. The temperature dependence is very sensitive. It appears that at $40^{\circ}C$ that there is not enough heat available to vaporize the ethanol from the membrane surface. Another possibilty is that the solubility and diffusivity of the ethanol in the membrane are very temperature dependent.

9.3.2 Reverse Osmosis

After the ultrafiltration experiments failed to separate the solvent from the ethanol, reverse osmosis with commercial membranes was tried. Feed solutions simulating the stripper product were used in these experiments also. The results are shown in Table .

As in the ultrafiltration results, the experimental technique for the three component analysis makes determinaton of small separations difficult. The preferential passing of water is a possibility and agrees with results reported in the literature (1,2). In the ethanol water system, a small increase in the water concnetration of the permeate was detected. Theoretically the separation obtainable by reverse osmosis would be

Table 9.6 Results of the General Pervaporation Studies.

Membrane	Feed		Permeate		Amount	Time	Pres.	Temp	α	J
	Etoh	H_2O	Etoh	H_2O						
Cellophane	79.0	2.0	-	-	-	1	100	Amb	-	-
Polyethylene	79.0	2.0	-	-	-	1	100	Amb	-	-
Polyethylene	85.1	1.6	86.9	1.7	7	1	180	75	0.96	0.16
GE MEM-213	70.8	0.8	66.8	0.9	5	1	260	Amb	0.94	0.12
GE MEM-213	50.0	50.0	50.0	50.0	100	1.5	260	60	1.0	1.7
GE MEM-101	70.8	0.8	-	-	-	-	260	60	-	-
GE MEM-101	53.0	47.0	72.0	28.0	10	6	160	60	2.28	0.04
Cellulose Acetate	44.5	55.5*	94.6	4.4*	0.5	2.5	220	60	26.8	0.005
Polypropylene	42.2	57.8*	15.2	84.8*	0.5	1	220	60	0.24	0.012
Polypropylene	86.0	1.2	71.3	14.6	0.3	6	220	60	0.68	0.001
Cellulose Acetate	50.0	50.0**	96.6	3.4**	0.5	3.5	220	60	28.	0.003
Cellulose Acetate	3.4	96.6**	85.0	15.0**	0.8	8	220	60	161.	0.002
Cellulose Acetate	3.4	96.6**	-	-	-	4	220		-	-

* Hexane   ** Isopar M

Fig. 9.3   Comparison of Separation by Vacuum Distillation with the Results of Pervaporation with GE MEM-101 Membrane.
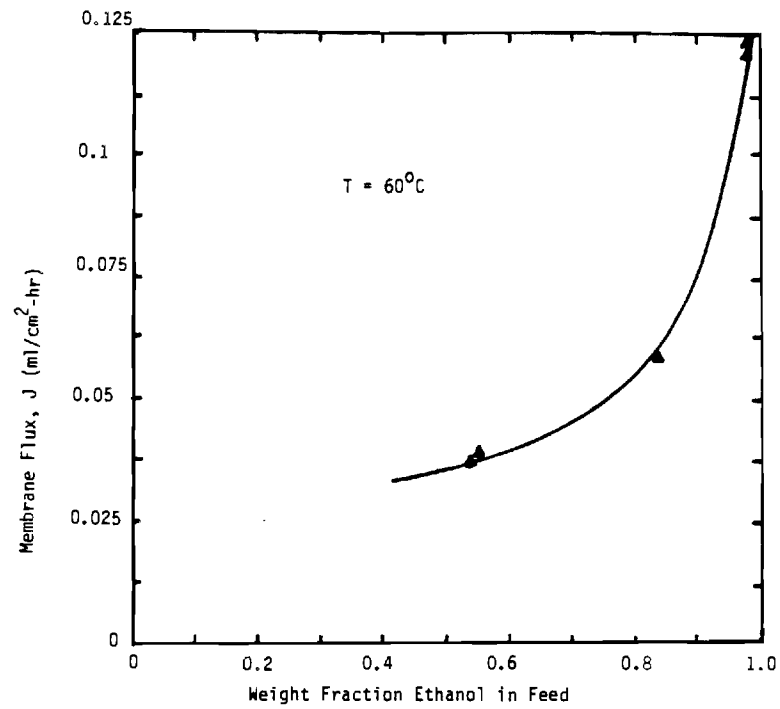
Fig. 9.4 Typical variation of ethanol flux with feed concentration and all other factors nearly constant.
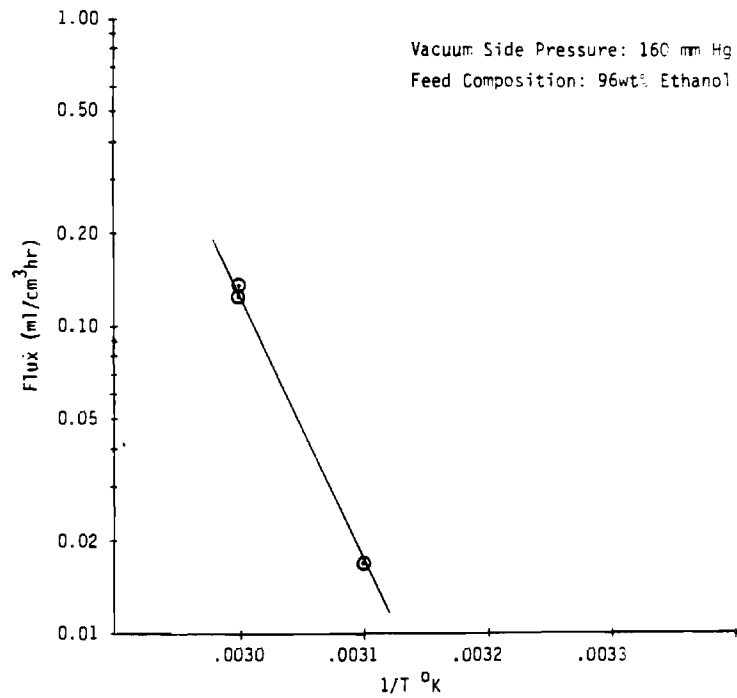
Fig. 9.5 Variation of Flux with Temperature for a Constant Composition System

greater if higher pressures were used. Unfortunately, the equipment was not designed to be operated at pressures above 250 psig.

9.3.3 Pervaporation

Pervaporation experiments were tried with the simulated stripper product or fifty-fifty mixtures of ethanol and solvents as the feed. The results of the pervaporation experiments are summarized in Table 9.7.

The three component feed of ethanol, water and Isopar L was tried first at ambient temperatures. The poor separation, or the unobservable fluxes, caused the operating temperatures to be raised. Still the separation was poor.

The lack of separation found with this technique did not agree with the results by Sweeny and Rose (4). In an attempt to duplicate their results, fifty-fifty mixtures of ethanol and hexane were tried. Cellulose acetate and polypropylene films were reported as providing the best separation, and therefore tried. The separation factors obtained for the cellulose acetate were within the range reported but the polypropylene did not perform as well as expected. The preferential passing of ethanol and retention of the non polar hexane made the cellulose acetate a prime candidate for removing ethanol from the solvent extract (18). A fifty-fifty solution of ethanol and Isopar M produced a 96 wt% ethanol product, therefore the low ethanol concentration feed was tried. The 3% ethanol feed produced a permeate which was 85% ethanol, this is an excellent separation in relation to the previous results, but is not as good as the separation obtainable by a flash. The flash, operated at 360 mm Hg and 70C produces a 90 wt% ethanol product.

The organic solvents swelled the GE membranes excessively, which resulted in them rupturing. A binary feed of ethanol and water was tried to avoid the previous compatibility and analytical problems. The GE MEM-101 and GE MEM-213 exhibited no adverse effects with the ethanol and water solution and determinaton of separation was more precise. The GE MEM-101 even showed a preferential passing of ethanol. A number of different feed compositions and temperatures were tried with the GE MEM-101 membrane and the results are summarized in Table 9.8.

162

Table 9.7   Results of the General Pervaporation Studies.

Membrane	Feed Etoh	Feed H_2O	Permeate Etoh	Permeate H_2O	Amount	Time	Pres.	Temp	α	J
Cellophane	79.0	2.0	-	-	-	1	100	Amb	-	-
Polyethylene	79.0	2.0	-	-	-	1	100	Amb	-	-
Polyethylene	85.1	1.6	86.9	1.7	7	1	180	75	0.96	0.16
GE MEM-213	70.8	0.8	66.8	0.9	5	1	260	Amb	0.94	0.12
GE MEM-213	50.0	50.0	50.0	50.0	100	1.5	260	60	1.0	1.7
GE MEM-101	70.8	0.8	-	-	-	-	260	60	-	-
GE MEM-101	53.0	47.0	72.0	28.0	10	6	160	60	2.28	0.04
Cellulose Acetate	44.5	55.5*	94.6	4.4*	0.5	2.5	220	60	26.8	0.005
Polypropylene	42.2	57.8*	15.2	84.8*	0.5	1	220	60	0.24	0.012
Polypropylene	86.0	1.2	71.3	14.6	0.3	6	220	60	0.68	0.001
Cellulose Acetate	50.0	50.0**	96.6	3.4**	0.5	3.5	220	60	28.	0.003
Cellulose Acetate	3.4	96.6**	85.0	15.0**	0.8	8	220	60	161.	0.002
Cellulose Acetate	3.4	96.6**	-	-	-	4	220		-	-

* Hexane   ** Isopar M

Table 9.8   Results of the Pervaporation Studies with the GE MEM-101 Membrane.

Membrane	Feed Etoh	Feed H_2O	Permeate Etoh	Permeate H_2O	Amount	Time	Pres.	Temp.	α	J
GE MEM-101	53.0	47.0	72.0	28.0	5	3.5	160	60	2.28	0.036
GE MEM-101	83.6	16.4	86.7	13.3	10	4	160	60	1.27	0.063
GE MEM-101	54.0	46.0	76.0	24.0	10	6	160	60	2.70	0.042
GE MEM-101	97.4	2.6	96.3	3.7	30	4.5	160	60	0.69	0.168
GE MEM-101	52.9	47.1	71.1	28.9	20	-	160	60	2.19	-
GE MEM-101	94.9	5.1	95.2	4.8	1	1.5	160	50	1.07	0.017
GE MEM-101	95.7	4.3	96.4	3.6	16	3	160	60	1.20	0.134
GE MEM-101	95.7	4.3	96.4	3.6	5	1	160	60	1.20	0.126
GE MEM-101	94.9	5.1	-	-	-	3	160	40	-	-

The efficiency of the separation by the GE MEM-101 membrane is compared to a vacuum distillation occurring at a similar temperature and pressures in Figure . The vapor liquid equilibrium data was plotted for the pressure range of 92 to 220 mmhg at a temperature of 50C. The points for the membrane separation fall above and below this curve, at low and high ethanol concentrations it was possible to obtain a 96 wt % ethanol product.

The separation factor appears to be concentration dependent with the results obtained here. On the other hand, the permeability of ethanol and water appears to be independent of feed concentration. The occurance of 96% ethanol from the varying feed concentrations supports this statement. An extended run was done for 26 hours which produced four permeate samples, 96%, 93%, 85% and 92% ethanol respectively. The samples were composited to get an average permeate of 92% ethanol and the shut down and start up of the apparatus was a possible source of the water contamination.

The fluxes that have been determined for this membrane and the others are on such a small scale that any correlations between flux and concentration are skeptical. The dependence of flux on temperature also cannot accurately be correlated, but it was obvious that at temperatures below $40^{\circ}C$ the GE MEM-101 had essentially zero flux. The data collected at the two different pressures on the vacuum side of the membrane showed, of course, a flux dependence on absolute pressure.

Table 9.9   Results of the Pervaporation Studies with the GE MEM-101 Membrane.(cont.)

Membrane	Feed Etoh	Feed H_2O	Permeate Etoh	Permeate H_2O	Amount	Time	Pres.	Temp.	α	J
GE MEM-101	8.0	92.0	-	-	-	4	220	60	-	-
GE MEM-101	35.0	65.0	96.4	3.6	0.8	2	220	60	50	0.009
GE MEM-101	35.0	65.0	96.4	3.6	1.0	2.5	220	60	50	0.01
GE MEM-101	8.0	92.0	20.0	80.0	-	-	220	75	2.8	-
GE MEM-101	29.0	71.0	83.0	17.0	4.3	6	220	60	12	0.018
GE MEM-101	32.0	68.0	93.0	7.0	3.5	6.5	220	60	29	0.014
GE MEM-101	30.5	69.5	62.5	37.5	6	6	220	60	3.8	0.025
GE MEM-101	54.5	45.5	96.0	4.0	2	2.5	220	60	20	0.02
GE MEM-101	54.5	45.5	92.0	8.0	15	26	220	60	9.6	0.015

9.4 Conclusions

The commercial separation of ethanol, water and solvent by a membrane process is not presently attractive using the tested membranes. Theoretically, osmotic pressure limits the permeating components flow through the membrane. The experimental results revealed that all the membranes tested passed all the species present -- only in different ratios which depended upon whether a liquid flowed through a porous solid or it evaporated away from the membrane.

The ultrafiltration process could be useful at other stages of the process. The separation of simular size molecules through a membrane whose pores are much larger than the molecules would need a membrane whose surface chemistry created a thick boundary layer with a steep concentration gradient. If the pore size was reduced further, the process would be referred to as reverse osmosis instead.

The reverse osmosis data presented here is inconclusive, but resembles data obtained by others ( ).

Pervaporation yielded the best separations for the membranes tested, but it requires the highest input of energy to operate. Placing a number of pervaporation units in series to form cascades may be impractical. The permeate, a vapor would need to be condensed between each stage, and the heat resupplied to vaporize the feed to the next stage. If a membrane was developed which would preferentially pass the lower concentration component and leave a nearly pure concentrate, then pervaporation would be more attractive.

9.5 References

1. Mehta, G. D., "Comparison of Membrance Processes with Distillation for Alcohol/Water Separation", J. Membrane Science, 12:1-26 (1982).

2. Schissel, P., "FY 1982 Annual Progress Report for the Membrane Research Subtask, Alcohol-Fuels Program", SERI/PR--255-1776, Golden, CO, Solar Research Institute, (1983).

3. Choo, C. Y., "Advances in Petroleum Chemistry", Vol 16, Ch 2, Interscience, NY (1962).

4. Sweeny, R. F. and Rose, A., "Factors Determining Rates and Separation in Barrier Membrane Permeation", I&EC Prod. Res. Dev. 4:248-251 (1965).

5. Beaton, N. C., "Applications and Economics of

Ultrafiltration", I. Chem. E. Symposium Series No. 51, 59-70.

6. Sourirajan, S. and Matsuura, T., "Science of Reverse Osmosis - An Essential Tool for the Chemcial Engineer", The Chemical Engineer, 359-376 (Oct. 1982).

7. Gill, W. N. and Soltanieh, M., "Review of Reverse Osmosis Membranes and Transport Models", Chem. Eng. Comm., 12:279-363 (1981).

8. Petty, S. E., and Maxham, J. V., "Ethanol - Water Separation Using a Reverse Osmosis Process", Department of Energy, DE-AC06-76RLO-1830, Pacific Northwest Laboratory, Richland, WA (1980).

9. Larkin, J. A., and Pemberton, R. C., "Thermodynamic Properties of Mixtures of Water and Ethanol Between 298.15 and 383.15 K", NPL Report Chem. 43, (Jan. 1976).

10. Tealdo, G. C., Canepa, P. and Munari, S., "Water - Ethanol Permeation Through Grafted PTFE Membranes", Journal of Membrane Science, 9:191-196 (1981).

11. Lee, T. S., Omstead, D. and Lu, N., "Membrane Separations in Alcohol Production", Annuals of the New York Academy of Science, 369:367-381 (1981).

12. "Summary of Progress on the Development of Ethanol - Selective Membranes at the Southern Research Institute", (Subcontract XB-1-1989-3).

13. "Summary of Progress on the Development of Ethanol - Selective Membranes for Contractor's Meeting May 16-18, 1982", Souther Research Institute, Birmingham, AL.

14. Pepper, D. and Smith, G. A., "The Design of Membrane Systems", I. Chem. E. Symposium Series No. 51, 1-16.

15. Lee, E. K. L. and Babcock, W. C., "Counter-Current Reverse Osmosis for Ethanol - Water Separation", Bend Research Inc., Bresnahan, PA, 66p DE83009725 (1983).

16. Nichols, L. D., Allen, M. B. and Celala, C., "Low-Energy Process to Extract Anhydrous Ethanol from Fermentation Beers", Moleculon Research Corp., DE 83 005012 (1983).

17. Reid, C. E. and Breaton, E. J., "Water and Ion Flow Across Cellulose Membranes", J. Appl. Poly. Sci., 1:133 (1959).

18. A. H. Ballweg, H. E. A. Bruschke, W. H. Schneider, G. F. Tusel, Homburg/Saar GFR. "Pervaporation Membranes - An Economical Method to Replace Conventional Dehydration and Rectification Columns in Ethanol Distilleries", GFT Engineering for Industrial Plants, 06650.

19. D. W. Tedder, W. Y. Tawfik, A. J. Eckles IV, Summary 1982.

20. Sourirajan, S. "The Science of Reverse Osmosis - Mechanisms, Membranes, Transport and Applications", Pure. Appl. Chem., 50:593-615 (1978).

21. Sourirajan, S., Reverse Osmosis, Academic Press (1970).

CHAPTER 10

MECHANISMS OF ETHANOL EXTRACTION INTO SELECTED SOLVENTS

(C. L. Liotta)

10.1 Introduction

It has been observed that a solution consisting of 30% (by volume) tri-n-butylphosphate (TBP) in hydrocarbon solvent (Isopar G or Isopar L) selectively extracts ethanol from a variety of aqueous ethanol solutions. It is generally believed that the TBP hydrogen bonds more effectively with ethanol than with water. In an attempt to understand the mechanistic origins of these observations, NMR techniques (^{31}P NMR) have been employed to probe the nature and degree of interaction of ethanol and water with TBP in Isopar G, Isopar L, and a variety of organic solvents. In addition, semi-empirical molecular orbital calculations (MINDO/3) have been employed in an attempt to understand the NMR observations on a molecular level.

10.2 Hydrogen Bonded Structures Involving Phosphorous Molecules

Hydrogen bonded structures involving oxygen and hydroxyl functionalities bound to phosphorus are well known in the chemical literature. In an excellent review (1) concerning very strong hydrogen bonding, J. Emsley comments that while hydrogen bonds in carboxylic acid dimers and polymers are weak, those involving phosphoric acid derivatives are often quite strong. The solid state structure of di-p-chlorophenylphosphoric acid has been determined from single crystal x-ray diffraction. The oxygen-oxygen distance associated with the hydrogne bond is 2.40 Å and is crystallographically symmetrical.

The infrared spectrum of this dimer shows no bond above 1500 cm^{-1} that could be assigned to the O-H-O vibration. Broad absorptions at 141 and 1115 cm^{-1}, which were absent in the deutero counterpart, were assigned to vibrations associated with O-H-O. The distance of 2.40 Å and the presence of the bands at 1410 and 1115 cm^{-1} imply a strong hydrogen bonded dimer. Oxygen-oxygen distances of 2.50 Å, 2.44 Å and 2.49 Å have been determined for dibenzylphosphate, calcium monohydrogenphosphate and potassium dihydrogenphosphate, respectively. Phosphate acid has been shown to form strong hydrogen bonds with urea.

Finally, the hydrogen bond formed between triphenylphosphine oxide and trichloroacetic acid has been measured to be approximately 15 kcal/mole.

P–CL–C$_6$H$_4$–O O····H–····O O–C$_6$H$_4$–P–CL

P

P

P–CL–C$_6$H$_4$–O O·····H–O O–C$_6$H$_4$–P–CL

|2.4 Å|
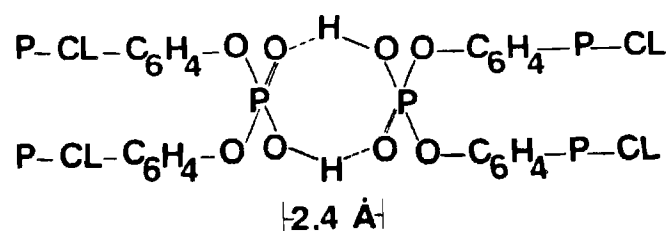
Fig. 10.   Solid state structure of
di-p-chlorophenylphosphoric acid based
on crystal X-ray diffraction

H$_2$N–C

O····H····O O–H

P

NH····H····O O–H

|1.0Å| |1.99Å|
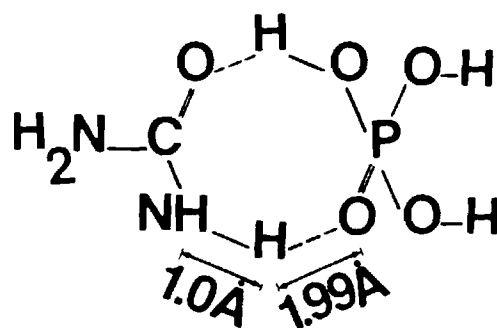
Fig. 10.   Urea-phosphoric acid
complex.

10.3 NMR Analysis

Since the ^{31}P nucleus occurs in 100% natural abundance and has a nuclear spin of 1/2, it is ideally suited for NMR studies. A wide variety of organic and inorganic phosphorous molecules have been reported in the literature. The range of ^{31}P chemical shifts vary from ca -250 ppm to ca +550 ppm with an average line width of ca 0.7 Hz. Two factors are thought to be largely responsible for the wide range of ^{31}P chemical shifts. FIrst, electrons in the 3p and sometimes 3d orbitals are alleged to contribute to the shielding, and second, in most of its compounds, phosphorus displays coordination numbers form three to six. The coordination number determines the shape of a given phosphorus molecule and in particular affects the electronic environment of the phosphorus atom.

To a first approximation, it is the substituents attached directly to the phosphorus atom which dictate the chemical shift. The effect which a change in these substitutents has on the chemical shift may be viewed in terms of (1) the change in electronegativity relative to phosphorus, (2) the effect of bond angle, and (3) the effect on the occupation of the phosphorus d orbitals, when one substituent is replaced by another. One further point is worthy of note. The charge on the phosphorus molecules, with phosphorus in a given valence state, has little effect on the magnetic shielding at the phosphorus atom. In general, substituents sterically protect the phosphorus atom from close-range magnetic and electronic effects due to surrounding (solvent) molecules which usually results in very small solvent effects. Nevertheless, the great sensitivity of the ^{31}P chemical shits makes this a useful tool for probing the environmental changes due to coordiantion of solvent molecules (especially hydrogen bonding solvents) to the pendant ligands around the central phosphorus.

10.4 Results and Discussion

A 30 volume percent stock solution of TBP in Isopar G containing benzene-d_6 was prepared from 15.00 ml of dry TBP, 25.00 ml of Isopar G, and 10.00 ml of benzene-d_6. A 2 ml volumetric pipet was used to accurately deliver 2.00 ml of solution into each NMR tube. Table 10.1 summarizes the change in ^{31}P chemical shift with addition of known quantities of anyhdrous ethanol to each of the 2.00 ml samples. These data are also represented graphically in Figure 10.1 Up to 220 mole percent of ethanol (based upon the amount of TBP) was added. Quite surprisingly, the change in chemical shift showed only a slight curivature over this large range. In fact, over the range covering the addition of one equivalent of ethanol (0 to 100 mole

percent), the plot of the ^{31}P chemical shifts vs. mole percent ethanol is essentially linear. This implies that there is probably a primary site on the TBP molecules for hydrogen bonding with ethanol. The possibilities are either at the phosphoryl oxygen or at one of the ether oxygens. With quantities of ethanol greater than 100 mole percent, the graph deviates from linearity, indicating that hydrogen bonding at secondary sites is occurring. Nevertheless, this deviation or curvature is relatively slight. This implies that the potential for ech of the oxygens of the TBP molecule to be involved in hydrogen bonding is close to being equal.

A similar series of experiments were performed using Isopar L in the absence of benzene-d$_6$. In contrast to the previous experiments, the amount of ethanol employed covered a range from 0 to 400 mole percent. The data are summarized in Tables 10.2 to 10.6 and graphically represented in Figure 10.2. The plot may be qualitatively divided into two linear segments. As in the previous experiments (Figure 10.1), the range of 0 to 100 mole percent ethanol is linear. This is followed by a curvature in the range of 100 to 200 mole percent, and then linearity from 200 to 400 mole percent ethanol. This behavior again suggests that a primary hydrogen bonding site exists on the TBP molecule and that subsequent addition of more than one equivalent of ethanol results in coordinaton with secondary sites. It is clear that it would be desirable to extend the present experiments to mole percents of ethanol greater than 400.

It was surprising to observe that, although the shapes and behavior of the curves in the two series of experiments (Figures 10.1 and 10.2) were similar, the ^{31}P chemical shifts of corresponding points were substantially displaced. The major difference between the two series was the presence and absence of benzene. It is well-known that when benzene is used as a solvent for NMR studies, the "normal" chemical shifts of nuclei are shifted in a direction consistent with deshielding. This is attributed to the interaction of the benzene molecules with the solute in question such that the diamagnetic ring currents of the benzene are felt by the nucleus in question. Thus, the comparison of Figures 10.1 and 10.2 demonstrate that benzene molecules are initimately associated with TBP. In addition, coordination of ethanol to TBP via hydrogen bonding is also effected by these non-passive solvent molecules.

In contrast to ethanol, water has only slight solubility in 30 volume percent TBP is Isopar G. Addition of varying quantities of water to this organic phase produced only slight changes in the ^{31}P chemical shift.

Table 10.1 [31]P Chemical Shifts (δ) as a Function of Mole Percent
Ethanol. 30 Volume Percent TBP in Isopar G and
Benzene-d_6.

mole % Ethanol	[31]P(δ), ppm	mole % Ethanol	[31]P(δ),ppm
0	0.461	120	0.162
20	0.397	140	0.140
40	0.334	160	0.103
60	0.303	180	0.085
80	0.261	200	0.052
100	0.225	220	0.030
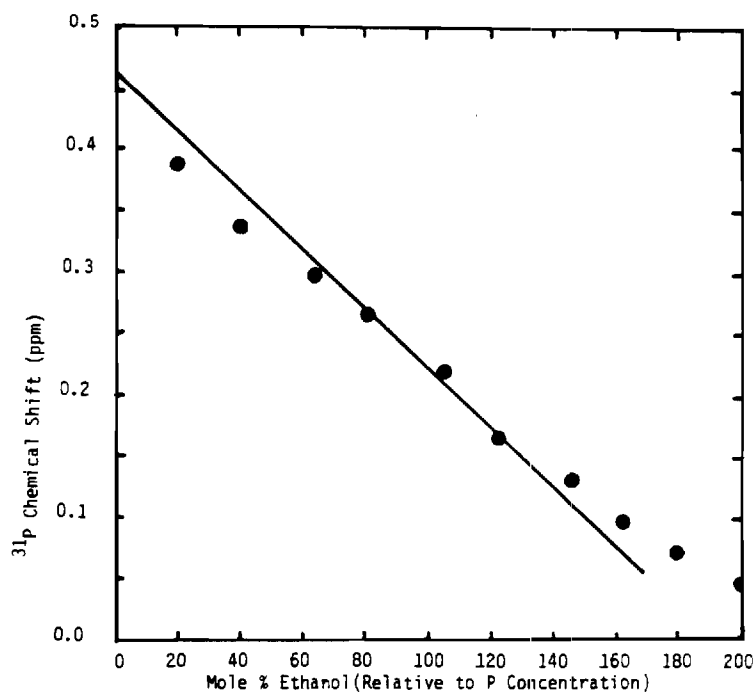
Fig. 10.1 [31]P Chemical Shift as a Function of Ethanol mole percent
in the solvent 30 vol% TBP in ISOPAR-G and benzene-d_6.
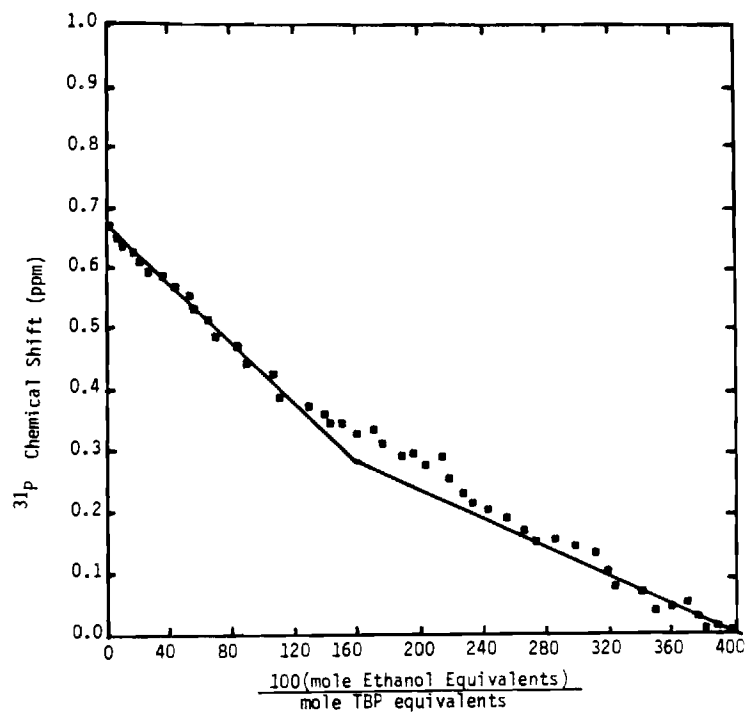
Fig.10.2 ^{31}P Chemical shift as a function of percent ethanol
in the solvent: 30 vol% TBP in ISOPAR-G and benzene-d$_6$

Table 10.2 ^{31}P Chemical Shifts (δ) as a Function of Mole Percent
Ethanol 30 Volume Percent TBP in Isopar L.

mole % Ethanol	^{31}P(δ), ppm	mole % Ethanol	^{31}P(δ), ppm
0	0.6630	26.7	0.5897
113.3	0.4097		
116.7	0.3958	30.0	0.5785
120.0	0.3878	40.0	0.5666
123.3	0.3798	43.3	0.5596
126.7	0.3777	50.0	0.5346
130.0	0.3697	53.3	0.5294
133.3	0.3657	80.0	0.4661
		90.67	0.4360
		103.3	0.4259

Table 10.3 ^{31}P Chemical Shifts (δ) as a Function of Mole Percent
Ethanol 30 Volume Percent TBP in Isopar L.

mole % Ethanol	$^{31}P(\delta)$, ppm	mole % Ethanol	$^{31}P(\delta)$, ppm
0	0.6642	210.0	0.2592
130.0	0.3787	220.0	0.2511
140.0	0.3747	230.0	0.2387
150.0	0.3375	240.0	0.2230
160.0	0.3346	250.0	0.2160
170.0	0.3104	260.0	0.2130
180.0	0.3044	270.0	0.2053
190.0	0.2953	280.0	0.1833
200.0	0.2853		

Table 10.4 ^{31}P Chemical Shifts (δ) as a Function of Mole Percent
Ethanol 30 Volume Percent TBP in Isopar L.

mole % Ethanol	$^{31}P(\delta)$, ppm	mole % Ethanol	$^{31}P(\delta)$, ppm
0	0.6610	33.3	0.5766
3.3	0.6490	36.7	0.5625
6.7	0.6409	40.0	-
10.0	0.6329	43.3	-
13.3	0.6249	46.7	0.5425
16.7	0.6128	50.0	-
20.0	0.6068	53.3	-
23.3	0.6048	56.7	0.5204
26.7	0.5867	60.0	0.5143
30.0	0.5817		

Table 10.5 ^{31}P Chemical Shifts (δ) as a Function of Mole Percent
Enthanol 30 Volume Percent TBP in Isopar L.

mole % Ethanol	^{31}P(δ), ppm	mole % Ethanol	^{31}P(δ), ppm
0	0.6620	86.7	0.4521
0	0.6691	90.0	0.4460
63.0	0.5164	93.3	0.4430
66.7	0.5053	96.7	0.4420
70.0	0.4973	100.0	0.4129
73.3	0.4832	103.3	-
76.7	0.4792	106.7	0.4099
80.0	0.4671	110.0	0.4039
83.3	0.4571		

Table 10.6 ^{31}P Chemical Shifts (δ) as a Function of Mole Percent
Ethanol 30 Volume Percent TBP in Isopar L.

mole % Ethanol	^{31}P(δ), ppm	mole % Ethanol	^{31}P(δ), ppm
0	0.6639	350.0	0.1236
280.0	0.1989	360.0	0.1226
290.0	0.1786	370.0	0.1195
300.0	0.1648	380.0	0.1115
310.0	0.1658	390.0	0.1075
320.0	0.1652	400.0	0.0995
330.0	0.1567		
340.0	0.1427		

These data are summarized in Table 10.7. These results were further substantiated by Karl Fischer titrations of water saturated TBP solutions. Maximum weight percents of 1.89, 0.86, and 0.50 weight percents of water in 30, 20 , and 10 volume percent TBP in Isopar G, respectively, could be achieved. Thus, in extraction experiments involving aqueous ethanol solutions, most of the extracted water must arise from the extraction of ethanol-water clusters.

Some initial experiments concerning the change in ^{31}P chemical shift were conducted using 20 volume percent TBP in Isopar L. The results are summarized in Table 10.8. Although there are only two points, it seems clear at this juncture that the results will be similar to those of Tables 10.1-10.6.

In order to probe the structure of the TBP molecule in hydrocarbon solvent (unperturbed by ethanol or water), the 31_P chemical shifts were determined for 30 volume percent solutions of TBP in ISOPAR G, tetrahydrofuran (THR), and methylene chloride. The results are summarized in Table 10.9. The polarity of the solvent increases in the direction Isopar G > THF > methylene chloride. As the polarity of the solvent increases, there is a dramatic change in the ^{31}P chemical shift. These obsevations may have some bearing on the possibility of TBP monomer-dimer equilibrium. Alternatively, they may be the result of specific solute-solvent interactions. Table 10.10 shows the effect of TBP dilution in Isopar G on the ^{31}P chemical shift. As the solution becomes more dilute, the chemical shifts moves to more positive ppm. It would be anticipated that as the solution becomes more dilute, greater concentrations of monomer would be present if a monomer-dimer equilibrium were operating. It is difficult to interpret these data at this point. It would be worthwhile to examine the colligative properties of these solutions.

10.5 Semiemprical Molecular Orbital Calculations

10.5.1 Phosphoric Acid

Table 10.11 summarizes the bond lengths, bond angles, and dihedral angles for geometry optimized-energy minimized phosphoric acid. Atom 2 represents the phosphoryl oxygen and atoms 4, 5, and 6 the ether oxygens. The geometry and the number associated with each position are pictorally represented in Figure 10.3.

It is interesting to note that the phosphoryl bond is shorter than the three other P-O bonds. This is consistent with the following valence bond representations (Figure 10.4) where structure B contributes more than structure C and its two remaining counterparts. Thus, there is more

Table 10.7 ^{31}P Chemical Shifts (δ) as a Function of Mole Percent
Water. 30 Volume Percent TBP in Isopar G and
Benzene-d$_6$.

mole % water	^{31}P(δ) ppm
0	0.461
10	0.450
20	0.446

Table 10.8 ^{31}P Chemical Shifts (δ) as a Function of Mole Percent
Ethanol 20 Volume Percent TBP in Isopar L

mole % Ethanol	^{31}P(δ),ppm
0	0.7032
17.2	0.6560

Table 10.9 ^{31}P Chemical Shifts (δ) as a Function of Solvent Polarity
30 Volume Percent TBP in Solvent Containing Benzene-d$_6$.

Solvent	^{31}P(δ) ppm
Isopar G	0.461
Tetrahydrofuran	0.300
Methylene Chloride	-0.300

Table 10.10 ^{31}P Chemical Shifts (δ) as a Function of TBP Concentration
(in the presence of Benzene-d$_6$).

Volume Percent	^{31}P(δ)ppm
30	0.461
10	0.548

Table 10.11 Bond Lengths, Bond Angles and Dihedral Angles for Geometry Optimized-Energy
Minimized Phosphoric Acid (H_3PO_4)

ATOM NUMBER (1)	ATOMIC NUMBER	BOND LENGTH (ANGSTROMS) NAO1	BOND ANGLE (DEGREES) NBONAO1	TWIST ANGLE (DEGREES) NCONBONAO1	NA	NB	NC
1[a]	99[a]						
2	8	5.00000			1		
3	15	1.52000	90.00000		2	1	
4	8	1.58000	115.88124	0.00000	3	2	1
5	8	1.58000	115.86518	119.81872	3	2	1
6	8	1.58000	115.98538	-120.05962	3	2	1
7	1	.95036	125.56489	0.00000	6	3	2
8	1	.94992	125.98083	0.00000	5	3	2
9	1	.95015	125.76481	0.00000	4	3	2

a. Dummy atom
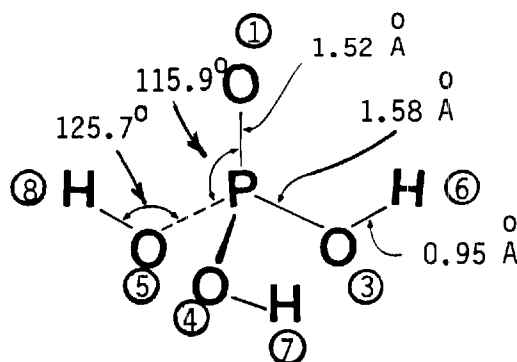
Fig. 10.3 Pictorial representation of the phosphoric acid-water complex
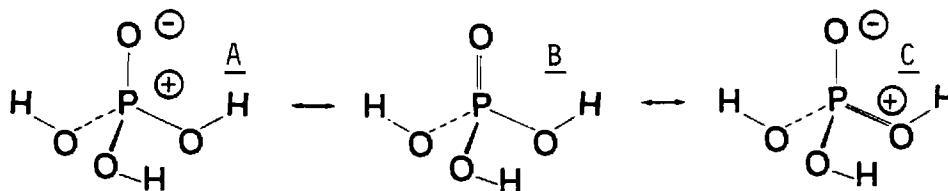
Fig. 10.4 Valence bond representations of the phosphoric acid-water complex. Additional representations are possible.

Table 10.12 Final Atomic Coordinates (Angstroms) For Geometry Optimized-Energy Minimized Phosphoric Acid (H_3PO_4)

ATOM NO.	ATOMIC NO.	X-COORDINATE	Y-COORDINATE	Z-COORDINATE
1	8	5.000000	0.000000	0.000000
2	15	5.000000	1.520000	0.000000
3	8	3.578473	2.209681	0.000000
4	8	5.706961	2.212264	-1.233489
5	8	5.711415	2.212264	1.229251
6	1	6.129965	1.759522	1.952462
7	1	6.123429	1.761069	-1.960133
8	1	2.742314	1.758440	0.000000

Table 10.13 Interatomic Separations (Angstroms) For Geometry Optimized-Energy Minimized Phosphoric Acid (H_3PO_4)

	1	2	3	4	5	6	7	8
1	0.000000							
2	1.520000	0.000000						
3	2.627478	1.580000	0.000000					
4	2.627208	1.580000	2.460073	0.000000				
5	2.628932	1.580000	2.461810	2.462746	0.000000			
6	2.860917	2.268546	3.244205	3.243227	.950164	0.000000		
7	2.864538	2.272076	3.243482	.949923	3.247184	3.912601	0.000000	
8	2.861688	2.270243	.950148	3.243513	3.245394	3.910024	3.908206	0.000000

Table IV. Net Atomic Charges For Geometry Optimized-Energy Minimized Phosphoric Acid (H_3PO_4)

ATOM NO.	CHARGE
1	-.7866
2	1.9082
3	-.6734
4	-.6741
5	-.6725
6	.1026
7	.1030
8	.1028

double bond character to the phosphoryl bond as compared to the other P-O bonds. Tables 10.12 and 10.13 summarize the atomic coordinates (x, y, z) and the interatomic separations, respectively, for geometry optimized-energy minimized phosphoric acid. The net charge associated with each of the atomic positions is summarized in Table 10.14 and is pictorially represented in Figure 10. 5.

The atomic site of greatest electron density is located at the phosphoryl oxygen. It is informative to note that the ether oxygens also contain a large amount of negative charge. The difference between the two kinds of oxygen is only 0.12 electronic charge. Thus, from electrostatic considerations alone, hydrogen bonding at the phosphoryl oxygen should be somewhat more favorable than at the ether oxygens. Nevertheless, it would be anticipated that both types of oxygens would be effective hydrogen bonding sites. Table 10.14 summarizes the eigenvalues and eigenvectors associated with all the occupied and unoccupied molecular orbitals of geometry optimized-energy minimized phosphoric acid. While molecular orbital # 16 is the highest occupied molecular orbital (HOMO) at -11.08 ev, the two immediately below are so close in energy to it (11.27 and -11.27 ev) that the three must be considered together in order to give an appropriate composite picture.

Since most of the orbital density is located on the phosphoryl oxygen atom, molecular orbitals 14, 15, and 16 represent the three lone pairs at this position. While there is a small amount of orbital density asociated with the ether oxygens, it would be anticipated that, as far as orbital controlled rections are concerned, these molecular orbitals would dominate the regiochemical behavior of the phosphoric acid molecule toward electrophilic species. Thus, the combination of greater charge density and greater orbital density (in the three highest occupied molecular orbitals) suggest that he primary site for the attack of an electrophilic species is at the phosphoryl oxygen. It follows that this would also be the most favorable site for hydrogen bonding with water or an alcohol. The lowest unoccupied molecular orbital is #17 at -1.04 ev. The largest coefficient associated with this molecular orbital z at the phosphorus atom. This atomic site is thus the most electrophilic position on the molecule in orbital cntrolled reactions. This, of course, is enhanced by the large positive charge associated with the phosphorus (+1.90 electronic charge). Finally, a dipole moment of 0.413 D was calculated for phosphoric acid (Figure 10.6).
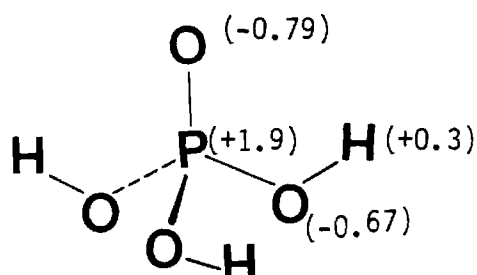
Fig. 10.5 Net charges associated with each of the atomic positions in phosphoric acid.
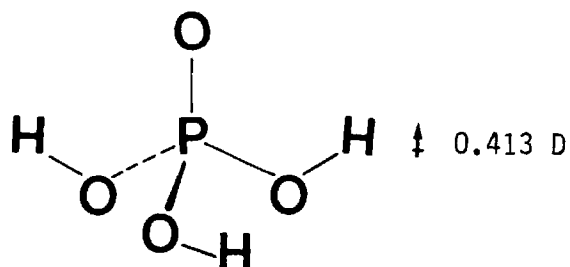
Fig. 10.6 Dipole moment of phosphoric acid.

Table 10.14 Eigenvalues and Eigenvectors for Geometry Optimized-Energy Minimized Phosphoric Acid Minimized Phosphoric Acid (H_3PO_4).

	1	2	3	4	5	6	7	8	9	10
	-32.387976	-29.686376	-29.672572	27.583012	-22.194399	-16.679291	-16.672697	-16.591648	-14.664819	-14.651376
1	.21098	.00109	.00012	.79209	.30946	-.01019	.00785	.38566	-.00142	.06102
2	-.00006	.02787	.04590	.00005	-.00003	.12181	.16851	-.00020	-.16956	-.19643
3	.11293	.00033	.00014	.14999	-.11648	.00861	-.00662	.33676	.00192	-.00138
4	.00002	.04593	-.02785	.00007	.00015	-.16851	.12127	-.00777	-.19648	.16941
5	.58215	.00073	.00054	.21021	-.42869	.00599	.00446	-.24592	.00074	-.00069
6	-.00032	.15664	.25785	.00029	-.00006	.22674	.31165	-.00058	-.14076	-.16222
7	.07112	.00060	.00001	-.15946	-.18502	-.00721	.00566	.26794	-.00151	.00103
8	.00011	.25818	-.15650	.00040	.00041	-.11375	.22577	-.01407	-.16310	.13990
9	.40605	.37015	-.61118	-.22872	.18881	.01879	-.01734	.16414	-.19248	-.22280
10	.09538	.02844	.04745	.02901	-.12119	-.11100	-.44884	.15994	-.11486	-.13408
11	-.08986	.05961	.09809	-.04014	-.01412	-.01566	-.00280	.34628	-.37302	-.43102
12	-.00000	.04200	-.02548	.00002	.00020	-.28211	.20375	-.01279	-.22197	.19085
13	.40498	.34488	.62663	-.22874	.18861	.02091	.00058	.16366	-.09765	.27774
14	-.04747	.02408	.06477	-.01445	.18688	-.24218	.32723	-.09298	-.21041	-.16741
15	-.08947	.05519	-.10011	-.04021	-.01198	.00156	.00575	.16481	-.18966	.53813
16	-.08270	.06440	-.03036	.02538	-.12229	.49531	.12522	.14841	-.18812	.09805
17	.40666	.427	-.01419	-.22271	.18896	-.01450	.02665	.16486	.28908	-.05442
18	-.04722	.02850	.04188	-.01436	.18587	.19186	-.13320	-.06207	-.13310	-.23357
19	-.09025	.11492	.00227	-.04024	-.01399	-.01181	.01821	.14807	.55910	-.10511
20	-.08235	.04716	-.02560	-.02483	.32128	.04166	-.51521	-.12768	-.12153	.17277
21	.12710	.27285	-.00544	-.06498	.22453	.11663	-.29875	-.16219	-.24529	.04627
22	.12615	.13170	.23938	-.06580	.22501	-.31706	.02986	-.17842	.08277	-.23641
23	.12671	.14138	-.23348	-.06557	.22469	.19185	.25874	-.12061	.16337	.18971
		.14138								

Table 10.14 (continued)

	11	12	13	14	15	16	17	18	19	20
	-12.700267	-12.696917	-12.452203	-11.267308	-11.265791	-11.082586	-1.044850	2.360176	2.364647	2.934806
1	.00024	.00020	.00000	-.00229	-.00012	.16860	.00695	-.00023	-.00053	-.21555
2	-.12306	.26546	.00612	.36702	-.76064	.00302	.00032	.19878	-.11609	.00002
3	-.00044	-.00048	.00000	.00752	.00115	-.62805	.39695	-.00063	-.00148	-.51546
4	.26513	.12211	.00288	.78105	.36685	.00955	.00003	-.11616	-.19857	.00033
5	.00014	-.00002	.00000	.00139	.00008	-.11607	-.52036	.00050	.00053	.24843
6	-.04573	.09864	.00190	.00679	-.01442	-.00018	-.00042	-.67025	.39164	-.00031
7	.00048	.00033	.00000	-.00364	-.00057	.26764	-.26609	-.00053	-.00157	-.64404
8	.09867	.04544	.00087	.01455	.00682	-.00027	.00018	.39171	.66995	-.00139
9	-.00333	.00619	.00018	.00858	-.01648	-.04496	.19865	-.27125	.12372	.10534
10	.10651	-.23021	.00561	.08815	-.19121	.17809	.18045	-.04679	.02701	-.08022
11	-.13722	.29386	.00678	-.14501	.32054	-.3808	-.21424	.24761	-.14454	.01209
12	-.58274	-.28469	.58359	-.00078	-.00047	.00040	-.00004	-.08468	-.14462	.00031
13	.00676	-.00081	.00022	.01139	.01560	-.04680	.19914	.21245	.12226	.10486
14	.06517	-.56848	.51142	-.05961	-.08530	-.06331	-.08925	.04952	-.13915	.03994
15	.32387	-.02972	.00606	-.19754	-.78943	-.18330	-.21386	-.24805	-.14239	.01330
16	-.25301	-.29946	.28778	.10282	.14968	.11359	.15607	.08180	-.04942	-.06978
17	-.00442	-.00592	.00003	-.01746	.00175	-.04714	.19873	-.00103	-.24390	.10654
18	.39852	-.43711	.48563	.10606	-.00820	-.06247	-.09049	.14517	.02624	.04039
19	-.18671	-.26520	.00074	.35567	-.02961	-.17445	-.21564	.00132	-.28707	.01018
20	-.39904	.01316	.28168	.18291	-.01614	-.10676	-.15679	-.08372	.04683	.07000
21	-.03842	-.05494	.00011	.02814	-.00268	.03991	-.22071	.00096	.21739	-.23156
22	.06750	-.00528	.00155	-.01745	-.02426	.01904	-.77126	-.20706	-.11951	-.22796
23	-.02802	.06147	.00165	-.01305	.02624	.01917	-.22076	.20557	-.12080	-.22917

Table 10.14 (Continued)

	21	22	23
	5.118021	5.130289	5.676785
1	-.00149	.00099	-.09203
2	.04055	.04622	-.00013
3	-.00225	.00150	-.12227
4	.04642	-.04052	-.00088
5	-.00129	.00095	-.16318
6	-.20674	-.23584	.00072
7	-.00646	.00433	-.44980
8	-.23661	.20671	.00456
9	.05977	.06902	-.02991
10	-.29752	-.14743	.32434
11	-.08298	-.09778	.11474
12	.02737	-.02386	-.00046
13	.02922	-.08630	-.03090
14	.10187	-.20419	-.16386
15	-.03961	.11934	.11513
16	-.10858	.37987	.28538
17	-.08958	.01764	-.02854
18	-.22058	.07616	-.15906
19	.12761	-.2567	.11304
20	-.39506	.06062	-.27535
21	.59467	-.11864	.35344
22	-.19115	.56712	.16780
23	-.39230	-.45653	.16189

10.5.2. Trimethyl phosphate

Table 10.15 summarizes the bond lengths, bond angles and dihedral angles for geometry optimized-energy minimized trimethylphosphate. The geometry and the number associated with each position are pictorally represented in Figure 10.7.

As in the phosphoric acid case, the phosphoryl bond is shorter than the other P-O bonds. The identical valence bond structures may be written for trimethylphosphate as were written for phosphoric acid. The overalp of a pair of electrons in a 2p orbital on the phosphoryl oxygen with the low lying unfilled orbitals on phosphorus (orbitals of proper symmetry) would give double bond character to the phosphoryl bond (structure B, Figure 10.4). Accompanying this would be a decrease in the negative charge associated with the phosphoryl oxygen. In general, it may be stated that the greater the contribution of Structure B, the shorter the phosphoryl bond and the smaller the negative charge at the phsophoryl oxygen. Accompanying this would be an increase in the negative charge associated with an ether oxygen (atoms 3, 4, and 5). As can be seen from Figures 10.3 and 10.7, all the P-O bond lengths are identical for both phosphoric acid and trimethylphosphate. Tables 10.16 and 10.17 summarize the atomic coordinates and the interatomic separations, respectively, for geometry optimized-enegy minimized trimethylphosphate. The conformation of lowest energy was calculated to be that shown in Figure 10.7. The methyl substituents are arranged so as to form an umbrella-like structure with a hydrophobic pocket. The net charge associated with each atomic position is summarized in Table 10.18 and is pictorally represented in Figure 10.8.

In contrast to the phosphoric acid molecule, the atomic sites of greatest electron density are those of the ether oxygens and not the phosphoryl oxygen. Since the P-O bond lengths for the two molecules are identical, the differnce in charge distribution must be due to the substitution of three methyl groups for three hydrogens. In the trimethylphosphate case, the difference between the two kinds of oxygen is 0.07 electronic charge. Thus, from electrostatic considerations alone, hydrogen bonding at the ether oxygens should be slightly more favorable than at the phosphoryl oxygen although both types of oxygen would be anticipated to be effective hydrogen bonding sites.

Table 10.19 sumarizes the eignevalues and eigenvectors associated with all the occupied and unoccupied molecular orbitals of geometry optimized-energy minimized trimethylphosphate. As in the case of phosphoric acid, the three highest occupied molecular orbitals (23, 24, and 25) must be considered together since they are so close in
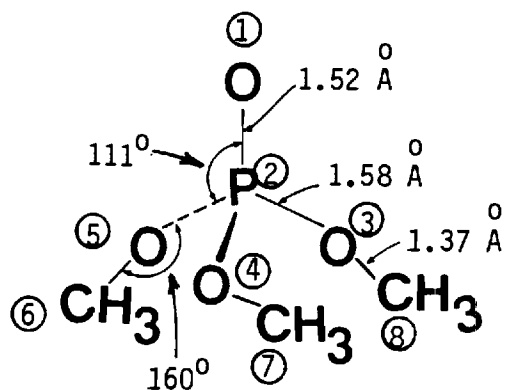
Fig. 10.7 Pictorial representation of trimethyl phosphoric acid showing bond angles and lengths and atom numbers.
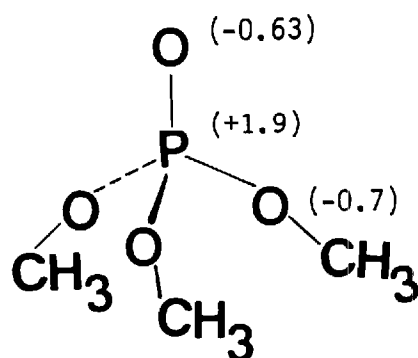
Fig. 10.8 Net charges and structure of trimethyl phosphate.
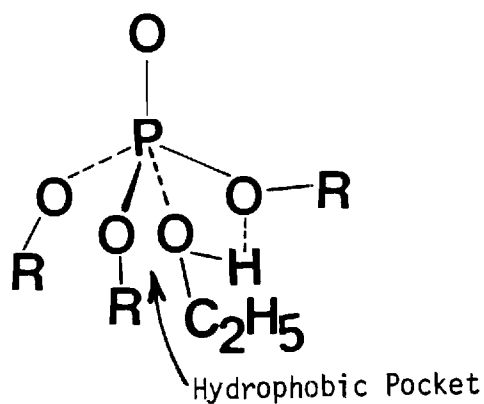
Fig. 10.9 Location of hydrophobic pocket in trialkyl phosphates.

Table 10.15 Bond Lengths, Bond Angles and Dihedral Angles for Geometry Optimized-Energy Minimized Trimethylphosphate [(CH₃O)₃PO]

ATOM NUMBER (I)	ATOMIC NUMBER	BOND LENGTH (ANGSTROMS) NAOI	BOND ANGLE (DEGREES) NBONAOI	TWIST ANGLE (DEGREES) NCONBONAOI	NA	NB	NC
1	99						
2	8	5.00000			1		
3	15	1.52000	90.00000		2	1	
4	8	1.58000	111.00000	0.00000	3	2	1
5	8	1.58000	110.53429	120.10099	3	2	1
6	8	1.58000	110.53428	-120.10100	3	2	1
7	6	1.37019	200.48581	0.00000	6	3	2
8	6	1.37019	200.48954	0.00000	5	3	2
9	6	1.36965	200.36676	0.00000	4	3	2
10	1	1.00000	109.00000	0.00000	7	6	3
11	1	1.00000	109.00000	-120.04198	7	6	3
12	1	1.00000	109.00000	120.04696	7	6	3
13	1	1.00000	109.00000	0.00000	8	5	3
14	1	1.00000	109.00000	-120.04695	8	5	3
15	1	1.00000	109.00000	120.04198	8	5	3
16	1	1.00000	109.00000	0.00000	9	4	3
17	1	1.00000	109.00000	-120.04103	9	4	3
18	1	1.00000	109.00000	120.04103	9	4	3

Table 10.16 Final Atomic Coordinates (ANgstroms) For Geometry Optimized-Energy Minimized Trimethylphosphate [(CH₃O)₃PO].

ATOM NO.	ATOMIC NO.	X-COORDINATE	Y-COORDINATE	Z-COORDINATE
1	8	5.000000	0.000000	0.000000
2	15	5.000000	1.52000	0.000000
3	8	3.524943	2.086221	0.000000
4	8	5.742063	2.074213	-1.280074
5	8	5.742063	2.074213	1.280074
6	6	6.260532	2.973504	2.174444
7	6	6.260531	2.973506	-2.174441
8	6	2.497026	2.991393	0.000000
9	1	6.072494	3.900556	1.850075
10	1	5.831420	2.830042	3.066230
11	1	7.247641	2.829989	2.245297
12	1	6.072492	3.900558	-1.850071
13	1	7.247639	2.829942	-2.245295
14	1	5.831419	2.830046	-3.066229
15	1	2.877560	3.916160	0.000000
16	1	1.939866	2.851310	-.818504
17	1	1.939866	2.851310	.818504

Table 10.17   Interatomic Separations (Angstroms) For Geometry Optimized-Energy Minimized Trimethylphosphate [(CH₃O)₃PO].

	1	2	3	4	5	6	7	8	9	10
1	0.000000									
2	1.520000	0.000000								
3	2.555017	1.580000	0.000000							
4	2.547863	1.580000	2.560148	0.000000						
5	2.547863	1.580000	2.560148	2.560149	0.000000					
6	3.893440	2.903416	3.605403	3.607109	1.370194	0.000000				
7	3.893440	2.903415	3.605481	1.370194	3.607107	4.368887	0.000000			
8	3.900426	2.903425	1.369653	3.606948	3.606949	4.346551	4.366549	0.000000		
9	4.448299	3.200011	3.633814	3.639031	1.941550	1.000000	4.114189	4.127145	0.000000	
10	4.254664	3.436457	3.908309	4.412440	1.941550	1.000000	5.260168	4.532768	1.638033	0.000000
11	4.254654	3.436449	4.610559	3.907199	1.941550	1.000000	4.530903	5.256971	1.638074	1.636952
12	4.448298	3.200009	3.633811	1.941549	3.639029	4.114188	1.000000	4.127142	3.700146	5.037275
13	4.254655	3.436468	4.410557	1.941549	3.907198	4.530902	1.000000	5.256969	4.393078	5.497088
14	4.254665	3.436457	3.908307	1.941549	4.412439	5.260168	1.000000	4.532766	5.037276	6.132459
15	4.454330	3.200989	1.941077	3.638232	3.638232	4.130534	4.130531	1.000000	3.691968	4.393940
16	4.261964	3.436096	1.941077	3.908149	4.411872	5.257455	4.530082	1.000000	5.029995	5.498710
17	4.261964	3.436096	1.941077	4.411872	3.908149	4.530084	5.257452	1.000000	4.386761	4.494098

	11	12	13	14	15	16	17
11	0.000000						
12	4.393078	0.000000					
13	4.490592	1.638074	0.000000				
14	5.497089	1.638032	1.636952	0.000000			
15	5.031772	3.691964	5.031770	4.393937	0.000000		
16	6.128606	4.386758	5.496719	4.494096	1.638025	0.000000	
17	5.496741	5.029991	6.128604	5.498708	1.638025	1.637009	0.000000

Table 10.18   Net Atomic Charges For Geometry Optimized-Energy Minimized Trimethylphosphate [(CH₃O)₃PO]

ATOM NO.	CHARGE
1	-.6286
2	1.8970
3	-.6979
4	-.6972
5	-.6972
6	.4638
7	.4638
8	.4648
9	-.0788
10	-.0553
11	-.0553
12	-.0788
13	-.0551
14	-.0553
15	-.0788
16	-.0555
17	-.0555

Table 10.19 Eigenvalues and Eigenvectors for Geometry Optimized Energy
Minimized Trimethylphosphate $[(CH_3O)_3PO]$

ROOT NO.	1	2	3	4	5	6	7	8	9	10
	-32.645682	-31.861998	-31.855559	-29.620415	-26.061861	-25.260641	-25.237139	-19.923343	-16.522180	-16.518890

Table 10.19 (Continued)

ROOT NO.	11	12	13	14	15	16	17	18	19	20
	-16.147312	-15.234887	-15.229855	-15.161990	-14.619026	-14.618106	-12.108031	-11.583313	-11.579865	-11.226074

Table 10.19 (Continued)

ROOT NO.	21	22	23	24	25	26	27	28	29	30
	-11.222851	-11.162024	-10.678710	-10.521703	-10.518771	-1.262389	1.155220	1.357863	3.605323	3.932426

Table 10.19 (Continued)

ROOT NO.	31	32	33	34	35	36	37	38	39	40	41
	3.938265	3.940366	4.681373	4.681986	4.707609	4.711172	4.713870	4.732556	4.596640	5.934512	5.915678

energy (-10.52, -10.52 and -10.68 ev). In contrast to phosphoric acid, however, most of the orbital density is located on the ether oxygens. Thus, in orbital controlled reactions, these sites would be predicted to control the regiochemical behavior of trimethylphosphate toward electrophilic species.

Combining the greater charge density at the ether oxygens with the greater orbital density at these positions (as compared to the phosphoryl oxygen) suggests that the primary site for attaching an electrophilic species is at the ether oxygen positions. It appears that the replacement of the three acidic hydrogens of phosphoric acid with three methyl substituents changes the preferred site of hydrogen bonding... Molecular orbital #26 at energy -1.26 ev represents the lowest unoccupied molecular orbital. This molecular orbital is primarily associated with the phosphoryl antibond. Since there are large s and py coefficients at phosphorus, and since the energy for this unfilled molecular orbital is quite low, this orbital may be important in bonding with the nucleophilic oxygen of the ethanol molecule. In addition to the potential overlap, electrostatic interactions between the positively charged phosphorus and the negatively charged oxygen of ethanol should also be considered.

10.6 Conclusions

The molecular orbital analysis of trimethylphosphate points to the relative importance of hydrogen bonding of water and ethanol to the ether oxygen sites of the molecule. The hydrophobic environment of the ether oxygens, as compared to the phosphoryl oxygen, points to the possible origin of the greater selectivity of trialkylphosphates toward ethnaol as compared to water. Hydrophobic-hydrophobic interactions between the ethyl group of the alcohol and the alkyl group of the phosphate may be pictorially represented by Figure 10.9.

10.7 References

1. J. Emsley, "Very Strong Hydrogen Bonding," Chem. Soc. Rev. 9, (1980) 91-124.